THREE DIMENSIONAL RIVER BASIN SIMULATION WITH DISTRIBUTED RUNOFF MODEL FOR WATER QUANTITY AND QUALITY

分布型流域モデルによる水・物質動態の三次元シミュレーションに関する研究

Amin Ismael Amin Nawahda

Doctoral Thesis
Department of Civil Engineering Systems
Graduate School of Engineering, Kyoto University

December 2004

To my wife, Samar, who, after 4 years of love and support, is still my strength, with the exception of Allah nothing is important. You have gone through a very tough time and carried most of the burden so that I didn't have to.

To my children, Aya and Yuna.

To my mother and father. Dad gave me the model of life that I live to this day. And Mom, my mother, friend, nurse, supporter, and so much more.

To a loving family that just never stopped giving themselves in countless ways.

ACKNOWLEDGMENTS

Firstly, I express my heartfelt gratitude to my supervisor, Professor Toshiharu KOJIRI, who first led me through this valley of darkness with his light of hope and knowledge, and to the members of the Water Resources Research Center at Kyoto University for their friendliness to provide the necessary data and information, and to the reviewers for reviewing the thesis and providing helpful comments. I would like also to sincerely thank Professor Shuichi IKEBUCHI, Professor Eiichi NAKAKITA, Professor Kaoru TAKARA, and Associate Professor Kunio TOMOSUGI for the unlimited support.

And also grateful to the Japanese Ministry of Education and Culture (Monbukagakusho) for the kind support.

ABSTRACT

Most of the existing distributed rainfall-runoff models simplify the interaction between the atmosphere and the groundwater processes. Nevertheless the correct representation of this interaction is very important in water resources management. The time scale of interaction between surface runoff and atmosphere is ranging from few minuets to few hours. The time scale of interaction between surface runoff and groundwater also has the range from few hours to few days (depending on the hydrological characteristics of the unsaturated and saturated layers). Because these scales are not the same, the hydrological modeling of the water cycle related processes is not straightforward. For lumped-typed runoff models, it is sufficient to simplify the interaction within large time scales. This creates the problem that large time scales in hydrological modeling do not include many of the physical processes that occur in small time scales.

The objective of this research has been to make an integrated hydrological model through the simulation of the hydrological interactions in the surface, ground and atmosphere. This resulted in a new distributed runoff model for watershed. For spatial interactions, it appeared that the existing distributed runoff models outputs could be improved considerably through considering atmosphere and ground interactions. The temporal interactions add much to the reliability and accuracy of the integrated hydrological model. The methodology is based on the dynamic linking among the transient hydrological models at different time scales, which implies that the quantity and quality of the distributed runoff at every time step is affected by the impact of atmosphere and groundwater interactions. Static linking of hydrological sub-models is normally used in distributed rainfall-runoff models. It is shown that the assumption of steady conditions for groundwater model during small time scales will not affect the accuracy of the model outputs. This is valid for many geological formations in the world. Using integrated hydrological modeling with dynamic linking between different sub-hydrological models is useful for water resources management. The developed integrated hydrological model has been applied for the Yasu River basin, Japan, and for the Seyhan River basin, Turkey. The performance of this model has been also compared with the available measured data.

Thus, as this dissertation gives a useful tool for simulating the hydrological interactions in the surface, ground and atmosphere. The developed approaches are important for integrated water resources management.

TABLE OF CONTENTS

LIST OF TABLES

LIST OF FIGURES

1 INTRODUCTION

1.1 General

The hydrological cycle involves complicated interactions between atmosphere layer, surface and ground layers. A large-scale model was developed for areas with a shallow groundwater table, and it was found that 5~20% of the groundwater evaporates from the watershed each year (Jennifer et al., 2002). The integrated hydrological modeling is achieved by dynamic linking and simultaneous calculation of the water cycle related processes. There will be almost no surface runoff unless the surface soil is saturated, or a relatively impermeable surface exists there. The saturation condition depends on the groundwater level, evaporation, water uptake by plants, infiltration, irrigation, and other existing sinks or sources. Precipitation infiltrates in grids and the excess forms the runoff. The runoff flows laterally to a seasonal stream during rain events through the surface and subsurface layers (Johansson, 1986).

Traditionally the lumped models simulate the formation of the surface runoff. Most of these models are based on the assumptions of uniformity and linearity in watersheds. In reality these assumptions include a high percentage of errors. The distributed rainfall-runoff modeling was introduced in order to overcome the shortcomings of these lumped models (Kojiri, 2000). In this distributed modeling, the watershed is divided into two types of grids; terrain grids that have only excess precipitation as input, and river grids having both excess precipitation and river flow as input. The surface runoff in each grid is transformed into the corresponding next terrain or river grid. Each grid includes five land use types; mountain, paddy, agriculture, urban, and water body. At each grid the heat balance method is used to calculate the evaporation and snowmelt, and then the kinematic wave model is used for calculating

the surface runoff. The linear storage model is used for groundwater flow modeling. The ground subsurface of the whole basin is divided into four uniform layers.

In this study the watershed is treated more extensively with specific details. These details include distributed criteria for each grid such as; geological cross sections, soil maps, dynamics of land uses, sinks and sources, and other hydroclimatic processes.

Recently most of the water quality studies, consider the mineralization of degraded pollutants without considering the transformation products, even though those products can be more toxic, more soluble, more persistent, or more bioaccumulated than the parent compound. Therefore a reliable understanding of the chemical fate of pollutants is required for the environmental impact assessment.

This study presents an approach to extend the concept of risk assessment for the distributed chemical transformations products of a parent compound (Fenner et al., 2000). The distributed hydrological model is used to provide detailed simulation of the spatial and temporal runoff including soil moisture simulation. The simulation of surface runoff quality is based on assumptions related to pollutant accumulation and transport process. These assumptions are: (1) the spatial and temporal pollutant concentration depends on the distributed runoff and the initial concentration of pollutant available for removal; (2) pollutant transformations due to chemical changes during the runoff process is considered, and (3) the amounts of pollutants percolating into the soil by infiltration are significant. The distributed concentration of pollutant is estimated based on land use types and population in each grid.

1.2 Synopsis description

The main question of this study is how to model the water quantitative and qualitative spatial and temporal interactions in atmosphere, surface and ground, making

use of the well-developed formulations for each system individually. This will be done by identifying the following requirements:

1) Which relationships can be reformulated in order to simulate the interaction?

2) How can one derive the parameterizations of the reformulated relationships?

3) How can these relationships be solved by using computer?

1.3 Objective

The main objective is to establish dynamically linked and physically based mathematical relationships with numerical approaches in distributed runoff models, groundwater and atmosphere models, in order to simulate the hydrological interactions in the atmosphere, surface and ground.

1.4 Case of the Yasu and the Seyhan River basins

The Yasu River is located in Shiga prefecture, Japan, and is one of the main water sources for Lake Biwa. Averaged annual precipitation for the regions ranges from 1550 - 2050 mm for the lower and upper catchments, respectively. The area of the whole basin is 445 km^2 (see Figure 1.1). The length of the river channel is 95 km. Small river flows and draw down of the groundwater level in the lower catchments and conservation of the water quality are the main concerns in the Yasu River basin. Many studies have been carried out for developing a hydrological model for the Yasu River basin. The tank model was used for simulating the runoff and the operation of reservoirs for the upper catchments (Kato, 2002). In the lower catchments of the basin a groundwater model was developed to investigate the impacts of land use changes (Kimaro, 2002) and the simulation results show a draw down of the groundwater levels. Though the mentioned studies were limited to sub-catchments in the Yasu River basin, the researchers thought

that there might be a strong relation between the exploding urbanization and the change in land uses, and the change of both groundwater levels and shape of the hydrographs of the Yasu River. The distributed spatial and temporal hydrological data for the Yasu River basin were collected at necessary monitoring stations. Spatial data includes geological formation, soil map, elevation, land uses, slope, flow direction, and existing sewers. Temporal data includes meteorological data, land utilization, groundwater level, operation of distributed sinks, water consumption, and seasonal measurements of the hydrological parameters.

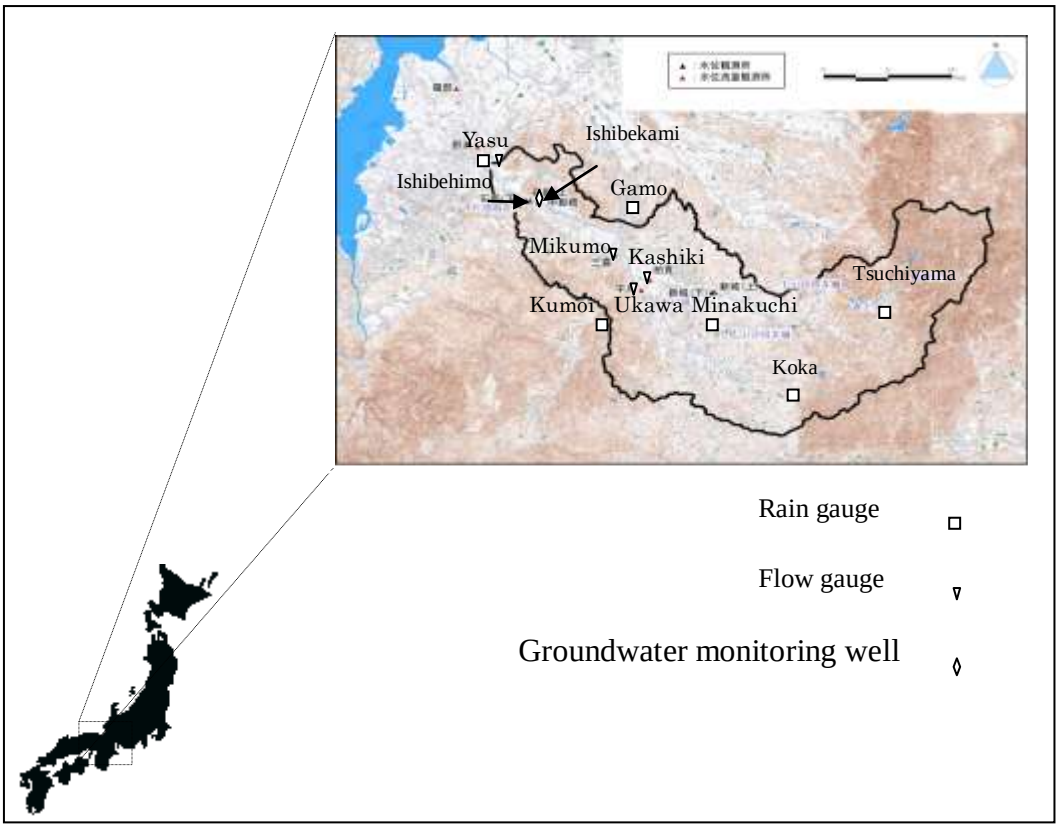

Figure 1.1 The Yasu River basin in Japan.

The Seyhan River basin, which is one of the main agricultural regions in Turkey, has an area of the basin is 22,300 km^2 (see Figure 1.2). The locations of rainfall gauges are shown in Figure B.1, Appendix B. There are four main land uses; forest and shrub (4.2 M ha), farmland (1.33 M ha) and pasture (0.36 M ha), maize, cotton and citrus fruits are mainly cultivated. For hydro-power generation and flood control the Catalan and the Seyhan dams were constructed. The annual average precipitation is 700-1000 mm. Due to climate change the evapotranspiration and consequently the irrigation water demand may increase. Also increase of precipitation in winter may increase the frequency of flood events, which have been observed recently.

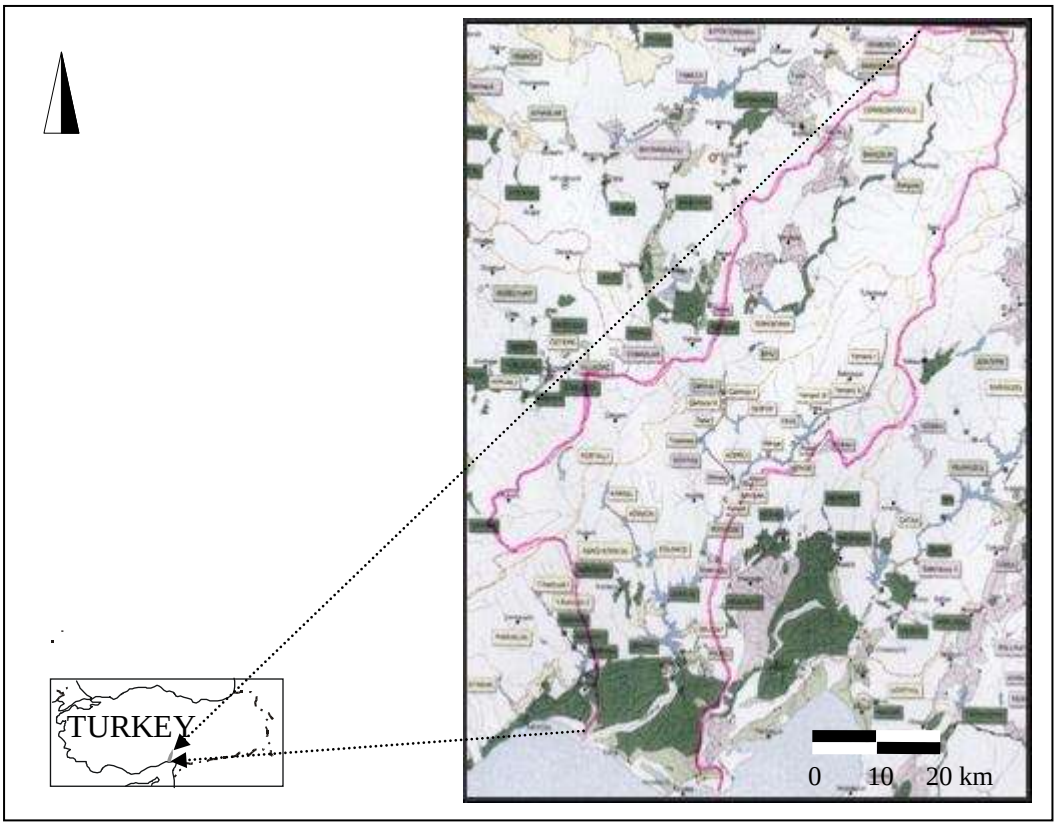

Figure 1.2 The Seyhan River basin in Turkey.

Flood simulation is relatively of high importance in the Seyhan River basin. Although the climate is generally dry and the total runoff is low, seasonal large floods occur there. Methods for modeling the flood hydrograph were first proposed in the Seyhan River basin by JICA before ten years ago (JICA, 1994), based on the translation of runoff by the time-area formulation.

Floods occur during springtime due to snowmelt in the upper catchments. The Seyhan streams are characterized by long periods of low flow with seasonal massive floods. For example the median of monthly flow rate for the 10,000 km^2 is about 10 (m^3/sec). The Department of Water and Irrigation (DSI) has published many documents related to river hydrograph and there are no manuals have been prepared by the DSI to be used for design work or future planning. These manuals are needed for flood estimation techniques. Unfortunately no much work has been done there for evaluating the infiltration and groundwater recharge, estimation of effective rainfall, which is the volume that is routed as a runoff, is based on a simplified models. For modeling the flood hydrographs there are many well-developed models and they have been widely used, such as synthetic unit hydrograph (Clark, 1945), and the storage routing models (Laureson, 1964). The distributed hydrological model has to be modified in order to be applied for the case of the Seyhan River basin. The modifications include; a) spatial and temporal of effective rainfall for each grid, b)runoff is routed realistically using simplified kinematic wave formulation, c)dynamic behaviors caused by land uses change in the watershed is included.

1.5 Dissertation innovations

The main objective of this dissertation, which is the mathematical formulation of the hydrological interactions in atmosphere, surface and ground layers using the dynamic linking between the governing equations for each layer, was explained in the preceding sections.

In Chapter 2, an introduction is given to the distributed-runoff sub-models. Various sub-models are discussed with regard to their mathematical equations and physical parameterizations. Thus, the innovation in this chapter is the flow chart of the HydroBEAM (Hydrological River Basin Environment Assessment Model) that illustrates the spatial and temporal interactions between surface, and ground.

In Chapter 3, methodologies are presented for watershed characterization using HydroBEAM that integrates numerical models and model-driven hydrological data. Then it has been implemented mathematically and physically at a very high resolution (1 km) land data, involving several categories such as: land uses, soil types, topography, and geology. Thus, the innovation in this chapter is to develop a computer program that can show the hydrological characteristics of a watershed and includes its hydrological systems. It includes reservoir routing, and an integrated hydrological parameterization in each grid. Earlier researches have used the GIS-based packages to extract these characteristics separated from their hydrological models. In HydroBEAM the characterization subroutines are dynamically linked with the main workspace and this allows for including the dynamic behavior of a watershed and its hydrological systems.

In chapter 4, the accurate evaluation of grid hydroclimatic parameters is described for distributed hydrological and meteorological models because of their spatial and temporal regulation of runoff, and energy fluxes between the ground and

atmosphere. The applied approach in this chapter is to construct numerical models that incorporate the essential physics that govern these parameters with very high resolutions. The method presented in this chapter uses the hourly records at few locations to derive the physical parameters that describe the annual spatial and temporal variability. For these locations the derived parameters have been compared with the theoretical parameters, to evaluate whether they accurately represent the hydroclimatic processes. Thus, the innovation in this chapter is to estimate the spatial and temporal ambient temperature, atmosphere pressure, and wind velocity in each grid. Also an empirical equation to describe the snowfall is derived.

In Chapter 5, the formulation of distributed water quality in atmosphere, surface, and ground zones is explained, with their numerical techniques, in order to extend the concept of risk assessment for the distributed chemical transformations products of a parent compound. HydroBEAM is used to provide detailed simulation of the spatial and temporal runoff including soil moisture simulation. The simulation of surface runoff quality is based on assumptions related to pollutant accumulation and transport process. The distributed concentration of pollutant is estimated based on land use types and population in each grid. Thus, the innovation in this chapter is to develop a compartmental ("well-mixed" media) model of environmental fate and transport, which describes the entry, movement, and spatial and temporal concentration of Nonylphyenol Ethoxylate within the watershed.

In Chapter 6, the developed HydroBEAM is applied for the case of the Yasu River basin. The spatial and temporal water quantity is presented and compared with the observed data, also the water quality simulations are presented.

In Chapter 7, HydroBEAM is modified in order to be applied to ungauged river basin, daily temperature and precipitation are extracted from global circulation models and downscaled to finer resolutions. The temperature is downscaled using the nonlinear interpolation method, and then it is modified with respect to topography. The precipitation is downscaled using an empirical interpolation method, and then snowfall and snowmelt are evaluated empirically. Also other simplifications, which is related to runoff and groundwater flow routing, are presented. The proposed methodologies are applied for the case of the Tone River basin, Japan, and the Seyhan River basin, Turkey. Thus, the innovation in this chapter is to downscale hydroclimatic data from GCM data by combining physical and empirical methods, and hydrological modeling for ungauged watersheds.

Chapter 8 gives a summary of the developed methodology and presents the conclusions and recommendations.

In this dissertation deterministic, physical, empirical, and numerical mathematics are employed. Only relatively simple numerical formulation is used for the atmosphere layer. The added value lies in the dynamic linking between different hydroclimatic processes, which have different spatial and temporal domains, this resulted in a new integrated hydrological model for numerical watershed management with relatively small spatial and temporal time steps.

2 THE DISTRIBUTED HYDROLOGICAL RUNOFF MODEL

2.1 Introduction

The water cycle related to hydrological processes such as surface water flow and groundwater flow are simulated in the distributed hydrological models, but are not directly linked to each other. When the intention is to model hydrological relations using distributed hydrological model as a tool, knowledge about the other hydrological processes that take place in atmosphere, surface and ground is necessary, such as evapotranspiration, snowmelt, and recharge. If the distributed spatial and temporal hydrological characteristics of the watershed are available, these characteristics can be used as input in distributed hydrological model. Hydrological processes such as evapotranspiration, snowmelt, and recharge depend on the distributed hydroclimatic processes, which cause the dynamic behavior of the watershed. The time scale for hydroclimatic processes is not similar. Therefore, it is important to have knowledge of:

1) Distribution of meteorological data
2) Energy budget method
3) Water budget method

These processes have been intensively viewed by many researchers who developed distributed hydrological models. Distributed models have been introduced in order to change the way the hydrologic system had been modeled, by characterizing the watersheds more realistically when simulating overland flow and river routing. Singh (1995) has developed a powerful model of watershed hydrology, other models such as TOPMODEL (Beven et al., 1995), the SLURP model (Kite, 1995), MIKE SHE (Refsgaard and Storm, 1995), SWMM (Huber, 1995), HEC-1 (Feldman, 1995) and HydroBEAM (Hydrological River Basin Environment Assessment Model) (Kojiri,

2000). All of these models are based on various levels of physical and mathematical descriptions of the watershed. But the common approach to all of them is the integrated modeling of watershed processes. Several researchers are using DEMs to define the hydrological characteristics of watershed such as boundary delineation and drainage network extraction. The models mentioned above also require data on soil characteristics, land use/cover distribution and vegetation indices as well as meteorological data. The extensive use of hydrological data in distributed modeling requires proper methodologies for distributing spatial data due to temporal changes which affects the setting of hydrological parameters such as infiltration, roughness, albedo, and others.

The original HydroBEAM has the following characteristics, which will be enhanced throughout the whole dissertation,

I. Definition

It is defined as a multi layer mesh-typed hydrological model for simulating the distributed runoff quality and quantity.

II. River basin characterizing

a) The basin boundary is determined manually or obtained from GIS-based software.
b) The basin is divided to uniform square grids (1 km x 1 km).
c) The geological cross sections and soil maps are not considered, the subsurface has four uniform layers, (A, B, C, D), and water can't pass from layer D.
d) One km elevation data is used for routing the runoff manually in four directions and cannot be visualized directly.
e) The calculation order for runoff simulation is done manually.

f) Land use data is assumed to be fixed thought the simulation except for the paddy field type.

g) The hydrological systems such as reservoirs, wells, sinks, and sources are not considered.

III. Hydrological processes

1) Evapotranspiration:

a) The heat budget method is used in order to calculate the daily potential evaporation. Wind speed is distributed horizontally by using the Thiessen polygons and vertically by using a simplified power low formulation for estimating the turbulent exchange terms. Ground heat flux is approximated by using an empirical equation that based on the cyclic fluctuation of the ground temperature; there is no relationship between the thermal conductivity, which is affected by the water content of the subsurface layers, and the fluctuation of the ground temperature.

b) The evaporation model is separated from the main model; this means the land use change due to runoff is not considered for updating the existing land use into wetted surfaces with different hydrological parameters.

c) Soil moisture content is not considered. Therefore, the actual evaporation is differs from the calculated one, the potential evaporation.

d) The calculated value can affect the four subsurface layers, and no relationship with groundwater since layer D has a zero downward vertical hydraulic conductivity.

e) Parameterization of the four layers is based only on the land use type and not based on the field sampling and soil data such as potential pressure, moisture content, and groundwater level.

f) Diffusion of evaporation, which affects the vapor pressure deficient, from a grid cell to other grid cells can't be considered since the wind direction is not considered. Also because the vapor pressure is distributed using the Thiessen polygons.

g) Mass balance is not calculated after calculating the evaporation in order to update the overall mass balance calculation for the surface and subsurface layers, since the distributed runoff is calculated based on an explicit formulation of the evaporation rate.

h) The calculated evaporation rate is used in the mass balance equation of the surface and subsurface layers, and no interaction with atmosphere.

2- Surface runoff

a) The kinematic wave model is used for routing the hourly runoff and the river flow rate. The hourly evaporation is calculated by averaging the calculated daily value. Infiltration is estimated by simulating the subsurface water flow in the four layers.

b) No reservoir routing.

c) Initial conditions such as the base flow in river, release from existing reservoir, are not considered.

d) The deferential equations of the kinematic wave model are solved using a linear scheme.

3- Subsurface water flow

a) The four layers are assume to be saturated, zero water potential and saturated hydraulic conductivity.
b) An analytical approximation of the subsurface water flow is done by using the Darcy equation and the mass balance equation for each layer.
c) Water extraction form layer A, is not considered in the formulation of the mass balance equation.

4- Groundwater flow is not considered.

IV. Atmospheric interactions

For water quantity simulation the atmospheric interactions are not considered, for water quality the following approaches are followed:

a) The runoff and the river flow are obtained from the kinematic wave model, and then the quantity and quality models are linked indirectly.
b) The atmosphere is considered as one layer.
c) Distributed point sources are considered and formulated as a function of land use and population distribution.
d) Simulations are achieved by assuming a simplified method for calculating wind velocity profile in the horizontal and vertical directions.
e) An elevated point source is not considered.
f) The impact of pollutant is used for ecological assessment.

In this chapter the formulation of each hydrological process is discussed and an overview is given of previous research regarding distributed hydrological models. The

discussed processes includes: evapotranspiration, surface runoff, subsurface and groundwater flows, snowfall and melt, and interception.

2.2 Evapotranspiration

Evapotranspiration can be defined as the change of water phase form liquid to vapor. Evapotranspiration occurs directly from surface water and indirectly from groundwater. Potential evapotranspiration occurs under the condition of unlimited water supply. The actual evapotranspiration depends on the spatial and temporal supply of water, and the plant physiology (Bras, 1990). For distributed hydrological model actual evapotranspiration should be constructed. However the spatial and temporal meteorological data is usually not sufficiently dense. Recent researches for evapotranspiration simulation have not progressed enough to describe the spatial hourly variability of evapotranspiration. Also intensive field studies for estimating and measuring the actual evapotranspiration from various irrigated crops, have been done using modified formulation of Penman method, the comparison between hourly and daily based formulations showed no advantage to either methods (Meyer et al., 1999). Unfortunately this conclusion cannot be used in distributed hydrological models. When simulating the evapotranspiration from a watershed with various land-uses and soil types the hourly time scale is of special importance.

2.2.1 Energy budget method

The energy budget equation can be written for each grid in the watershed, as follows:

$$Q_o = Q_s - Q_r + Q_a - Q_{ar} - Q_{bs} - Q_e - Q_{lh} - Q_h - Q_g \tag{2.1}$$

where Q_o is the change in the grid energy; Q_s is the incident solar radiation; Q_r is the reflected solar radiation; Q_a is the incoming long wave atmospheric radiation; Q_{ar} is the long wave radiation emitted by the grid; Q_{bs} is the long wave radiation emitted by the water body; Q_e is the energy used in evaporation; Q_{lh} is latent heat; Q_h is the sensible heat; and Q_g is the ground heat flux. The units of all terms are in watts per unit area.

Radiation energy

The effective solar radiation intensity at the watershed has a spatial and temporal variation, given by

$$I_o = \frac{W_o}{\left(1+0.017\cos\left[\frac{2\pi}{365}(186-D)\right]\right)^2}\sin\alpha \tag{2.2}$$

where I_o is the insolation, W_o is the solar constant, D is the Julian day, and α is the angle between the plan tangent to the earth and the projection of the solar radiation, $\sin\alpha$ is donated by the solar altitude (Eagleson, 1970), given by

$$\sin\alpha = \sin\delta\sin\Phi + \cos\delta\cos\Phi\cos\tau \tag{2.3}$$

where δ is the declination of the sun, Φ is the latitude, and τ is the hour angle, δ is approximated for a Julian day D by the Tennessee Valley Authority (TVA) equation, or

$$\delta = \frac{23.45\pi}{180}\cos\left[\frac{2\pi}{365}(172-D)\right] \tag{2.4}$$

Shortwave radiation

The high temperature of the sun causes the shortwave radiation; the shortwave radiation can be estimated as reported by Curtis and Eagleson (1982), as

$$\frac{I_c}{I_o} = \exp(-na_1 m) \tag{2.5}$$

where n is the turbidity factor for air, it has the value of 2.0 for clear air to 5.0 for smoggy air, m is the optical air mass, and a_1 is defined as a function of the effective thickness of the atmosphere,

$$a_1 = 0.128 - 0.054 \log_{10} m \tag{2.6}$$

m is estimated by the following equation,

$$m = \left[\sin\alpha + \frac{0.1500}{(\alpha + 3.885)^{1.253}} \right]^{-1} \tag{2.7}$$

The cloud type, thickness, and elevation affect the shortwave radiation, TVA (1972) proposed an empirical equation in order to account this effect,

$$\frac{I_s}{I_c} = 1 - 0.65N^2 \tag{2.8}$$

where I_s is the net shortwave radiation, and N is total opaque could cover. Buildings and vegetation also reflects the shortwave radiation, the net radiation at the ground level can be obtained using

$$I_{sg} = K_t I_s \tag{2.9}$$

where K_t is the transmission coefficient function of density, type, and condition of buildings and vegetations. The effective incoming shortwave radiation is given by

$$I_s^* = I_s \left(1 - albedo(t)\right) \tag{2.10}$$

Effective incoming shortwave radiation on snow surface is given by

$$\frac{I_s}{I_s^*} = \exp(-kz) \tag{2.11}$$

where k is a function of snow pack density, and z is the depth of the snow pack. The values of K_t vary from 0.28 to 0.106 according to snowpack density (26%-45%).

Longwave radiation

The earth surface, vegetations, and buildings are heated by the shortwave radiation from the sun, and then cause a Longwave radiation. Longwave radiation for clear sky is,

$$I_l = \left(1 - albedo(t)\right)\sigma E_a T_a^4 - \sigma E T^4 \tag{2.12}$$

where E_a is the atmosphere emissivity, σ is the Stefan-Boltzmann coefficient, T is the surface temperature, T_a is the air temperature (^{0}C), and E is the atmosphere emissivity near the surface. E_a is related strongly to the vapor pressure e (hPa), which can be measured directly or calculated using the relative humidity measurements, (Idso, 1981),

$$E_a = 0.70 + 5.95 \times 10^{-5} e \times \exp\left(\frac{1500}{T_a}\right) \tag{2.13}$$

Over the snow pack E_a is taken as a constant and equal to 0.757.

Sensible heat

The energy transferred due to sensible heat can be estimated by (Kojiri, 2000),

$$Q_h = c_p \rho_a C_H U \left(T - T_a\right) \tag{2.14}$$

where C_H is the bulk transfer coefficient for sensible heat, c_p is the specific heat of air, ρ_a is the density of air (kg/m^3), and U is the wind speed (m/sec) measured at (2 m) above the ground surface, however wind speed is measured most commonly at (10 m) above the ground surface. Therefore, the wind speed at (2 m) is estimated using Deacon's power relationship as illustrated by Figure C.1, Appendix C. The density of air is given by,

$$\rho_a = \frac{P_a}{RT_a}\left(1 - 0.378\frac{e}{P_a}\right) \tag{2.15}$$

where P_a is the atmosphere pressure (Pa). The temperature of the ground is affected by meteorological, terrain, and subsurface conditions. The meteorological conditions include net solar radiation, air temperature, and precipitation. Snow is considered as one of the important factors that affect the ground temperature. Also the distributed characteristics of the land uses and soil types affect the thermal coefficients of heat transfer such as the volumetric heat capacity, thermal conductivity, and the thermal diffusivity. If the ground has constant thermal proprieties, the fluctuation of ground temperature is approximated by Crawford (1957),

$$T(z,t) = T'' + A_d \exp\left(-z\sqrt{\frac{\pi}{\alpha' t_o}}\right)\cos\left(\frac{2\pi t}{t_o} - z\sqrt{\frac{\pi}{\alpha' t_o}}\right) \tag{2.16}$$

where T'' is the ground seasonal average temperature, A_d is the difference between the maximum and minimum temperatures for the period, t is the time, t_o is time for one complete cycle, and $\acute{\alpha}$ is thermal diffusivity. The ground temperature decreases exponentially with depth. Many studies showed that the ground temperature below 5 meters is constant. The temperature elapse rate is around 1 degree per 50 m depth. The heat flow in the vertical direction is given by Baker (2000),

$$\frac{\partial T}{\partial t} = D_T \frac{\partial^2 T}{\partial z^2} \tag{2.17}$$

where D_T is the thermal diffusivity. The ground thermal conductivity is strongly affected by the water content. An empirical equation is used to describe the relation with soil moisture is given by Jansson (1991),

$$\lambda = A_\lambda + B_\lambda - (A_\lambda - D_\lambda)\exp\left(-(C_\lambda\theta)^4\right)$$
$$A_\lambda = \frac{(0.5 + 1.73\theta + 0.93S)}{(1 - 0.74\theta - 0.49M - 2.8S)}$$
$$B_\lambda = 2.8S \qquad (2.18)$$
$$D_\lambda = 0.03 + 0.7S^2$$
$$C_\lambda = 1 + 2.6\sqrt{MT}$$

where θ is the soil moisture. The variables S, M, and MT are percentages of solids, quartz, and clay in soil respectively.

Latent heat

The latent heat is evaluated by the bulk-transfer method as follows,

$$Q_l = l\rho_a C_E U(q_s - q_a) \qquad (2.19)$$

where l is the latent heat of vaporization, C_E is the bulk-transfer coefficient, q_s is the specific humidity at the water and atmosphere contact, q_a is the specific humidity of atmosphere.

Ground heat

The ground heat flow is estimated by using the soil temperature gradients measured near the surface with the one dimensional steady-conductive heat flow equation, or

$$Q_g = \lambda\frac{dT}{dz} \qquad (2.20)$$

The change rate of the stored energy in the system during small time step is assumed constant; therefore the summation of all energy terms in Eq. (2.1) equals the available energy for evaporating the existing water.

Evapotranspiration

Evapotranspiration is the summation of evaporated and transpired water from water bodies and vegetations, the evapotranspiration is strangely affected by the soil moisture conditions, and also it is affected by the cropping type and stage. Many empirical equations have been developed for estimating the evapotranspiration (Singh, 1992). In this study evapotranspiration from each grid is evaluated by two steps, at first the evapotranspiration amount is calculated by using the FAO (1998) proposed crop factorization,

$$ET_1(grid,t) = k_f\,(type,t)\,EP(grid) \tag{2.21}$$

where k_f is the crop factor, *type* is the crop type, and *EP* is the potential evaporation. At second the output of the first step is updated according to the mass balance equation in the subsurface model,

$$\begin{aligned} ET_2(\text{grid,t}) = {} & \text{eprecipitation} + \text{irrigation} + \text{unsaturated/moisture} \\ & + \text{saturated/moisture} - EP - \text{recharge} - \text{runoff} \end{aligned} \tag{2.22}$$

2.3 Snowfall and snowmelt

Snowfall is one of the water resources in watersheds, in the study the simulation of the snowfall occurrence and snow pack is estimated using an empirical formula which was derived from historical data, or

$$Snowfall : e - T_a > 0.1 \tag{2.23}$$

2.3.1 Snowmelt and energy budget

The heat budget method is used for simulating the following processes within the snowpack,

$$Q_o = Q_h + Q_l + I_s + I_c + Q_v + Q_g + Q_f \tag{2.24}$$

where Q_o is the total energy available for snowmelt, if Q_o is less than the cold content of the snowpack, then snowmelt occurs and given by

$$H_m = \frac{Q_o}{80\left(\frac{L_{ms}}{L_m} - \frac{C_s T_a}{L_m}\right)} \tag{2.25}$$

where H_m is the snow melt per unit time (cm/sec), L_{ms} is the latent heat of melting for snow, L_m is the latent heat of melting for ice, and C_s is the snowpack specific heat.

The advected heat in precipitation, Q_v , is given by

$$Q_v = C_p \rho_w P T \tag{2.26}$$

where P is the water equivalent of precipitation, C_p is the specific heat of precipitation, and T is the precipitation temperature. The energy released by freezing the water content in the snowpack is given by

$$Q_f = \frac{\rho_s D_s W L_f}{\Delta t} \tag{2.27}$$

where L_f is the latent heat of freezing, D_s is the snowpack depth, W is the liquid-water content, ρ_s is the snow density, and Δt is the period of simulation.

Snowpack physical processes

1) Snowpack compaction and fresh snow density are simulated as given by Anderson and Crawford (1964),

$$\Delta D_s = \frac{P_n \times D_s}{P_p}\left(\frac{D_s}{10}\right)^{0.35} \tag{2.28}$$

$$\begin{aligned} \rho_s &= 0.05 + \left(\frac{T_a + 32}{55.6}\right)^2; && \text{for } T_a > 18^\circ C \\ \rho_s &= 0.05; && \text{for } T_a \le 18^\circ C \end{aligned} \tag{2.29}$$

where P_n is the new snow water equivalent, and P_p is the snowpack water equivalent.

2) Cold content: is the threshold energy needed before snowmelt, it is given by

$$Q_{cc} = -\rho_s C_s D_s T_a \tag{2.30}$$

3) Liquid-water content is calculated according to the empirical equation of Amorocho and Espildora (1966), or

$$W = 100\left(1 - \frac{L_{ms}}{L_m} + \frac{C_s T_a}{L_m}\right) \tag{2.31}$$

The physical processes, which occur most commonly in the snowpack are illustrated by Figure 2.2.

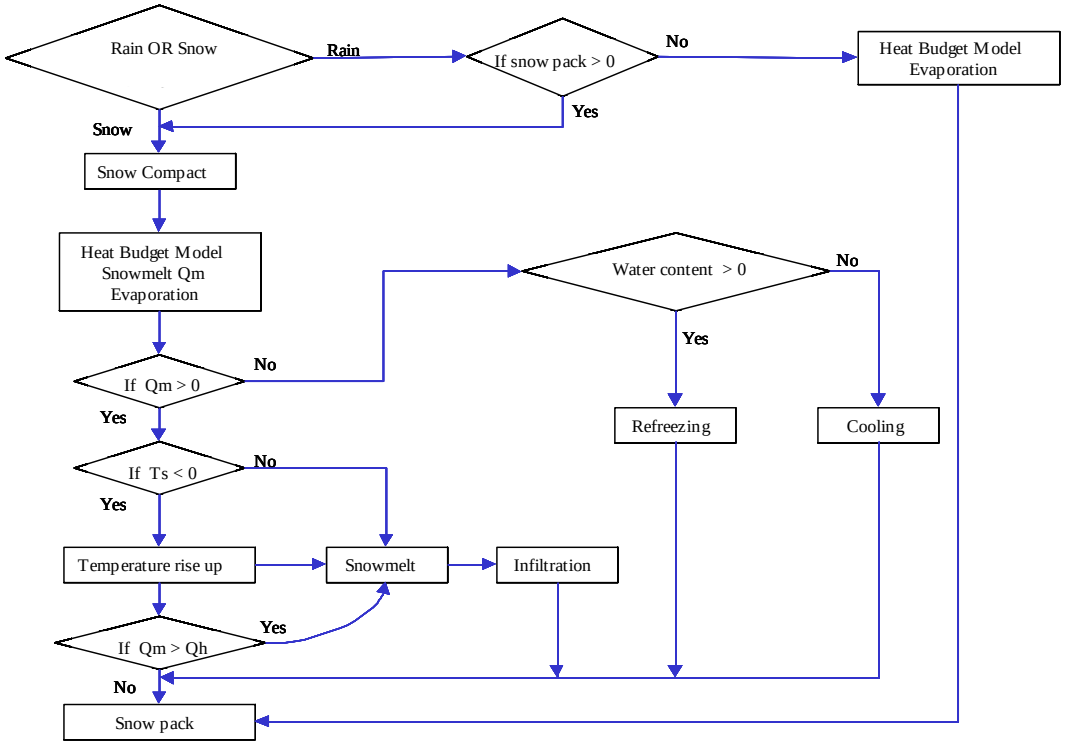

Figure 2.1 Snowfall and snowmelt related physical processes.

2.4 Surface runoff

In this dissertation the surface runoff is simulated according to the kinematic wave model. It is based on the continuity and the kinematic assumptions,

$$\frac{\partial A}{\partial t} + \frac{\partial Q}{\partial s} = q(t,s) \tag{2.32}$$

$$A = f(x, Q) = \alpha Q^{\beta} \tag{2.33}$$

where A is the discharge area, Q is the flow rate, q is the spatial and temporal effective rainfall, and α and β are parameters. The Manning's equation is used to estimate the kinematic wave parameters,

$$Q = \frac{\sqrt{sin(\varphi)}}{n_r} A H^{\frac{2}{3}} \tag{2.34}$$

where φ is the grid average slope, n_r is the roughness coefficient, and H is the hydraulic radius. Table 2-1 gives α and β for variety of shapes useful in approximating natural and man-made channels.

Table 2-1 Kinematic-parameter definitions for various hydraulic elements.

Type of segment	Alpha (α)	Beta (β)	Term definitions
Rectangular channel	$\frac{\sqrt{sin(\varphi)}}{n_r H^{2/3}}$	1.67	
Triangular channel	$\frac{1.6\sqrt{sin(\varphi)}}{n_r}\left(\frac{z}{1+z^2}\right)^{1/3}$	1.33	z : horizontal component of lateral slope
Gutter flow	$\frac{1.26\sqrt{sin(\varphi)}}{n_r}\left(\frac{z^{1/2}}{1+\left(1+z^2\right)^{1/2}}\right)^{1/3}$	1.33	
Overland flow	$\frac{\sqrt{sin(\varphi)}}{n_r}$	1.67	

2.5 Groundwater flow

2.5.1 Subsurface unsaturated flow

Richards's equation for unsaturated flow in one dimension (Richards, 1931) is used to simulate the distribution of the soil moisture and to estimate the spatial and temporal groundwater recharge,

$$C\frac{\partial \Psi}{\partial t} = \frac{\partial}{\partial z}\left[K(\Psi)\left(\frac{\partial \Psi}{\partial z} + 1\right)\right] \tag{2.35}$$

where, C is the specific water capacity, ψ (m) is the water potential head, K is the hydraulic conductivity (m/sec), z (m) is the vertical coordinate and t is time. The potential pressure-saturation relation is simulated using van-Genuchten style equations,

$$S_t = \frac{\theta - \theta_r}{\theta_s - \theta_r} = \left[\frac{1}{1 + \left(\Psi/\Psi_d\right)^{\alpha}}\right]^{\lambda/\alpha} \tag{2.36}$$

$$K = K_s S_t^{\eta} \tag{2.37}$$

where S_t is the effective saturation, θ_r is the residual water content, θ_s is the saturated water content, α and λ are the van-Genuchten fitting parameters, Ψ_d is the displacement pressure head, K_s is the saturated hydraulic conductivity and η is the exponential soil parameter.

2.5.2 Saturated groundwater flow

Quasi-three dimensional differential equation for the transient unconfined groundwater flow with Dupuit assumptions is given by

$$\frac{1}{2}\left(K_x \frac{\partial^2 h^2}{\partial x^2} + K_y \frac{\partial^2 h^2}{\partial y^2}\right) = S\frac{\partial h}{\partial t} - R(t) \tag{2.38}$$

where h is the groundwater level, K is the hydraulic conductivity, S is the specific yield, R is the volume of recharge per unit time per unit aquifer area, x and y are the displacement coordinates, and t is time.

2.6 Interception

A fraction of rainfall is not contributing to the runoff formation due to interception. The interception occurs at the roof of houses in city grids, and also occurs over the vegetation cover which has a certain storage capacity. A fraction of the intercepted water evaporates. Another fraction falls to the ground in large drops or flows over the body of the interceptor to reach the ground surface. The interception process is highly affected by the rainfall intensity and the conditions of the interceptor. Similar to the interception by vegetation that was derived by Horton (1919), the interception caused by residential buildings is given by,

$$I = D + VEt \tag{2.39}$$

where I is the interception loss, D is the interception storage depth, V is the ratio of building's surface area to its projected area on the ground, E is the evaporation rate, and t is the storm duration. The interception by plants is formulated in order to include the seasonality, also the fluctuation of the leaf area indices is included in the estimation of both interception and evaporation rates according to rainfall intensity.

2.7 Numerical methods

The finite difference method is used to approximate Eq. (2.32) as shown by Eq. (2.40), the numerical solution of the nonlinear implicit Eq. (2.40) is achieved by using the Iterative Newton Method.

$$\frac{Q_{s+1}^{t+1}-Q_{s}^{t+1}}{\Delta s}+\frac{A_{s+1}^{t+1}-A_{s+1}^{t}}{\Delta t}=\frac{q_{s+1}^{t+1}-q_{s+1}^{t}}{2}$$

$$A_{s+1}^{t+1}=\alpha\left(Q_{s+1}^{t+1}\right)^{\beta}$$

$$A_{s+1}^{t}=\alpha\left(Q_{s+1}^{t}\right)^{\beta}$$

$$\frac{\Delta t}{\Delta s}Q_{s+1}^{t+1}+\alpha\left(Q_{s+1}^{t+1}\right)^{\beta}=\frac{\Delta t}{\Delta s}Q_{s}^{t+1}+\alpha\left(Q_{s+1}^{t}\right)^{\beta}+\Delta t\left(\frac{q^{t+1}-q^{t}}{2}\right) \tag{2.40}$$

The numerical solution for Eq. (2.35) is achieved by using the finite difference implicit scheme as illustrated by Eq. (2.41). The boundary conditions can be introduced by using Eq. (2.42) and Eq. (2.43) in order to include the boundary contribution from the subsurface layers as shown in Figure 2.2.

$$C_z\frac{\Psi_z^{t+1}-\Psi_z^{t}}{\Delta t}=\frac{1}{\Delta z}\left(K_{ip}\frac{\Psi_{z+1}^{t+1}-\Psi_z^{t+1}}{\Delta z}+K_{ip}-K_{im}\frac{\Psi_z^{t+1}-\Psi_{z-1}^{t+1}}{\Delta z}-K_{im}\right) \tag{2.41}$$

Deep node:

$$\left(C_z+\frac{\Delta t}{\Delta z^2}(K_{im}+K_{ip})\right)\Psi_z^{t+1}-\frac{\Delta t}{\Delta z^2}K_{ip}\Psi_{z+1}^{t+1}=C_z\Psi_z^{t}+\frac{\Delta t}{\Delta z}(K_{ip}-K_{im})+\frac{\Delta t}{\Delta z^2}K_{im}\Psi_0 \tag{2.42}$$

Surface node:

$$\frac{\Delta t}{\Delta z^2}K_{im}\Psi_{np-2}^{t+1}+\left(C_{np-1}+\frac{\Delta t}{\Delta z^2}K_{im}\right)\Psi_{np-1}^{t+1}=C_{np-1}\Psi_{np-1}^{t}-\frac{\Delta t}{\Delta z}\left(K_{im}+q^{t+1}\right) \tag{2.43}$$

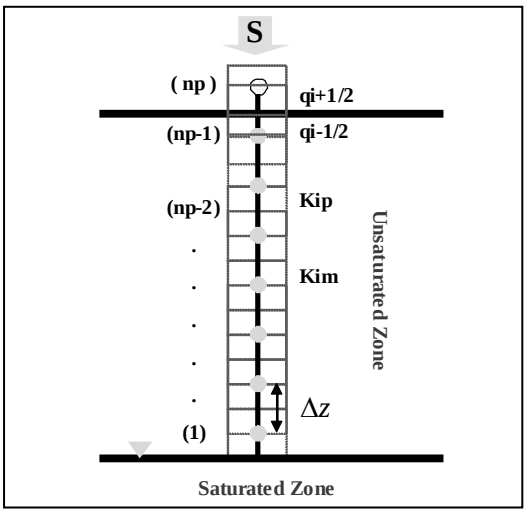

Figure 2.2 Definition sketch for finite-difference grid.

Iterative implicit Crank-Nicolson equation form is used to approximate the solution of the quasi-three dimensional partial differential equation for groundwater flow (Wang, 1982) as follows;

$$v_{ij}^{n+1} = \frac{1}{\left(\frac{a^2 S}{4K\sqrt{v_{ij}^n \Delta t}} + \alpha\right)}\left(\alpha vm_{ij}^{n+1} + \frac{a^2 S}{4K\sqrt{v_{ij}^n \Delta t}} v_{ij}^n + (1-\alpha)\left(vm_{ij}^n - v_{ij}^n\right) + \frac{a^2 R_{ij}^n}{2K}\right) \tag{2.44}$$

where $v = h^2$, $a = \Delta x^2 = \Delta y^2$, i and j are displacement coordinates, n is time step index, $\alpha = 0.5$, and vm is the arithmetic mean of the surrounding star heads.

2.8 Calculation layout in HydroBEAM

The integrated hydrological modeling is achieved by dynamic linking and simultaneous calculation of the water cycle related processes. There will be no surface runoff unless the saturation of the soil is satisfied at the surface, or an impermeable surface exists there. The saturation condition depends on the groundwater level,

evaporation, water uptake by plants, infiltration, or irrigation, and other existing sinks or sources. The precipitation infiltrates in grid-cells and the excess forms the runoff. The runoff flows laterally to a seasonal stream during rain events through the surface and subsurface layers. Figure 2.3 shows the flow chart for the HydroBEAM.

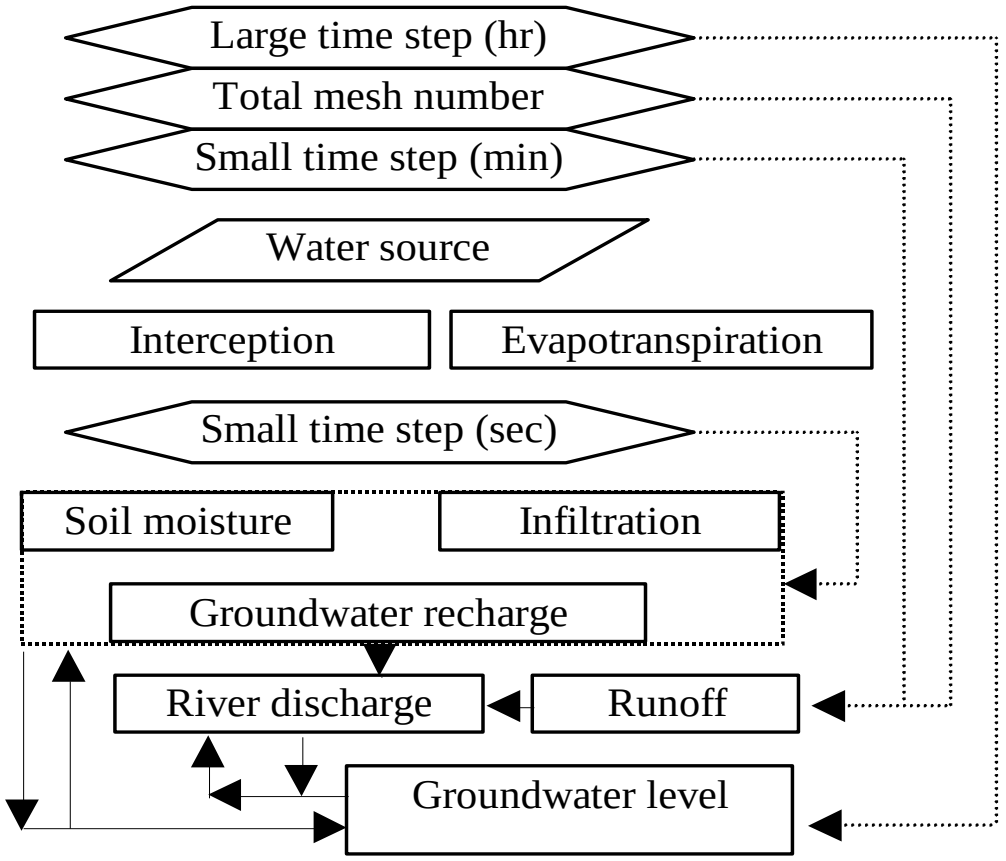

Figure 2.3 Calculation layout of HydroBEAM, quantitative spatial and temporal interactions between hydrological processes in surface and subsurface domains.

3 HYDROLOGICAL CHARACTERIZATION OF WATERSHED IN HYDROBEAM

3.1 Introduction

In this chapter, it is shown that the spatial and temporal surface runoff conditions are strongly related to the spatial and temporal characteristics of the atmosphere. Also the spatial and temporal conditions of groundwater are strongly related to the surface runoff and to the characteristics of the atmosphere.

3.2 Integrated hydrological characterization

Modeling of land water resources conditions is of critical importance to real-world applications such as water resource management, agricultural production, and flood. This has motivated the development of HydroBEAM that integrates numerical models and model-driven hydrological data. To fully address the applicability of HydroBEAM, this model has been implemented mathematically and physically at a high resolution (1km) land data, which involves several categories such as: land uses, soil types, topography, and geology, numerical simulations, and visualization tools, the watershed is divided into identical grids. In the Yasu River basin the stations used are Tsuchiyama, Minakuchi, Koka, Mikumo, Gamo and Yasu. This section briefly describes the differences in climate between these stations. Table 3-1 presents the details of the stations and Figure 3.1 shows the locations on the map. The mean annual rainfall at Tsuchiyama (1746 mm/y) is on average is higher than that at Minakuchi (1520 mm/y), Koka (1315 mm/y), Kumoi (1595 mm/y), Gamo (1454 mm/y) and Yasu (1589 mm/y).

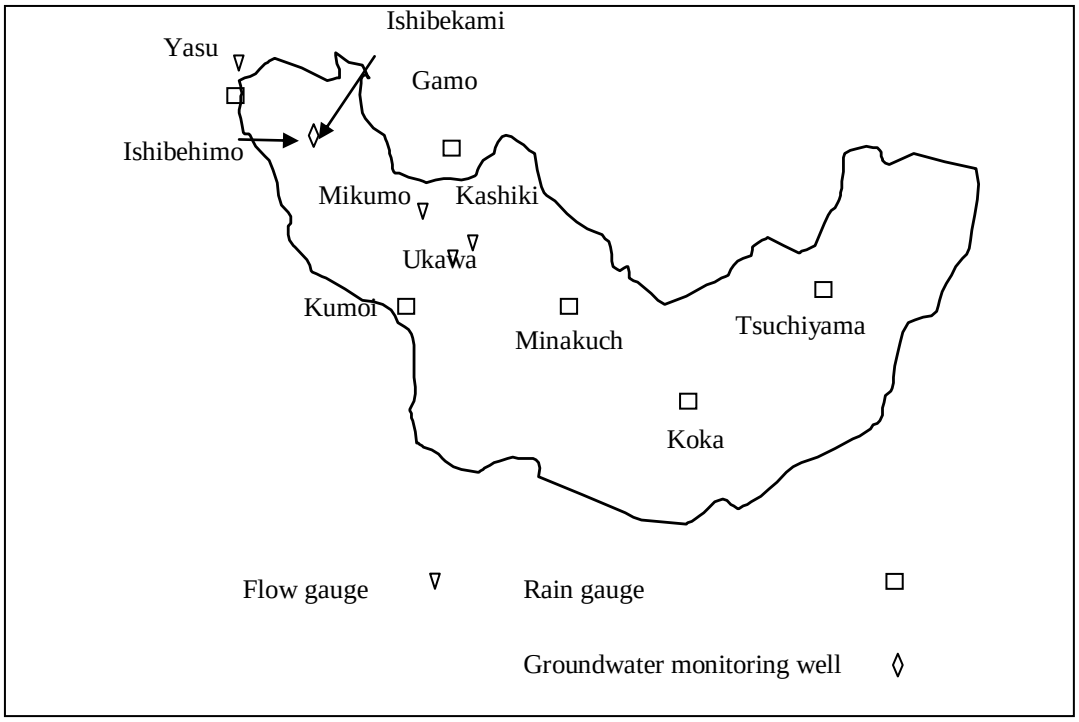

Figure 3.1 Distributed weather and gauging stations at the Yasu River basin.

Table 3-1 Details of the stations from which precipitation data are used throughout the dissertation.

	Tsuchiyama	Minakuchi	Koka	Kumoi	Gamo	Yasu
mean annual rainfall (mm/y)	1746	1520	1315	1595	1454	1589
Latitude	34° 55′42″	34° 58′06″	34° 54′07″	34° 58′57″	35° 03′06″	34° 04′30″
longitude	136° 18′00″	136° 10′09″	136° 13′18″	136° 07′16″	136° 11′06″	136° 00′24″
altitude (m)	263	174	230	141	88	95
data period	1989-1998	1989-1998	1989-1998	1989-1998	1989-1998	1989-1998
missing data		1992,1995				1992

Table 3-2 Details of the stations from which river flow data are used throughout the dissertation.

	Mikumo	Ukawa	Kashiki	Yasu
mean annual flow (m^3/sec)	10	4	6	12
distance from basin mouth (km)	32.2	23.2	19.5	8.1
catchment area (km^2)	160	125	297	445
altitude (m)	157	154	142	100
Data period	1989-1998	1989-1998	1989-1998	1989-1998
missing data	1991,1992			

Table 3-3 Details of the stations from which the water depth of river flow data are used throughout the dissertation.

	Mikumo	Ukawa	Yasu
mean annual flow depth (m)	0.17	-0.06	0.16
distance from basin mouth (km)	32.2	23.2	8.1
catchment area (km^2)	160	125	445
altitude (m)	157	154	100
data period	1989-1998	1989-1998	1989-1998

Table 3-4 Details of the stations from which groundwater table data are used throughout the dissertation.

	Ishibehimo	Ishibekami
mean annual groundwater table (m)	3.5	7.1
latitude	35° 01′17″	35° 01′07″
longitude	136° 12′27″	136° 020′59″
altitude (m)	119	117
data period	1989-1998	1989-1998

3.3 Hydrological characteristics of river basin.

3.3.1 Topography

HydroBEAM includes an automated extraction techniques that produce fast and accurate stream networks if the input from Digital Elevation Model (DEM) has a high resolution. In early times HdroBEAM had been designed to incorporate four directions routing approach, then it has been upgraded by incorporating the eight directions routing approach. Table 3-5 lists a comparison between the four and eight directions routing approaches. In eight directions routing approach, flow from a grid is directed towards one of its eight neighbors with the steepest slope as shown in Figure 3.2. HydroBEAM assigns a flow direction to each grid and a calculation index that represents the accumulated area down slope along the flow paths connecting each catchment's grids. However, the use of eight directions routing method has certain drawbacks in complex topographies as it permits flow only in one direction away from a DEM grid. Therefore, in HydroBEAM an automatic adjustment of sinks and grids with problems such as flat grids is performed before the delineation of the drainage network. This grid processing technique in HydroBEAM is considered as a preliminary step for hydrological modeling.

Table 3-5 Comparison between the four and eight directions routing approaches.

Hydraulic elements	Four directions	Eight directions
River channel length (km)	50	36
Travel time for 10 m^3/sec	53.5 (min)	41.0 (min)

The Yasu River basin is divided into one kilometer by one kilometer square grids as shown in Figure 3.3, (a). (DEM) for the Yasu River basin are available in the forms of raster or grid-based data. The DEM is used to extract hydrology-related information such as watershed delineation and drainage network extraction. A digital elevation map is shown in Figure 3.3, (b). Stream data in the Yasu River basin are extracted from both available stream data and systematically derived from the DEM by using HydroBEAM. Also surface drainage and channel network can also be automatically extracted from DEM.

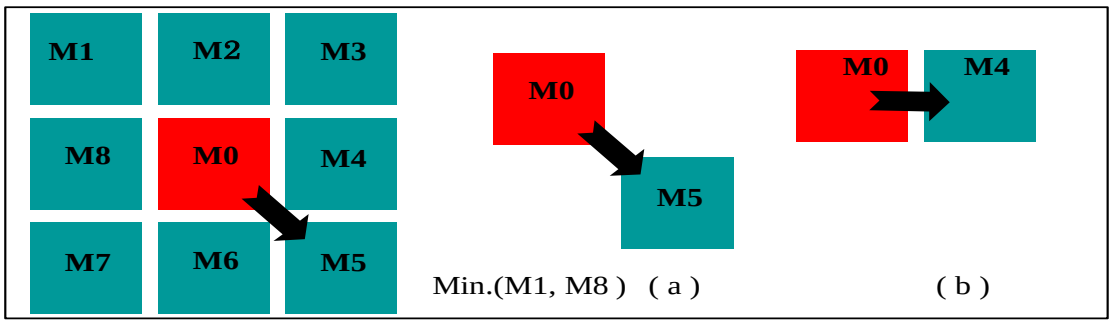

Figure 3.2 Runoff routing algorithm, (a) eight directions based routing, (b) four directions based routing.

Land use data at the Yasu River basin is obtained from remotely sensed digital images. Land use data is coupled with the soil characteristics for each grid in HydroBEAM in order to estimate the surface roughness that affects the velocity of runoff, and to estimate infiltration of precipitation. Leaf area index is estimated from the land use data. Land uses are classified into five types as follows: a) mountains, forests; b) paddy fields; c) farms; d) urban areas; e) water bodies. Figure 3.4 shows the land use and population distributions at the Yasu River basin.

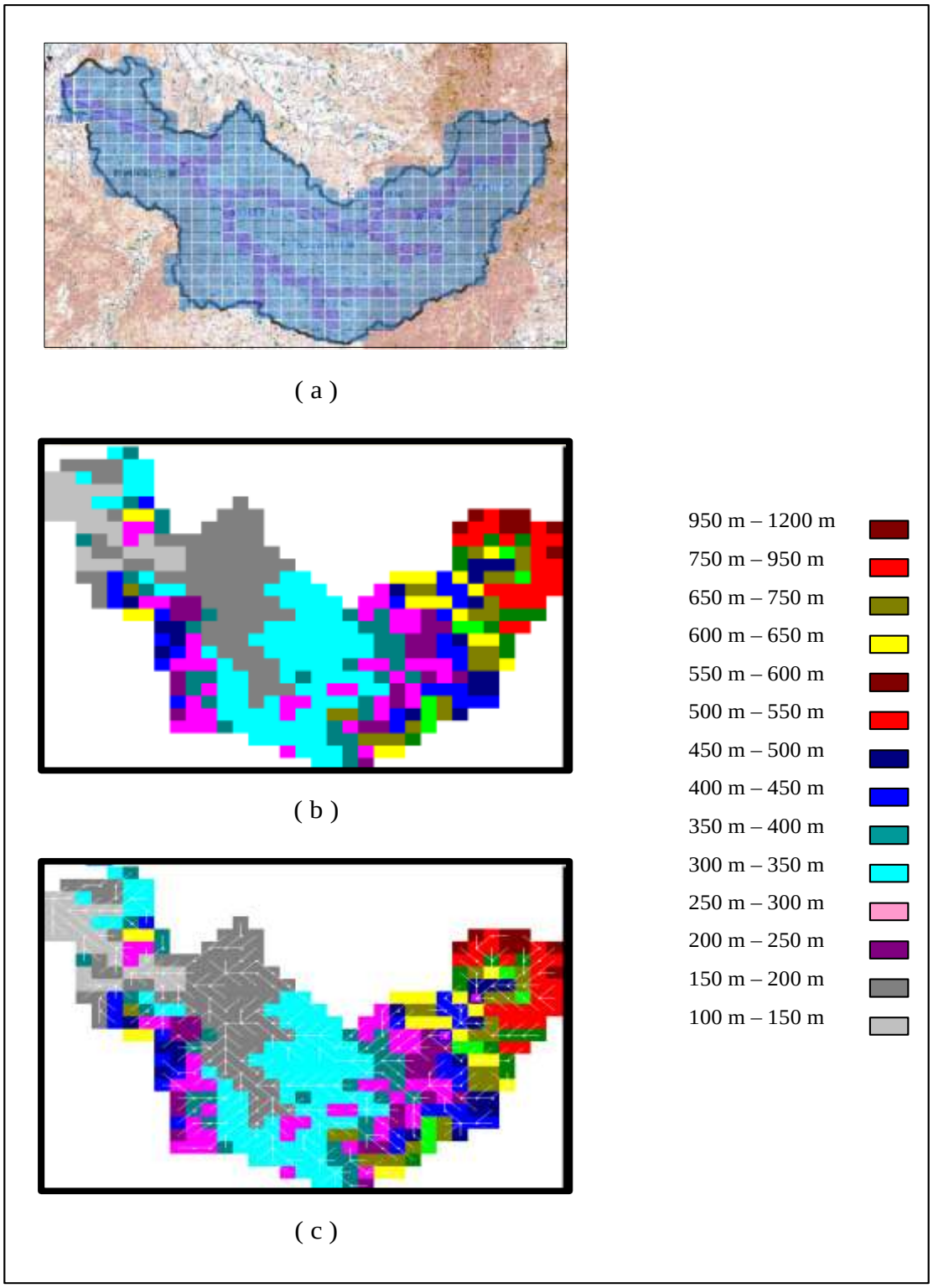

Figure 3.3 (a) The Yasu River basin divided to 1 km square grids, (b) Digital elevation map, (c) Grid-to-grid drainage network.

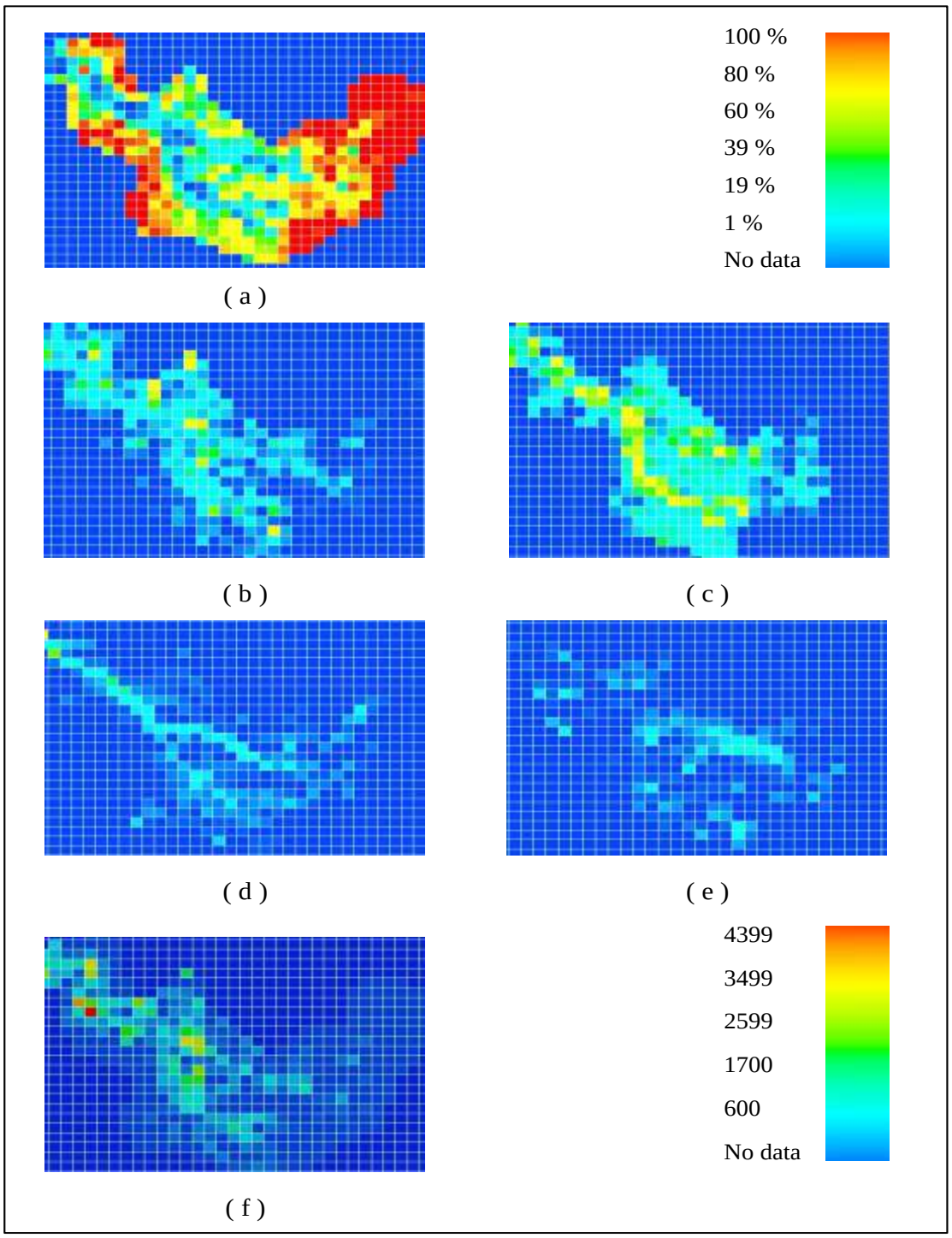

Figure 3.4 Land use and population distributions at the Yasu River basin, a) Mountains, forests; b) Paddy fields; c) Farms; d) Urban areas; e) Water bodies; f) Population (cap.)

3.3.2 Hydrograph characteristics

There are many factors affecting the hydrograph of the Yasu River basin. These factors are (1) basin characteristics, (2) land use and soil, and (3) distributed hyetographs. Figure 3.5 shows the relationship between the hydrograph at the outlet of the Yasu River basin and the summation of the distributed hyetographs there. Hydrograph is generally analyzed by using certain methods, which are used in order to estimate groundwater flow within the stream flow. In HydroBEAM the hydrograph is accurately analyzed due to dynamic linking between groundwater model and runoff model. The analysis of the hydrographs in Figure 3.6 shows that the hydrograph is highly affected by the spatial and temporal distribution of rainfall.

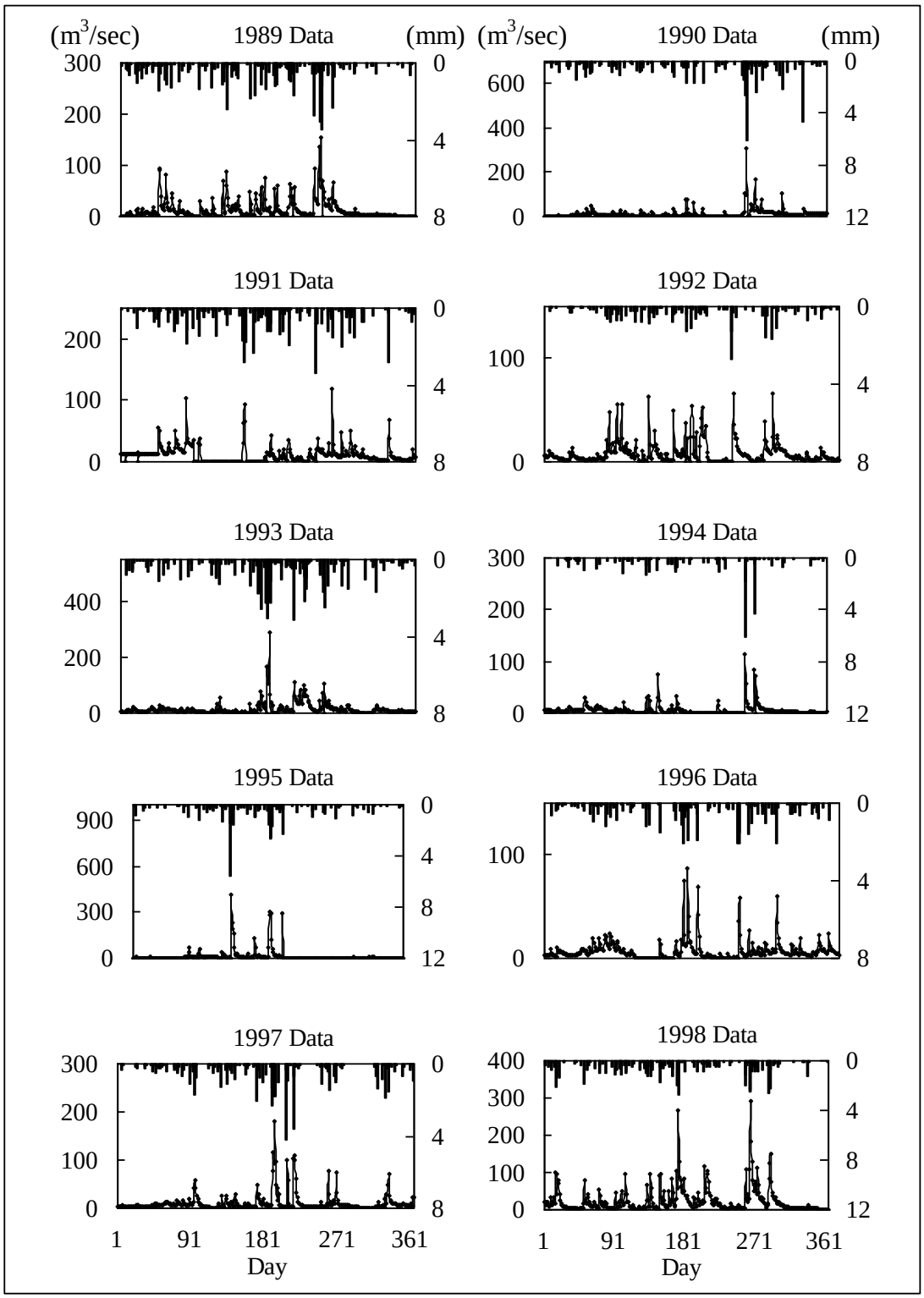

Figure 3.5 Relationship between the Yasu River hydrograph and the daily average rainfall intensity.

3.3.3 Groundwater geology and soil analysis

The soil characteristics data is vital in HydroBEAM. Most of the simulated hydroclimatic processes require specific geological data and soil data like soil type, porosity and hydraulic conductivity. Despite the need of soil and geological data in HydroBEAM, fine resolution data is generally not available in digital form. The soil characteristics and geological data are extracted from the already available hardcopy soil maps (See Appendix A). The geological structures are used to determine the boundaries of the groundwater model in HydroBEAM. The data used for the geological analysis also extracted from drillers' logs. This information was used to prepare geological cross sections in the Yasu River basin. Data from seventy groundwater monitor wells were analyzed. For groundwater modeling the geological cross sections are analyzed, the soil and the geological maps are used in order to distribute the soil types and geological formations for each grid. There are five main soil types: (a) grey low land soil; (b) gray soil; (c) peat soil; (d) not matured soil; (a) dry brown forest soil. Table 3-6 lists some of the field sampling analysis. There are four main rocks types: (a) granite; (b) chert; (c) sandstone; (d) limestone. The hydrological parameters for the geological formation such as the hydraulic conductivity and the storage coefficient are not available for the whole basin, therefore it is optimized through the model calibration by trial and error.

Table 3-6 Physical soil parameters of the Yasu River basin.

sampling point	depth (cm)	Wet weight (g)	Dry weight (g)	Saturated weight (g)	Volumetric water content (%)	Porosity (%)	Saturated hydraulic conductivity (cm/s)
A1	2.5-7	221.1	185.1	235	36	49.9	3.22 x 10-2
M1	0-5	144	116.3	184.6	27.7	68.3	6.07 x 10-1
B1	2.5-7	259.4	210.5	259.5	48.9	49	3.43 x 10-4

A1: Agricultural field, M1: Mountain, B1: Paddy field

According to the drillers' logs and geological cross sections of the study area, there are mainly unconfined and confined layers respectively. The number of boring wells is so large, they are available at every 100 m between section A and section B as shown in Figure 3.6. The unconfined layer is not the same in all grids as shown in Figure 3.7, therefore a constant average thickness is assumed all over the basin, and the unconfined layer has an average thickness of 11 m. The ranges for hydraulic conductivities for each sub-layer are listed in Table 3-7.

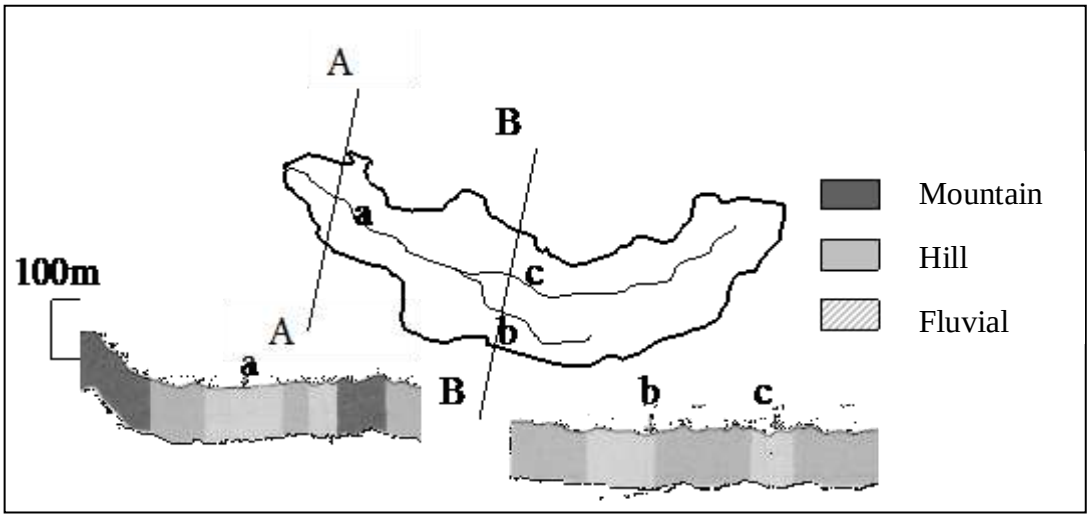

Figure 3.6 Geological cross sections at the Yasu River basin.

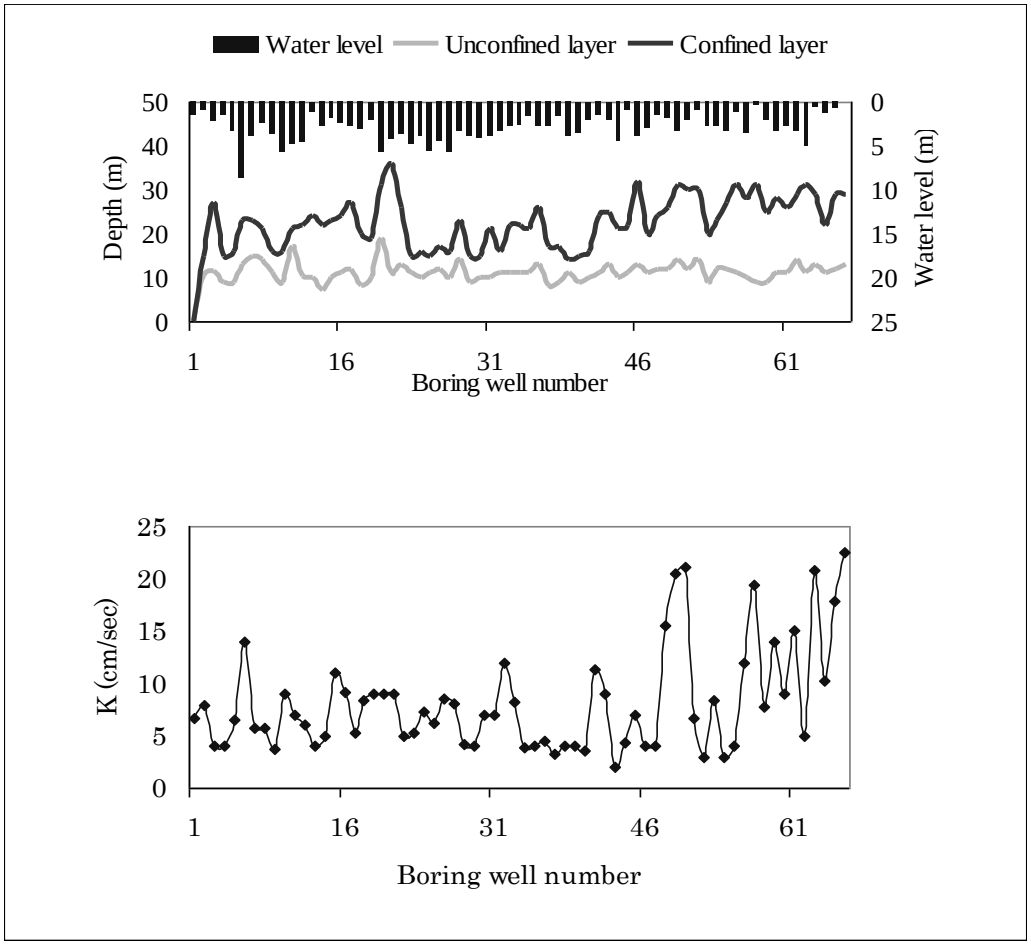

Figure 3.7 Quantitative and qualitative information from the boring logs at the Yasu River basin.

Table 3-7 Distributed stratigraphy in the lower Yasu River basin.

Layer name	Height (m)	K (cm/sec)
Ag	3	10E-2 – 1.0
Ks	2	10E-6 – 10E-5
Ksg	1	10E-3– 10E-4
Kg	11	10E-2 – 10E-4

The groundwater divide in south, north, and east of the Yasu Basin forms the basin boundaries. These boundaries are assumed to be no-flow boundaries. The western boundary will be used for calibrating the groundwater model. The recharge sources are

mainly the rainfall and irrigation. The time series data of the observed groundwater levels and groundwater extraction amounts have not been sufficiently available for the whole basin. Limited investigations conducting the amounts of pumped water were carried out. Therefore the involved uncertainty is evaluated by the manual calibration of the model. Three-dimensional simulations for the unconfined groundwater levels were also carried out. A one-year simulation was done by using these data and by applying physical parameters obtained from field. These data was set as initial conditions for the groundwater flow model. The analysis of the groundwater level data in Figure 3.8 shows that the groundwater level is highly affected by the spatial and temporal distribution of rainfall.

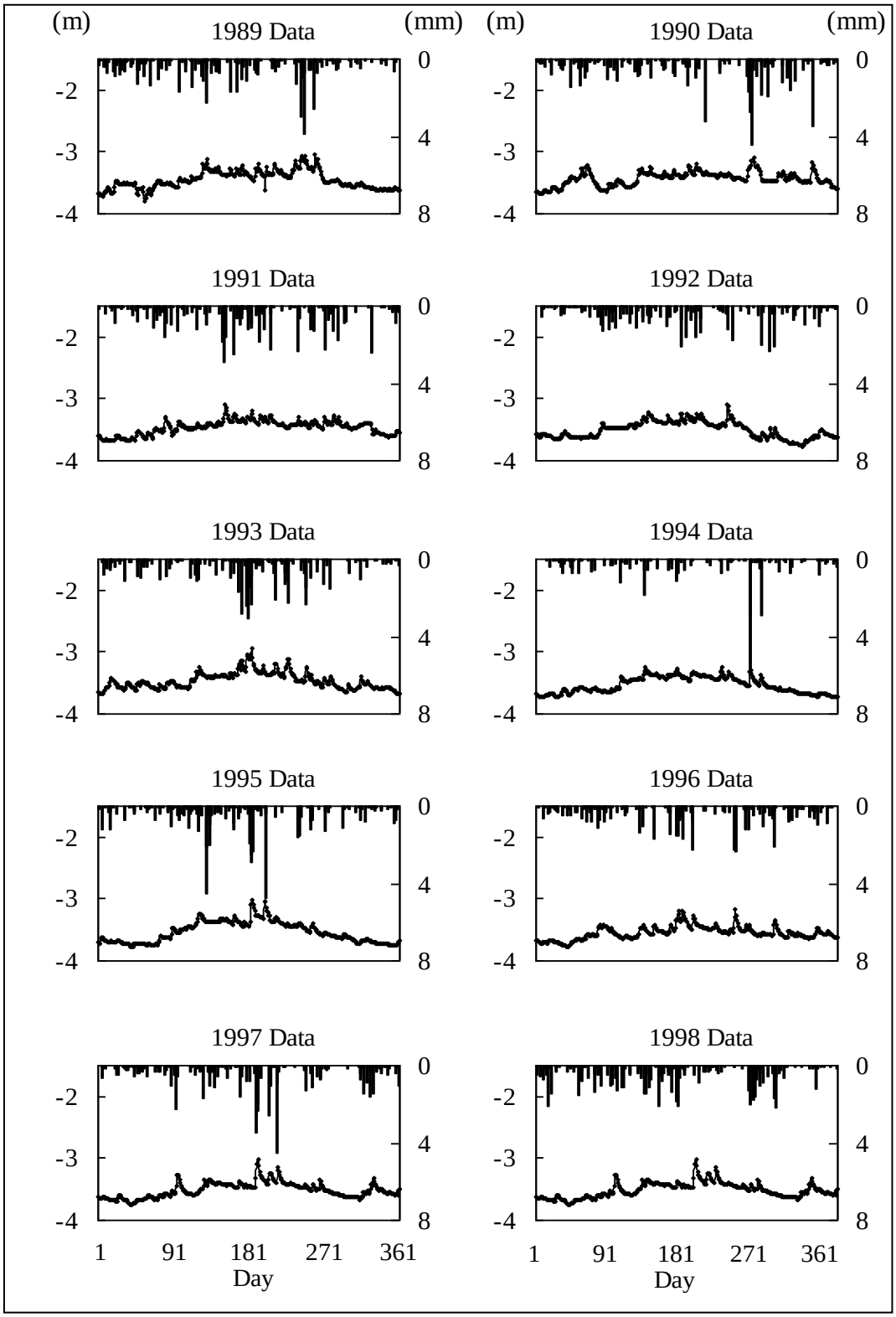

Figure 3.8 Relationship between groundwater level (m) and daily average rainfall intensity (mm) at the Yasu River basin.

3.4 Formulation of reservoir operation

There are two reservoirs are located in the upper catchments of the Yasu River basin, the *Yasu* dam is used to supply water for irrigation when shortages occur in the downstream area, and to control floods, and it has a capacity of (7.8 to 10) x 10^6 m^3, the *Ozuchi* dam is used to supply domestic water (0.080 m^3/sec) and to satisfy industrial water demand (0.533 m^3/sec). The operation of *Ozuchi* dam depends on the flow at *Minagutchi*, and the monitored flow is 1.68 m^3/sec. The basin division is used in order to simulate the operation of the two reservoirs and to set the base flow in the river channel. The basin division can be defined as dividing the watershed that has a reservoir into upper part and lower parts. Compared with the lower catchments, the upper catchments of the watershed are subjected to precipitation that differs in time and amount, also the stratigraphy of the lower part differs from the upper part. The numerical solution for the equations of mass and momentum conservations, Eq. (2.40), shows that the speed of the kinematic wave is affected by the runoff depth. Therefore the wave propagation from the upper catchments to the lower catchments will be subjected to the kinematic wave shock (Shen, 1979). On the other hand, the reservoir operation can be considered as a strong down stream control for the developed kinematic wave from the upper catchments, and then the kinematic wave approximation will be no longer valid if the reservoir operation is not involved (Ishihara, 1959). Also the probabilistic nature of the reservoir operation hardens the process of integrating with the physical hydrological models, due to different simulation and operation times. Therefore, the seasonality of the reservoir operation, and the extremes of the seasonal water demands and safety operation are set in the hydrological model, and then linear storage model is used for

routing the water in the reservoir. Two approaches are introduced in this study for estimating the release of the reservoir:

(a) *Formulated operation rules*: For immediate supply from the reservoir, and according to this approach the reservoir is operated according to certain specified rules which can be represented by the polynomial formulation of an objective release as follows;

$$Release = Qbase + Qdom + Qele + Qind + Qirr + QM \quad (3.1)$$

where *Qbase* is the river base flow, *Qdom* is the domestic water supply, *Qele* is the hydropower water supply, *Qind* is the industry water supply, *Qirr* is the irrigation water supply, and *QM* is the monitoring flow rate.

(b) *Iterative operating*: For far supply from the reservoir, this approach is introduced for reservoirs which have detailed operation rules that involve maintaining a minimum base flow in the downstream or supplying fluctuation human needs, or maintaining a specific temporal storage. At first HydroBEAM is initialized with an actual storage and release amounts. Then the seasonal user-defined main operation constrains such as maximum and minimum storage and/or allowed water levels, are formulated into the iterative method, because the calculating order in HydroBEAM is achieved form the upstream to the downstream simultaneously. Therefore, a reservoir in the upper catchments will be operated before the runoff contribution in the lower catchments is calculated. An initial guess of release is assumed, then HydroBEAM simulates the runoff up to the monitoring point then the river discharge is compared with the desired discharge *QM* as illustrated by Figure 3.9. This procedure is repeated until a certain conversion or a maximum number of iterations are achieved. The iterations are performed according to the user-defined operation time in order to save computing time.

The output of the iteration method is used to simulate the fluctuation of the storage. In order to calculate the storage, the calculated releases and the HydroBEAM simulated inflow at the reservoir, are routed linearly. There will be a deficit between the observed and simulated storages. This deficit can be used to estimate the hidden losses of the reservoir.

The operation of the *Yasu* dam is analyzed for a period of ten years. The operation of the dam illustrates some of the unique problems, associated with a dam designed for flood protection and for water supply. This type of dams requires a seasonality-based operation rules. Therefore, in HydroBEAM the monthly operation is simulated according to the formulated operation method. The operation can be formulated as a polynomial of the order six as illustrated by Eq. (3.2). Table 3-8, illustrates the monthly formulation of the storage- release functions.

$$Release = \sum_{i=1}^{6} a_i RS^i \tag{3.2}$$

where a_i is the polynomial coefficients, *RS* is the reservoir storage. Then the unsteady inflow from the upper catchments is routed through the reservoir, the initial outflow and as well as the initial storage, must be known. Using continuity the storage for a time step is given by

$$2RS_j = I_{j-1} + I_j - Rl_{j-1} - Rl(RS_j) \tag{3.3}$$

where *I* is the inflow and *Rl* is the release. The *RS* value can be used to calculate *Rl* for a time step by applying an iteration method.

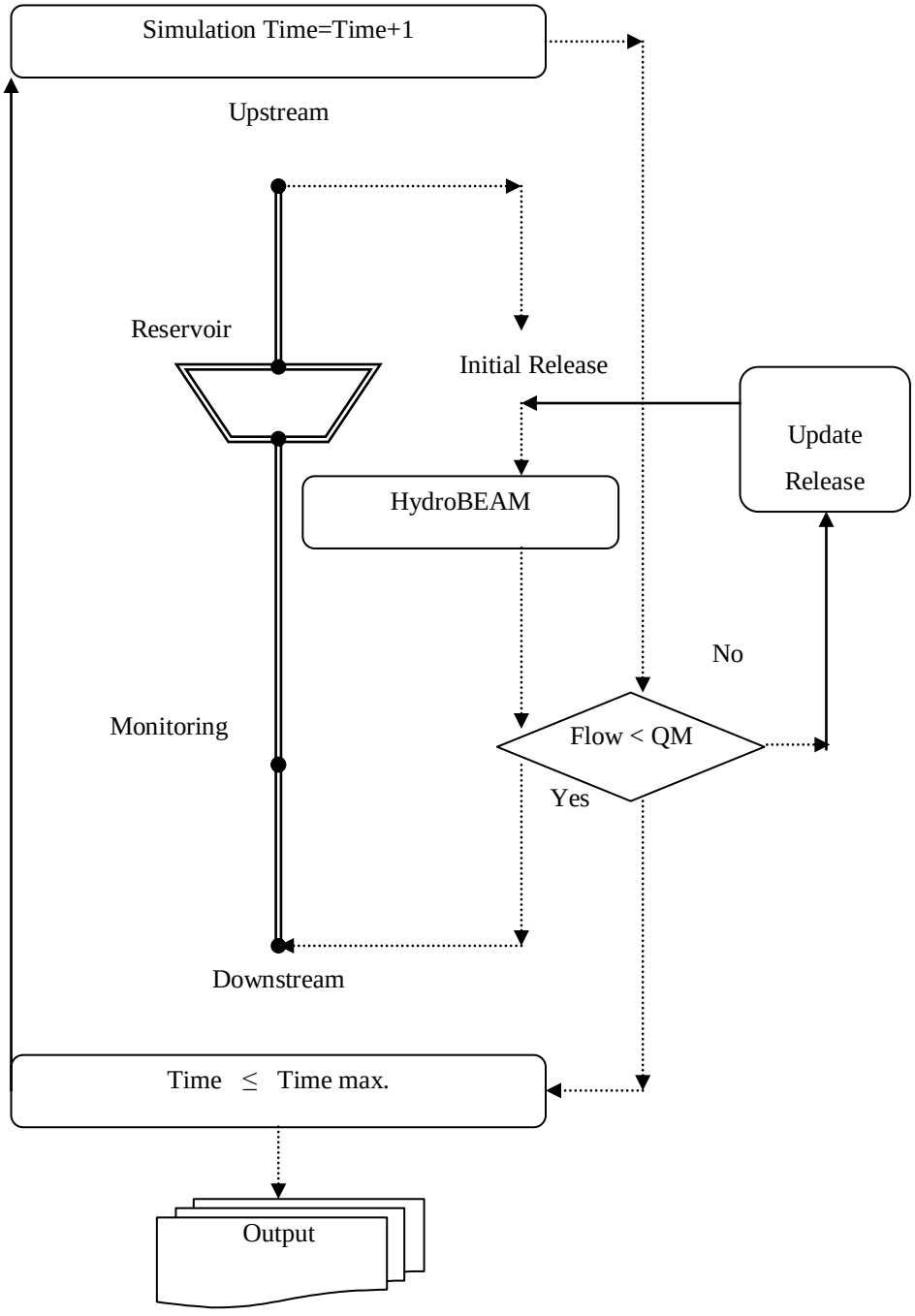

Figure 3.9 Illustration of the iterative method for reservoir flow routing at the Yasu River basin.

Table 3-8 Formulated monthly operation rules for the Yasu dam.

Month	a_1	a_2	a_3	a_4	a_5	a_6
1	0	298.7	-32278	12992	-23820	10400
2	0	2.00E-15	-4.00E-11	4.00E-07	-0.0017	2.689
3	8.00E-18	-3.00E-13	4.00E-09	-2.00E-05	7.83E-02	-1.03E+02
4	0	2.00E-15	-6.00E-11	6.00E-07	-0.0025	4.176
5	0	2.00E-16	-6.00E-12	5.00E-08	-0.0002	0.3352
6	3.00E-19	-7.00E-15	7.00E-11	-4.00E-07	9.00E-04	-9.48E-01
7	0	0.00E+00	2.00E-11	-4.00E-07	0.0029	-6.289
8	1.00E-20	-3.00E-16	2.00E-12	-9.00E-09	2.00E-05	-1.28E-02
9	3.00E-19	-6.00E-15	4.00E-11	-2.00E-07	3.00E-04	-1.81E-01
10	0.00E+00	5.00E-15	-5.00E-11	2.00E-07	-2.00E-04	1.16E-01
11	1.00E-18	-1.00E-13	1.00E-09	-6.00E-06	1.10E-02	-7.48E+00
12	4.00E-19	-7.00E-15	5.00E-11	-2.00E-07	4.00E-04	-2.75E-01

3.5 Spatial and temporal variability of hydrological parameters

The surface and subsurface hydrological parameters vary in space and/or time; this variability causes a significant change in the shape of the river hydrograph. The variability can be caused by the basin characteristics, precipitation, and human utilization of land. Therefore, the watershed is divided into the catchments, each catchement is divided into square grids, and each grid is connected to a drainage network represented by a channel segment. The variability of the hydrological parameters for each grid is integrated, and then each grid is divided into elements of uniform parameters. The number of elements is decided by the surface properties and availability of hydrological data.

In the kinematic wave model soil roughness affects both the speed of runoff and the infiltration rate that affects both the depth of the surface runoff and the groundwater

recharge. Therefore, for each type of soil and land use there is preliminary sets of roughness and infiltration coefficients. These coefficients are evaluated by using a scaling method. The scaling factors are derived by two steps; first is soil sampling from different locations in the watershed. Second is to use the occupation ratio. The rational method for calculating the representative infiltration and roughness coefficients for each grid is shown in Figure 3.10. It shows the soil map based parameterization n_j*, and the land use based parameterization n_j, where n can be a surface hydrological parameter, L_j is the area percentage of the sub- parameter n_j, j is the number of the considered land uses or soils, and AM_i is the area of the i^{th} grid. An example is illustrated by Figure 3.10. An infiltration coefficient for a grid with sandy soil (normalized $n^* \approx 1.0$) and city-typed land use ($n \approx 0.0$) has a value that is not large as if the parameterization is only based on soil map, and is not small as if it is only based on land use map. In other words the two values n and n* represent the limits of the variability domain; therefore the value of infiltration coefficient is selected within this domain. In HydroBEAM the harmonic mean value is selected.

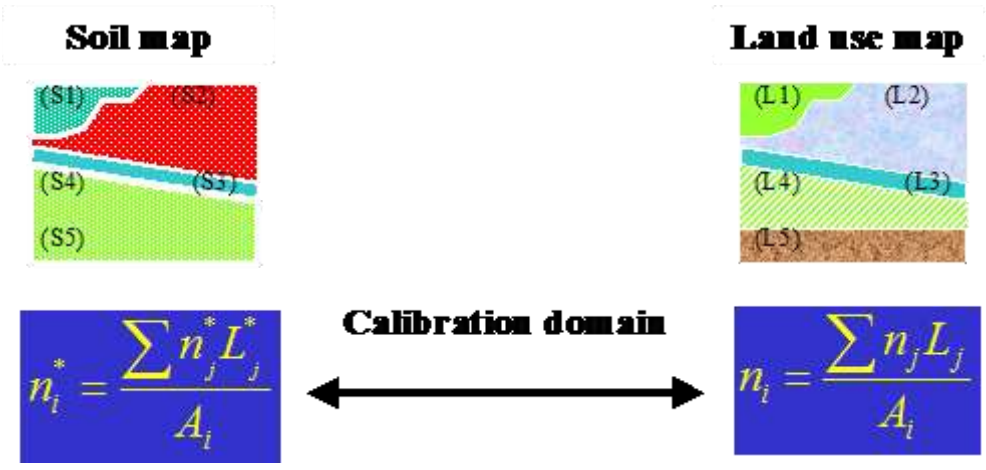

Figure 3.10 Integrated hydrological parameterizations based on distributed soils (S) and land uses.

The changes of land uses within the watershed occur dynamically in space and/or in time. In order to model the hydroclimatic processes in the watershed such as stream flows, evapotranspiration and soil moisture, HydroBEAM allows for an automatic adjustment of the distribution of land uses for each grid. On the other hand the hydrological parameters are also subjected to the same dynamic behavior. This requires that a seasonal parameterization for surface roughness, infiltration, and irrigation amounts have to be prepared to simulate the dynamics of land uses. This behavior of land is related to the residence time of water in the watershed and to the human utilization of land. The land use dynamics approach can be applied for deterministic schemes or stochastic schemes by considering several scenarios of hypothetical changes in land uses.

4 METEOROLOGICAL FORMULATION OF THE ATMOSPHERE

4.1 Introduction

An accurate evaluation of grid hydroclimatic parameters is described for distributed hydrological and meteorological models, because of their spatial and temporal regulation of runoff, and energy fluxes between ground and atmosphere. The approach in this chapter is to construct numerical models that incorporate the essential physics that govern these parameters with very high resolutions. The method presented in this chapter uses the hourly records at a few locations to derive the physical parameters that describe the spatial and temporal variability. For these locations, the derived parameters have been compared with the theoretical parameters, to evaluate whether they accurately represent the hydroclimatic processes. The spatial and temporal vertical temperature, pressure, and wind filed in each grid are calculated. And then the calculated data at an altitude of (2m) is to be used in the heat budget relationship as explained in chapter 2. Also the output data at a point source height is used for simulating the plume rise according to Gaussian plume model. The horizontal and vertical wind speeds and directions are calculated by using the linear interpolation scheme for the horizontal pressure gradients, and the Ekman layer approach. Also an empirical equation to describe the snowfall is derived.

4.2 Distribution of temperature

The atmosphere is heated from each grid. The amount of solar energy received by a grid depends on time of day, seasonality, latitude, altitude and dynamic behaviors of land. The horizontal distribution of temperature is widely varied. Usually the vertical ambient temperature is reasonable assumed to be linear, and the vertical

profile of temperature is calculated by using the lapse rate; it is usually varies between 5 and 8 ^{0}C/km;

$$T_{i,j} = T^*_{i,j} - \Gamma.\Delta z \tag{4.1}$$

where $T_{i,j}$ is the horizontal ambient temperature, $T^*_{i,j}$ is the measured ambient temperature, Γ is the lapse rate, and Δz is the change of altitude above the ground surface. In order to select the best lapse rate value for the distributing horizontal and vertical temperatures at the Yasu River basin. Temperature data form meteorological stations was analyzed in order to identify the correlation coefficient (R^2) among the weather stations as follows:

a) The correlation coefficient between the measured hourly temperatures at Tsuchiyama and Gamo is calculated.
b) The hourly temperature at Tsuchiyama is calculated by substituting the measured hourly temperature at Gamo in E.q. (4.1) with an altitude deference of (175 m).
c) The correlation coefficient between the calculated hourly temperature and the measured one at Tsuchiyama is calculated.
d) The calculations in b) and c) are repeated using another lapse rate value (5 to 8).
e) A representative lapse rate that shows the highest correlation coefficient is selected.
f) The calculation procedure, a) to e), is repeated for another hourly temperature data in another year (1989 to 1998).

Figures 4.1 and 4.2 show the deference between measured hourly temperature and the calculated one at Tsuchiyama based on two different lapse rates respectively. Figure 4.3 shows a sample from the calculation procedure, a) to f), and the calculated

correlation coefficients based on a constant lapse rate throughout each year. The final outputs at f) for twos years are shown in Figure 4.4. A lapse rate of 6.5 can be considered as a representative lapse rate for the analyzed data set, since it shows the highest correlation coefficient.

This kind of analysis is introduced here in order to discuss whether the lapse rate can be considered constant throughout the annual hydrological simulation in HydroBEAM. Even though the use of constant lapse rate throughout the year has shown a high correlation coefficients, the correlation analysis dose not fully account for the spatial and temporal characteristics of the watershed. According to theoretical considerations the calculation of the distributed heat budget at each grid can be used for estimating the ambient temperatures in the lower layer of the atmosphere because the ground mainly heats it. In this case an iterative solution for the governing equations in the heat budget method is required since the ambient temperature at each grid must be identified in advance. The iteration is applied and continued until a certain stopping criterion is satisfied. In HydroBEAM it has to be done for each grid within the watershed which might be a time-consuming process.

Usually, ambient temperature increases during the day and decreases at night, the peak temperature lags behind the daily incoming radiation as shown in Figure 4.5. This lag is caused by the lag in maximum radiation that leaving the earth relative to the maximum daily incoming radiation. The calculation of the net daily radiation, which was explained in chapter 2, shows that the shortwave radiation and the longwave radiation are highly affected by the surface conditions. Therefore, an approach is introduced in this desertion that is based on the analysis of historical data of temperature at different locations and another hydroclimatic process such as precipitation.

Precipitation is selected because of the relationship with the heat budget calculation, and because it is the main process that changes the surface hydrological characteristics and parameters. The relationship between temperature and the occurrence of precipitation is not handled by many researchers since the temperature accounts for a minor factor when it is compared with the oceans, which is a major humidity source. As a result precipitation is used in order to identify seasonality.

Figure 4.6 shows that there is a relationship between the optimum lapse rate and seasonality, which is characterized by wet and dry conditions respectively. Figure 4.7 shows the impact of seasonality-based lapse rate on the correlation between calculated and observed temperatures, for dry condition the lapse rate takes the value of (6.5) and for wet condition it takes the value of (8).

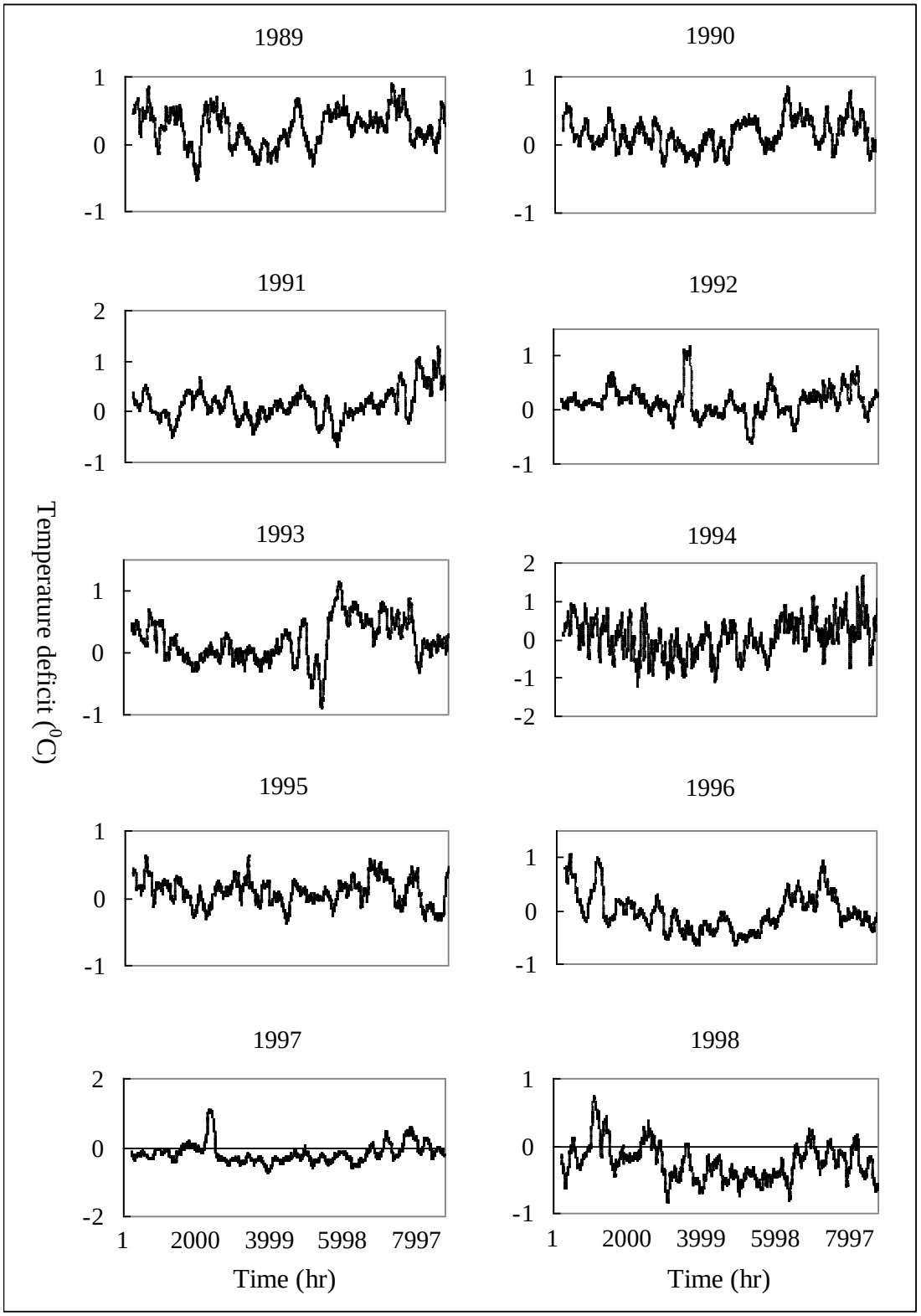

Figure 4.1 Lapse rate adjustment at Tsuchiyama weather station (6.5 ^{0}C/km)

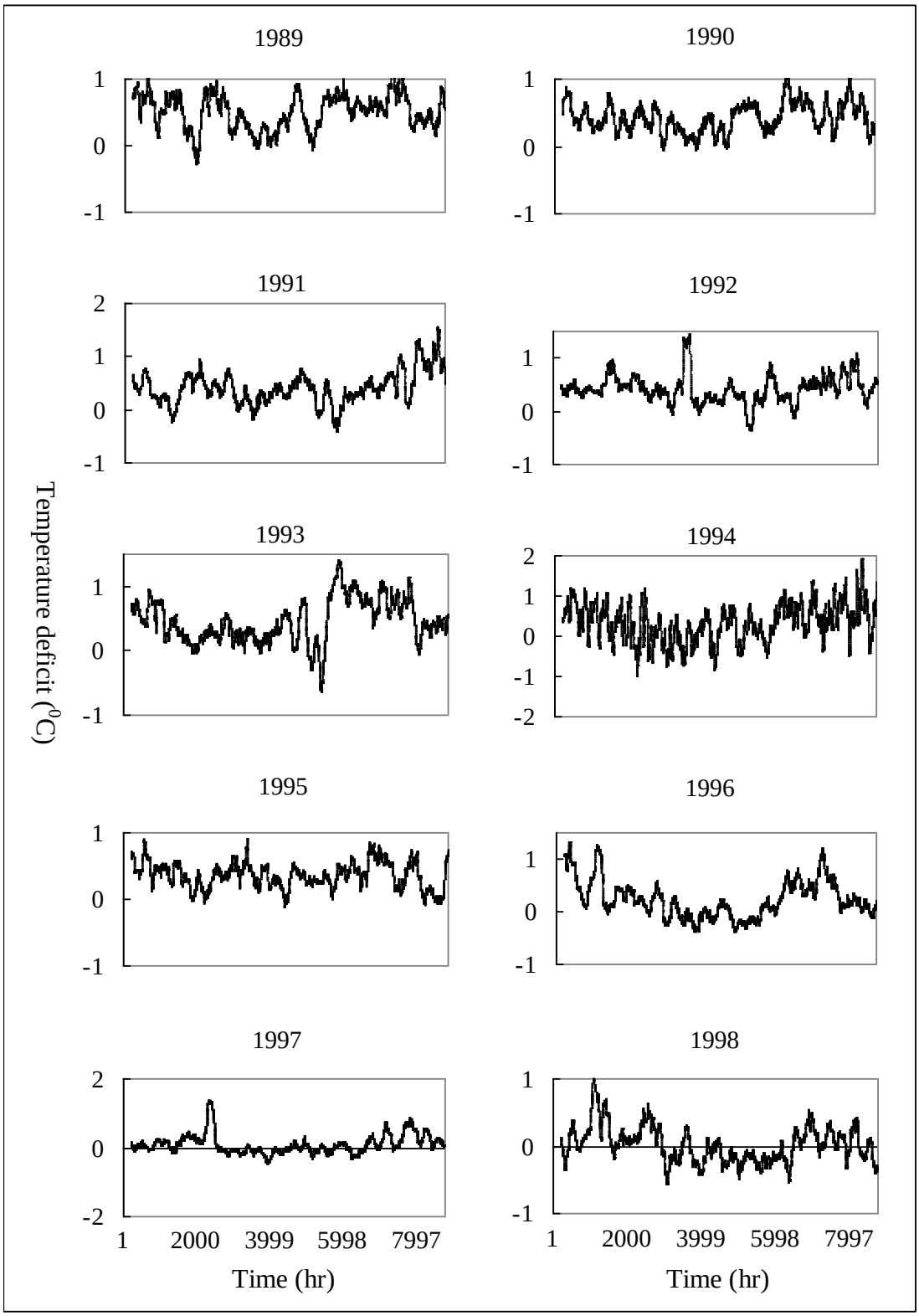

Figure 4.2 Lapse rate adjustment at Tsuchiyama weather station (8.0 ^{0}C/km).

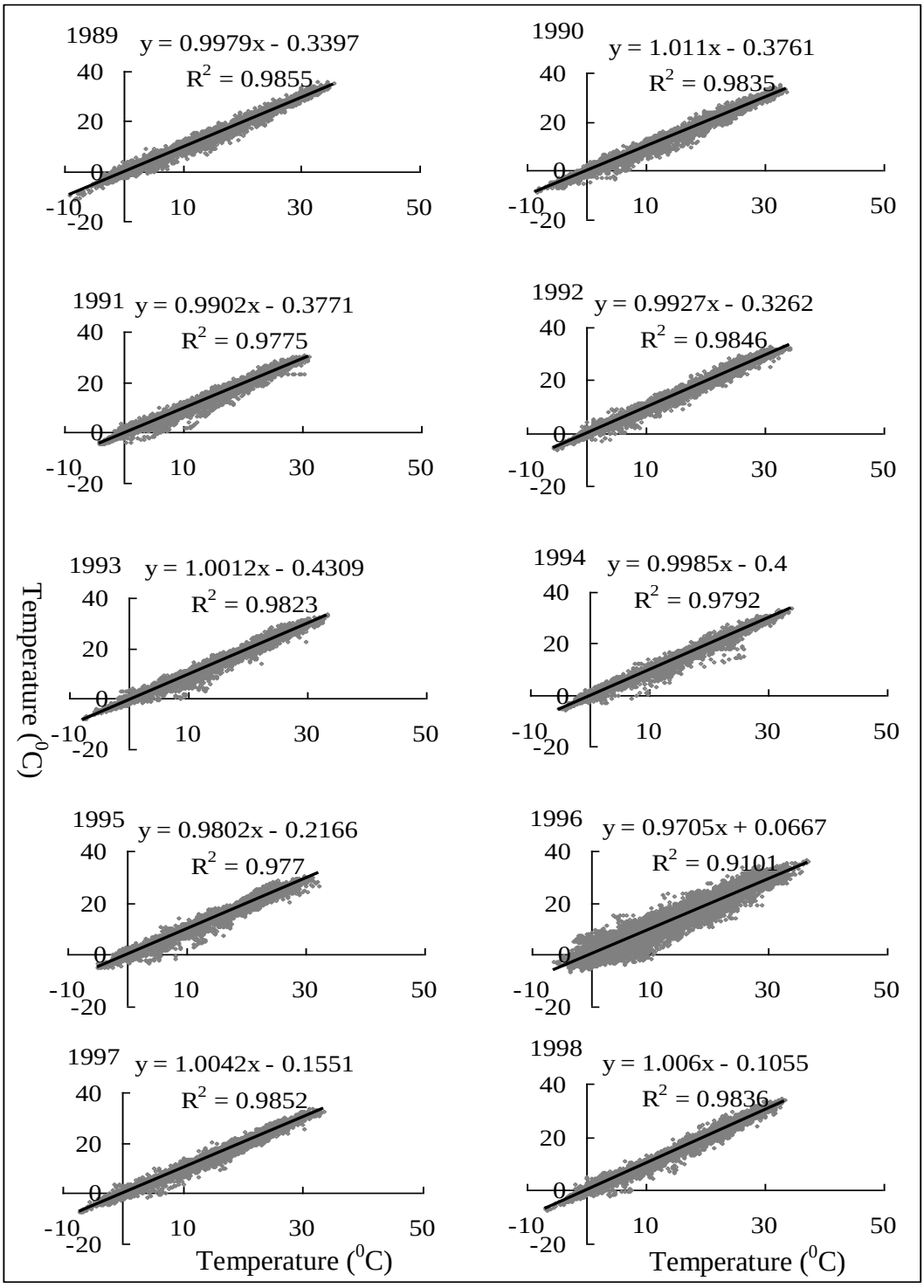

Figure 4.3 Correlations between observed and measured temperatures at Tsuchiyama weather station (Lapse rate: 6.5 ^{0}C/km).

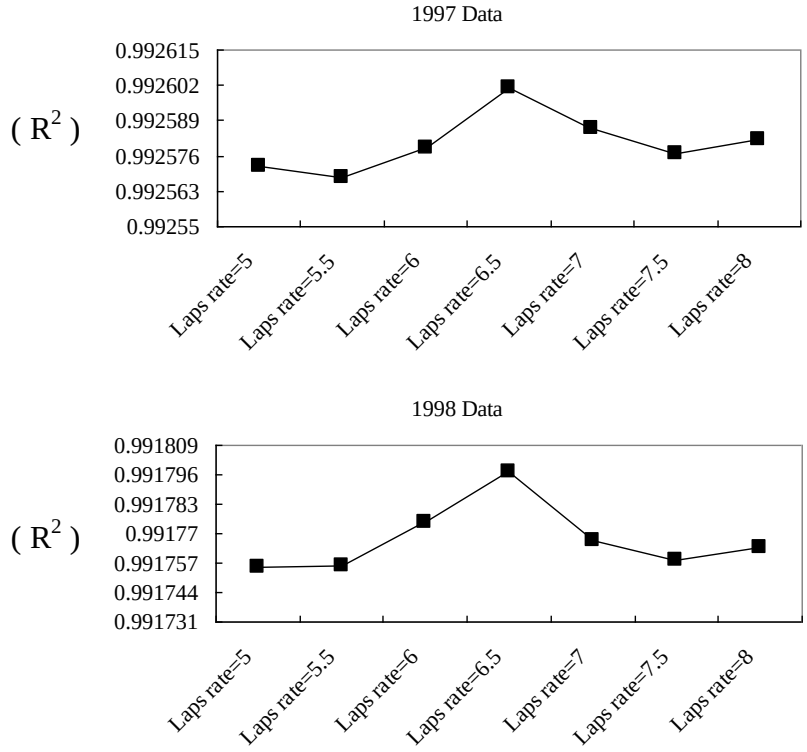

Figure 4.4 Correlation coefficients at Tsuchiyama considering different lapse rates.

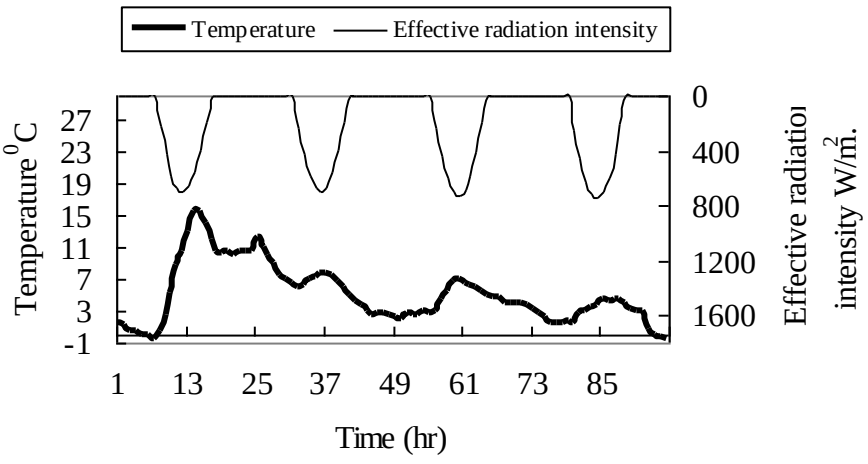

Figure 4.5 Peak periods of measured hourly ambient temperature and effective radiation intensity.

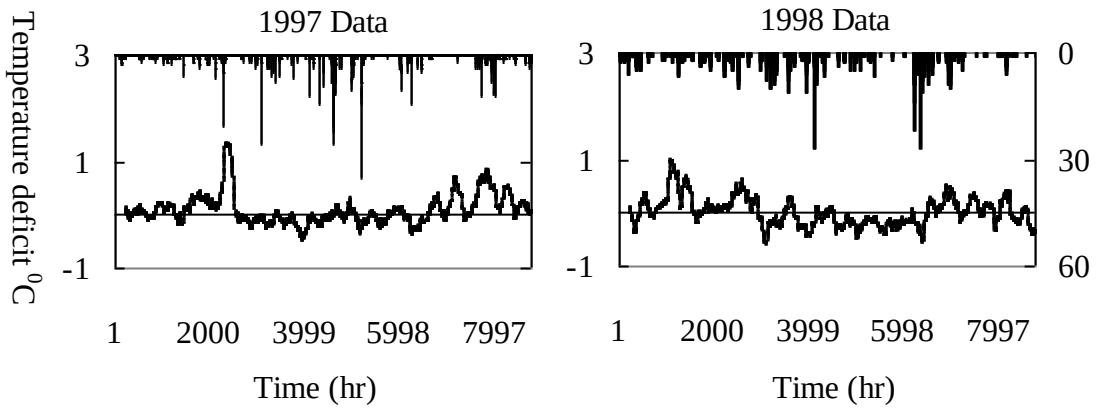

Figure 4.5 Relationship between the impact of rainfall intensity (mm) on the difference between measured and calculated temperatures based on constant lapse rate.

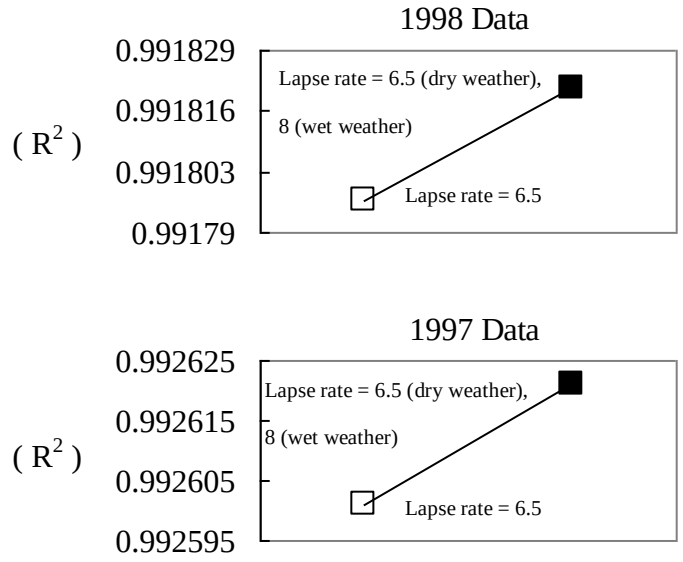

Figure 4.6 The impact of seasonality-based lapse rate on the correlation between calculated and observed temperatures.

4.3 Distribution of Pressure

The distribution of air pressure is obtained by assuming that the atmosphere layers are in hydrostatic condition and considered as an ideal gas. The distribution of the vertical and horizontal air pressures at a grid is derived as follows,

$$
\begin{aligned}
&dP_{i,j} = -\rho g dz \\
&\rho = \frac{RT_{i,j}}{P_{i,j}} \\
&dP_{i,j} = -\frac{P_{i,j}}{RT_{i,j}} g dz \\
&dz = -\frac{dT_{i,j}}{\Gamma} \\
&\frac{dP_{i,j}}{P_{i,j}} = \frac{g}{R\Gamma}\frac{dT_{i,j}}{T} \\
&P_{i,j} = P^*_{i,j}\left(\frac{T_{i,j}}{T^*_{i,j}}\right)^{\frac{g}{R\Gamma}}
\end{aligned}
\tag{4.2}
$$

where P is the spatial and temporal air pressure, T is the spatial and temporal ambient temperature, * refers to measured values, i is the grid number, j is the time step, R is the dry air gas constant, and g is the gravitational acceleration. The derivation of Eq. (4.2) is based on the assumption of constant lapse rate, however the use of a seasonal lapse rate is more reliable, which was shown in the previous section, but it doesn't affect much the related daily simulation of hydrological processes. Then the distributed pressure and temperature are used to calculate the distributed air density using Eq. (2.15). Figure 4.7 and Figure 4.8 show the distribution of the hourly ambient temperature and pressure in the Yasu River basin respectively.

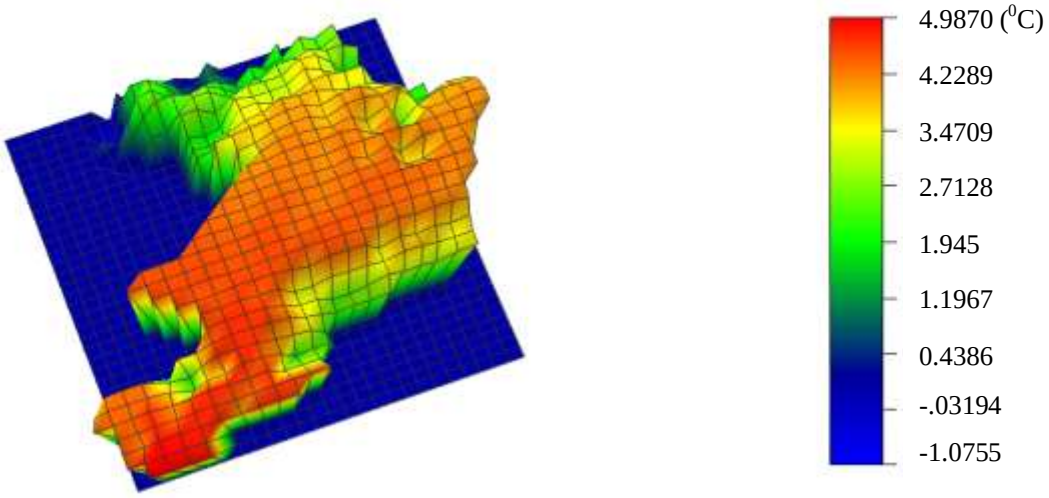

Figure 4.7 Distribution of the ambient temperature at the Yasu River basin. (1997/01/01, time: 00 hr).

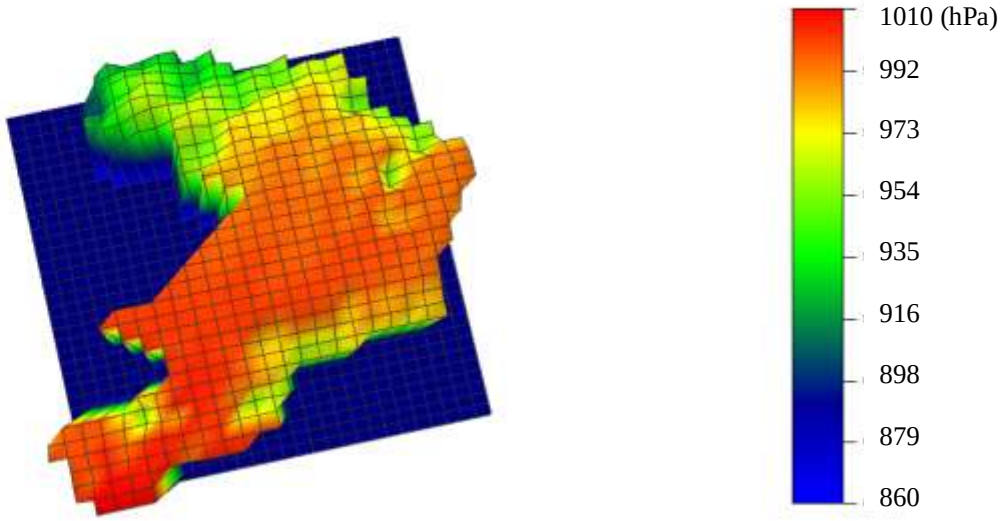

Figure 4.8 Distribution of the air pressure at the Yasu River basin. (1997/01/01, time: 00 hr).

4.4 Distributed wind field

There are many theoretical and numerical models have been developed for generating wind fields. In large scales the variation of wind velocity in the horizontal flow direction is small, but it is not the same for small scales. In the case of a distributed hydrological model, wind velocity is observed at randomly spaced meteorological stations within the watershed, and then an interpolation scheme is applied in order to estimate the wind field at each grid. This technique is based on averaging the wind velocities from distributed meteorological stations. Wind field is needed for calculating of the turbulent flux terms in the heat budget equation, and for calculating the concentration of air pollutants, *C*, in the equation of diffusion,

$$\frac{\partial C}{\partial t}+u\frac{\partial C}{\partial x}+\upsilon\frac{\partial C}{\partial y}+w\frac{\partial C}{\partial z}=K_x\frac{\partial^2 C}{\partial x^2}+K_y\frac{\partial^2 C}{\partial y^2}+K_z\frac{\partial^2 C}{\partial z^2} \tag{4.4}$$

where *u*, *υ*, and *w* are the components of the wind velocity, *K* is the diffusion coefficient. The solution for Eq. (4.4) can be approximated by using the Gaussian plume model if the Cartesian coordinate is replaced by new coordinate that is defined in terms of the wind velocity vector as follows,

$$\xi=\frac{\Phi(x,y)}{\sqrt{u^2+\upsilon^2}},\qquad \eta=\frac{\Psi(x,y)}{\sqrt{u^2+\upsilon^2}} \tag{4.5}$$

where Φ is the potential velocity, and Ψ is the stream function. Substituting of Eq. (4.5) into the homogenous and the two dimensional form of Eq. (4.4) gives,

$$\sqrt{u^2+\upsilon^2}\frac{\partial C}{\partial \xi}=K\left(\frac{\partial^2 C}{\partial \xi^2}+\frac{\partial^2 C}{\partial \eta^2}\right) \tag{4.6}$$

According to Gaussian plume model the solution of Eq. (4.6) is given by,

$$C(\xi,\eta)=\frac{Q}{\pi\sigma_\eta\sigma_z}\exp\left(-\frac{\eta^2}{2\sigma_\eta^2}-\frac{H^2}{2\sigma_z^2}\right) \tag{4.7}$$

where Q is the emission rate from a point source, and H is the effective height of a point source. The calculation procedure of H is illustrated in Appendix C.

The continuity equation can be applied in order to eliminate the divergence between successive grids as given by (Hiroh et al., 1992),

$$\frac{\partial h}{\partial t}+\frac{\partial(uh)}{\partial x}+\frac{\partial(vh)}{\partial y}=0 \tag{4.8}$$

where h is the inversion height, u and υ are the horizontal components of the wind velocity. The steady state form of Eq. (4.8) is solved numerically by an iterative method. The iteration is done in order to minimize the divergence between two grids that is caused by the change of topography. At a grid point (i,j), the finite difference approximation of Eq. (4.8) is given by,

$$D_{i,j}^{n}=\frac{\left(u_{i+1,j}^{n}h_{i+1,j}-u_{i-1,j}^{n}h_{i-1,j}\right)}{2\Delta x}+\frac{\left(\upsilon_{i,j+1}^{n}h_{i,j+1}-\upsilon_{i,j-1}^{n}h_{i,j-1}\right)}{2\Delta y} \tag{4.9}$$

where D is the divergence of the wind field, and n is the nth iteration. The velocity adjustments U and V,

$$\begin{aligned}
u_{i+1,j}^{n+1}&=u_{i+1,j}^{n}+s_{i+1,j}U_{i+1,j}^{n}h_{i+1,j}\\
u_{i-1,j}^{n+1}&=u_{i-1,j}^{n}+s_{i-1,j}U_{i-1,j}^{n}h_{i-1,j}\\
\upsilon_{i,j+1}^{n+1}&=\upsilon_{i,j+1}^{n}+s_{i,j+1}V_{i,j+1}^{n}h_{i,j+1}\\
\upsilon_{i,j-1}^{n+1}&=\upsilon_{i,j-1}^{n}+s_{i,j-1}V_{i,j-1}^{n}h_{i,j-1}
\end{aligned} \tag{4.10}$$

where s has a value of zero except for a grid, where there is no weather station, and a unity for other grids. Substitution of Eq. (4.10) into Eq. (4.9) yields

$$\frac{\left(s_{i+1,j}+s_{i-1,j}\right)U_{i,j}^{n}}{2\Delta x}+\frac{\left(s_{i,j+1}+s_{i,j-1}\right)V_{i,j}^{n}}{2\Delta y}+D_{i,j}^{n}=0 \tag{4.11}$$

The two terms in Eq. (4.11) are assumed to contribute equally to the divergence,

$$U_{i,j}^{n} = -D_{i,j}^{n} \frac{\Delta x}{\left(s_{i+1,j} + s_{i-1,j}\right)}$$
$$V_{i,j}^{n} = -D_{i,j}^{n} \frac{\Delta y}{\left(s_{i,j} + 1 + s_{i,j-1}\right)} \qquad (4.12)$$

The initial values of wind velocity in each grid, u^0 and v^0, are approximated using an empirical interpolation equation,

$$u_{i,j}^{0} = \frac{\sum_k u_k / r_k^2}{\sum_k 1/r_k^2}, \qquad \upsilon_{i,j}^{0} = \frac{\sum_k \upsilon_k / r_k^2}{\sum_k 1/r_k^2} \qquad (4.13)$$

Then, wind field is generated by using the approach that is based on the developed distributed pressures at each grid. The boundary and initial conditions in this approach are not only evaluated from the measured wind velocity from distributed weather stations, but also from large-scale output data from other atmosphere models. The output from the mesoscale model has a spatial resolution of 20 km and a time step of 6 hours. Then wind velocity is calculated by using the distribution of horizontal pressure gradients and then routed within the boundaries of the watershed. The wind flows from a higher pressure-grid to the least pressure-grid from the nearest neighboring grids as shown in Figure 4.9.

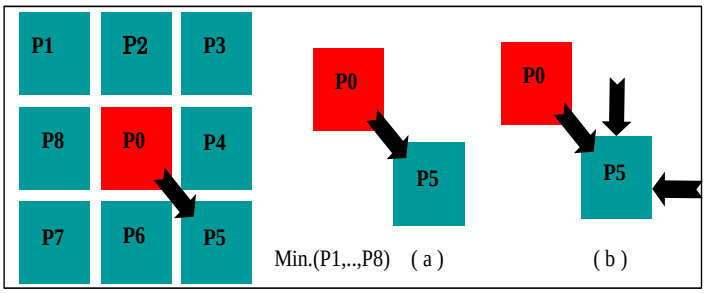

Figure 4.9 Wind velocity routing algorithm, (a) 8-dierections based routing, (b) the case of sink-grid.

The distributed wind vectors are substituted in Eq. (4.9) and modified by using the Eq. (4.10) to Eq. (4.12). Figure 4.10 shows the different approaches for generating the wind field in the case of the Yasu River basin.

The drawbacks of using the air pressure gradient-based approach for generating the wind filed for a river basin are,

a) The horizontal distribution of atmospheric pressure is based on the assumption of hydrostatic conditions, which means that the resulted pressure gradient is resulted form the deference in topography.
b) The iteration method in Eq. (4.11) doesn't guarantee a unique solution for the continuity equation, Eq. (4.9).
c) The vertical profile of the wind velocity doesn't consider the change in direction.
d) It depends on the number of weather stations, in the case of large number the divergence is eliminated easily, but in the case of small number of stations the method might be inefficient.

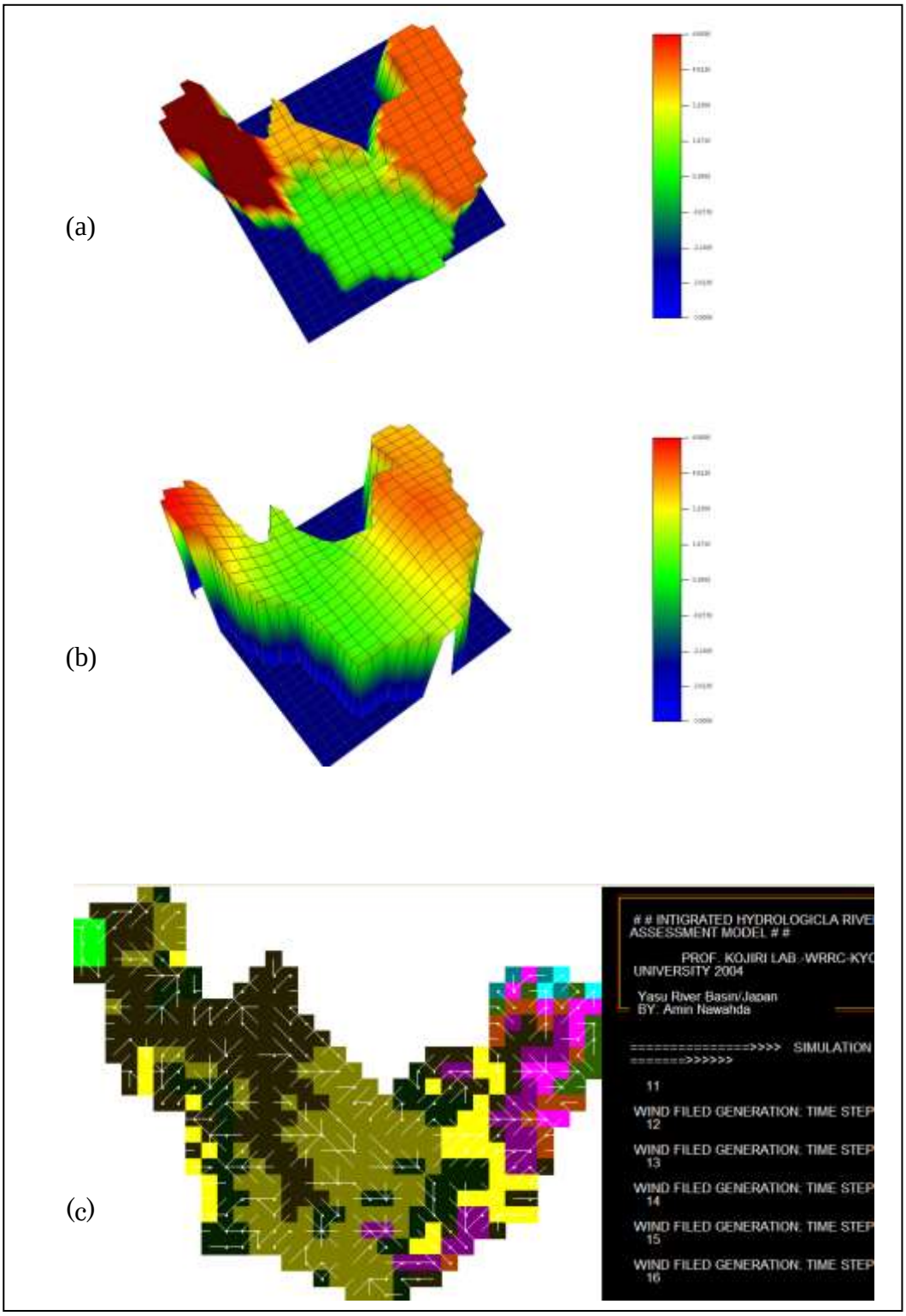

Figure 4.10 (a) Wind field based on Thiessen method, (b) Wind field based on Eq. (4.13), (c) Grid-to-grid wind field network.

In order to overcome the drawbacks of the distributed pressure-based method, the Ekman boundary layer can be used in order to approximate the wind vector profile at each grid based on a data-driven approach, and by considering the physical characteristics of the atmosphere near the surface of the ground. The wind field is simulated at every time step within the distributed hydrological model.

The wind velocity, which is observed at the ground level, is distributed in the vertical direction by using the Ekman boundary layer approach, which is based on the balance among coriolis, pressure gradient and frictional forces, within the transition layer that ranges from 100 m to several kilometers or more, Pielke (1984). Above the surface layer the mean wind changes direction with height and approaches the free-stream velocity, geostrophic wind, at the top of the transition layer. The mass balance equation can be rewritten as,

$$\begin{aligned} 0 &= \frac{1}{\rho_\circ}\frac{\partial}{\partial z}\rho_\circ \overline{w''u''} - \alpha_\circ \frac{\partial P_\circ}{\partial x} + f\upsilon \\ 0 &= \frac{1}{\rho_\circ}\frac{\partial}{\partial z}\rho_\circ \overline{w''\upsilon''} - \alpha_\circ \frac{\partial P_\circ}{\partial y} - fu \end{aligned} \tag{4.14}$$

where f is the coriolis force. The subgrid flux terms are approximated with a constant exchange coefficient K_E. And then Eq. (4.14) can be written in terms of the geostrophic wind components, υ_g and u_g ,

$$\begin{aligned} 0 &= K_E \frac{\partial^2 u}{\partial z^2} + f(\upsilon - \upsilon_g) \\ 0 &= K_E \frac{\partial^2 \upsilon}{\partial z^2} + f(u_g - u) \end{aligned} \tag{4.15}$$

The geostrophic wind components are given by,

$$f\upsilon_g = \frac{1}{\rho_g}\frac{\partial P_g}{\partial x}, \qquad fu_g = -\frac{1}{\rho_g}\frac{\partial P_g}{\partial y}, \tag{4.16}$$

where ρ_g is the air density at the top of the transition layer, and P_g is the atmosphere pressure at same altitude. ρ_g is calculated using the ideal gas equation. The horizontal pressure gradients in Eq. (4.16) are estimated by using the linear interpolation method as illustrated by the following steps,

a) Identifying the location of three additional weather stations as shown in Figure 4.11.

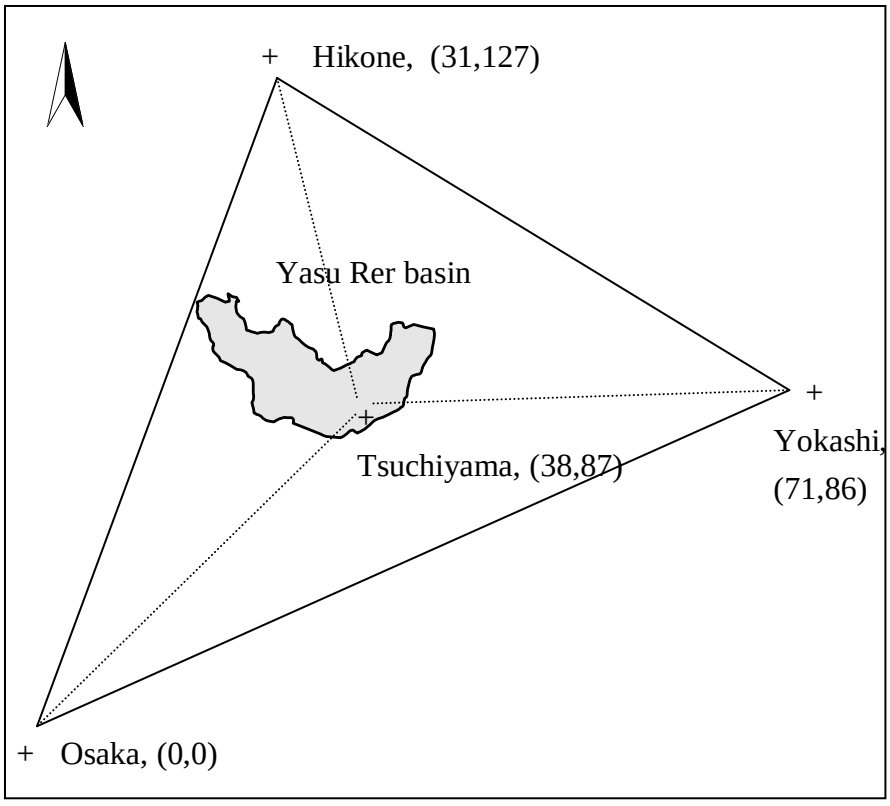

Figure 4.11 The locations of the weather stations around the Yasu River basin, coordinates are in kilometers.

b) Calculating the vertical temperature and pressures profiles up to several kilometers above the ground surface at the surrounding weather stations by using Eq. (4.2).

c) The horizontal pressure gradients in Tsuchiyama at any altitude, *z*, is derived as follows,

The pressure in Tsuchiyama, $P(x,y,z)$ can be interpolated from the three surrounding weather stations using the following relationship,

$$
\begin{aligned}
&P(x,y,z) = \sum_{k=1}^{3} L_k P(x_k, y_k, z_k) \\
&L_k = \frac{1}{D}(a_k + b_k x + c_k y) \\
&D = \begin{bmatrix} 1 & x_1 & y_1 \\ 1 & x_2 & y_2 \\ 1 & x_3 & y_3 \end{bmatrix} \\
&a_1 = x_2 y_3 - x_3 y_2, \quad b_1 = y_2 - y_3, \quad c_1 = x_3 - x_2 \\
&a_2 = x_3 y_1 - x_1 y_3, \quad b_1 = y_3 - y_1, \quad c_1 = x_1 - x_3 \\
&a_3 = x_1 y_2 - x_2 y_1, \quad b_1 = y_1 - y_2, \quad c_1 = x_2 - x_1
\end{aligned}
\tag{4.17}
$$

where D is the determinant of the array, and L is the area of a sub-triangle that can be drawn from the location of a weather station inside the river basin and the locations of two reference weather stations that are located outside the river basin as shown in Figure 4.11.

The horizontal pressure gradients can be calculated by taking the derivatives of the pressure from Eq. (4.17) or,

$$
\begin{aligned}
&\frac{\partial P(x,y,z)}{\partial x} = \sum_{k=1}^{3} \frac{\partial L_k}{\partial x} P(x_k, y_k, z_k), \\
&\frac{\partial P(x,y,z)}{\partial y} = \sum_{k=1}^{3} \frac{\partial L_k}{\partial y} P(x_k, y_k, z_k) \\
&\frac{\partial L_k}{\partial x} = \frac{b_k}{D}, \quad \frac{\partial L_k}{\partial y} = \frac{c_k}{D}
\end{aligned}
\tag{4.18}
$$

d) The components of the geostrophic velocity are calculated by using Eq. (4.16) at deferent altitudes within the transition layer. The calculation stops when the divergence between successive geostrophic velocities is small. The analytical solution for Eq. 4.19 is given by,

$$u(z) = u_g\left(1 - e^{\frac{-z}{\Delta}}\cos\left(\frac{z}{\Delta}\right)\right)$$
$$\upsilon(z) = u_g e^{\frac{-z}{\Delta}}\sin\left(\frac{z}{\Delta}\right), \qquad \Delta = \sqrt{\frac{2K_E}{f}} \tag{4.19}$$

where z is the height above the ground surface. If the value of K_E is assumed 10 m/s^2 then, the vertical profile of the wind velocity at various altitudes can be illustrated by Figure 4.12.

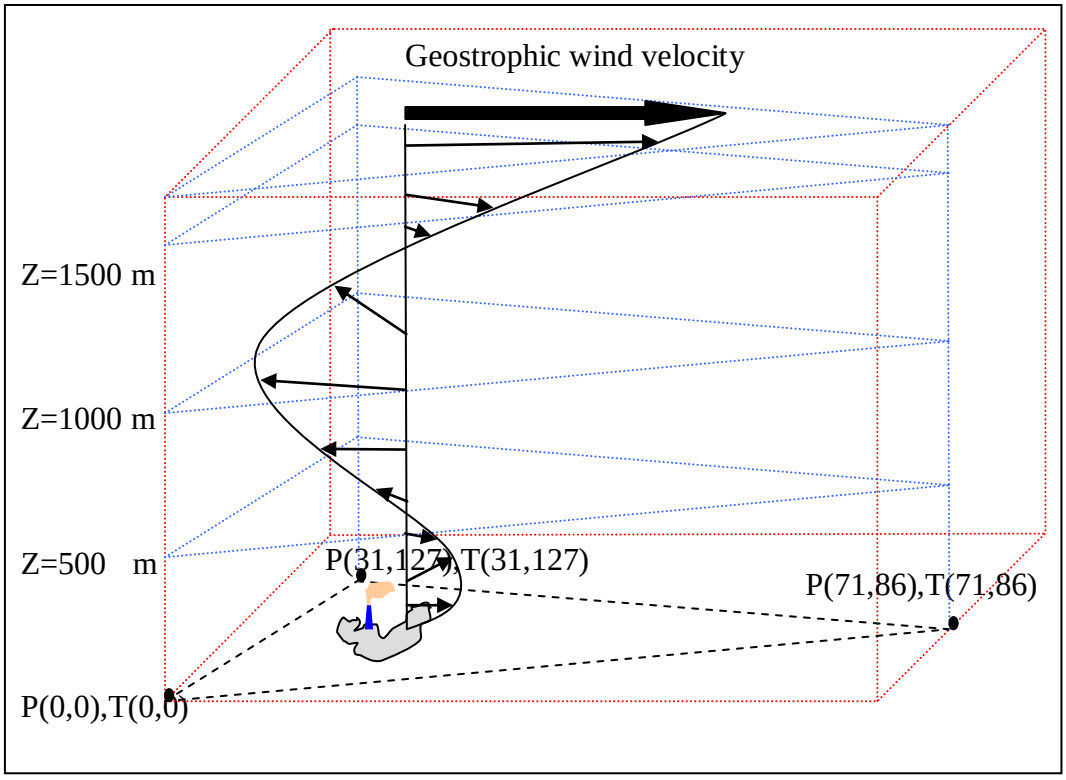

Figure 4.12 A plot of the vertical profile of the Ekman wind velocity.

The value of K_E can be estimated by substituting the measured wind velocity, which is taken form the weather stations inside the river basin at 10 m height, and apply the following formulas,

$$f = 2\Omega\sin(\Phi_s), \qquad Tsuchiyama: \Phi_s = 35^\circ$$
$$= 2\times 7.292\times 10^{-5}\times\sin(35^\circ) = 8.365\times 10^{-5}$$
$$1-\frac{u(z)}{u_g} = e^{\frac{-z}{\sqrt{2K_E/f}}}\cos\left(\frac{z}{\sqrt{2K_E/f}}\right)$$
$$z=10 \Rightarrow \cos\left(\frac{10}{\sqrt{2K_E/f}}\right)\approx 1 \Rightarrow \ln\left(1-\frac{u(z)}{u_g}\right) = \frac{-z}{\sqrt{2K_E^0/f}}$$
$$K_E^0 = \frac{fz^2}{2\left(\ln\left(1-\frac{u(z)}{u_g}\right)\right)^2}$$
$$K_{E(z=10)}^0 = \frac{8.365\times 10^{-5}\times(-10)^2}{2\left(\ln\left(1-\frac{u(10)}{u_g}\right)\right)^2}$$
$$\frac{\upsilon(10)}{u_g} = e^{\frac{-10}{\sqrt{2K_E/8.365\times 10^{-5}}}}\sin\left(\frac{10}{\sqrt{2K_E/8.365\times 10^{-5}}}\right)$$
$$\frac{\upsilon(10)}{u_g} - e^{\frac{-10}{\sqrt{2K_E/8.365\times 10^{-5}}}}\sin\left(\frac{10}{\sqrt{2K_E/8.365\times 10^{-5}}}\right) = \varepsilon \qquad (4.20)$$

where ε is a very small number that approaches zero, and K^0_E is the constant exchange coefficient that is calculated by simplifying the equation of $u(z)$, Eq. (4.19), this value is considered as an initial guess for the last iterative equation in Eq.(4.20). The stopping criteria are; a very small ε, and the deference between K_E and K^0_E is minimum.

If there is more than weather station in the river basin the same procedure is repeated, this results in another value for K_E. Therefore, an average value of K_E can be considered as a representative value for any location within the river basin. Also at a point source the vertical wind velocity profile can be identified, and then Gaussian plume model can be applied.

4.5 Distributed potential precipitable water

The distributed potential precipitable water in a grid can be estimated if the distribution of moisture is identified within the spatial and vertical dimensions. In the case of a hydrostatic distribution of pressure the potential precipitable water is given by,

$$w_p = \frac{0.622}{g} \int_{p}^{p_0} e \frac{dP}{P} \tag{4.21}$$

The above equation gives an exaggerated amount of precipitation since it assumes that all the moisture is condensed and then precipitates. However since there are other necessary conditions for initiating precipitation which is not covered in this dissertation, the calculated amount is weighted by a coefficient τ, in order to be close to the gauged precipitation,

$$\text{Rainfall} = \tau \cdot w_p \tag{4.22}$$

The occurrence of snowfall in a grid is examined; the relationship between ambient temperature and vapor pressure has been derived from snowfall data,

$$\rho = \frac{e}{RT}, \tag{4.23}$$
$$\text{Pricipitation} \Rightarrow \textit{Snowfall} \Leftrightarrow \text{density lower limit} \le \rho < \text{density lower limit}$$

Figure 4.13 depicts sample of the precipitation data that has been used for the derivation of Eq. (4.23).

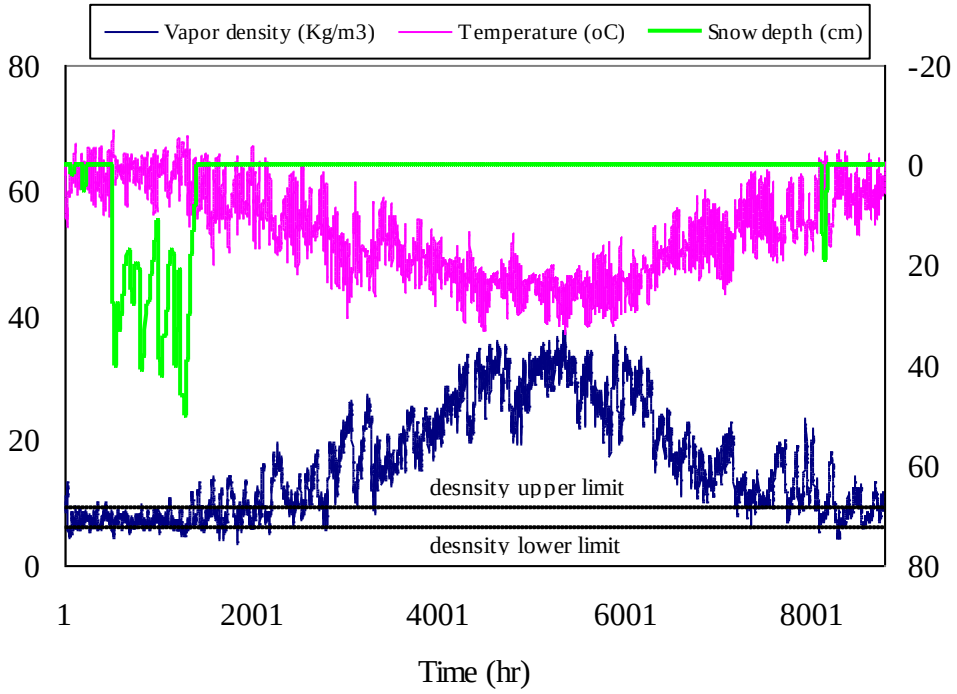

Figure 4.13 Snowfall occurrence based on density upper and lower limits, (5-9 kg/m^3).

5 WATER QUALITY MODELING

5.1 Introduction

The water related pollution sources are yearly increasing due to exploding urbanization and extensive use of detergents and chemicals in agricultural and industrial production. The degradation of water quality can be easily figured out in many places all over the world. Therefore a reliable understanding of the chemical fate of pollutants is required for the environmental impact assessment. This study presents an approach to extend the pollutant transport for the distributed chemical transformations products of a parent compound. First the residence time in a steady state scenario and the lifetime in a pulse scenario are compared with respect to their mathematical formulations and with respect to their spatial and temporal concentrations functions are calculated. Second it is shown how to modify the transient hydrological model in order to include the parameterization of transformations products.

Recently most of the pollutant transport studies consider the mineralization of degraded pollutants without considering the transformation products, even though those products can be more toxic, more soluble, more persistent, or more bioaccumulated than the parent compound. In order to encounter the delay in formation of transformation products two persisting measures are used the joint persistence and secondary persistence (Fenner et al., 2000). There are many obstacle in considering the transformation compounds because many of those compound are poorly characterized, and most of the recent research consider the conceptual modeling for the assessment of the transformation kinetics, also, the setting of the boundary condition of the model illustrate some of the unique problems for simulating the interactions between hydrological layers while the contribution of neighboring areas is hardly evaluated.

HydroBEAM is used to provide detailed simulation of the spatial and temporal runoff including soil moisture simulations. The simulation of surface runoff quality is based on assumptions related to pollutant accumulation and transport process. These assumptions are: (1) the spatial and temporal pollutant concentration depends on the distributed runoff and the initial concentration of pollutant available for removal; (2) pollutant transformations due to chemical changes or biological degradation during the runoff process is considered, and (3) the amount of pollutants percolating into the soil by infiltration are significant. The distributed concentration of pollutant is estimated based on land use types and population in each grid.

Nonylphenol (NP) is selected as a case study in order to illustrate the methodology in this study, because it has been detected by many researchers in surfactant groundwater, sediment, aquatic organisms, wastewater effluent, air, and human food. (NP) differs from other persistence synthetic organic compounds such as: (PCBs), (DDT), and (PAHs) because it is not released directly into the environment, but it results from the anaerobic degradation of widely used nonionic surfactants, NPEO, which are neither toxic nor have an estrogenic effects, it is typically used in domestic liquid Landry detergents and used in cleaners (Porter *et al.*, 2001).

5.2 Pollutant transport

The compartmental ("well-mixed" media) model of environmental fate and transport are used in order to describe the entry, movement, and spatial and temporal concentration of pollutants within the watershed. It is assumed each the watershed consists of a number of well-mixed subcompartements. The dimensions of each compartment depend on the distributed meteorological and hydrological characteristics of each grid, as well as the definition and quantification of the phase-transfer processes

between the phases are the same as those introduced by Scheringer (1996). Biotic and abiotic first order degradation processes have been considered; which are donated by K_i in each phase i. Advective and diffusive transfer between the phases are donated by U_{ik}, where the sequence i-k means the transfer from i phase to phase k .The following general form of the chemical balance equation, which takes into account all the degradations and interphase transfer processes in the compartments with volumes v_i and v_k, it considers each of the chemical species (x_i) in the model system (Finner, 2000);

$$\frac{dC_i^{x_1}(t)}{dt} = -K_i^{x_1} C_i^{x_1}(t) - \sum_k U_{ik}^{x_1} C_i^{x_1}(t) + \sum_k \frac{v_k}{v_i} U_{ki}^{x_1} C_k^{x_1}(t) + \sum_k \theta_i^{x_1 x_2} K_i^{x_1}(t) \quad (5.1)$$

where the first term on the right-hand side of Eq. (5.1) represents degradation, the second term describes transfer between compartments, and the last term is the transfer form other compartments to the considered compartment. This equation is formulated for each compound x_i. Figure A.3 and Figure A.4, Appendix A, show the spatial distribution of wastewater, COD, T-P, and T-N at the Yasu River basin.

5.3 Transformation product of the Nonylphyenol Ethoxylate

The main source of the Nonylphyenol Ethoxylate (NPE) is the wastewater, which is released from wastewater treatment plants. Wastewater treatment can be techniques can be based on aerobic conditions, anaerobic conditions and combination of aerobic and anaerobic conditions. Figure 5.1 shows the way that wastewater in the Yasu River basin is treated, and the reuse of the sludge from the activated sludge champers.

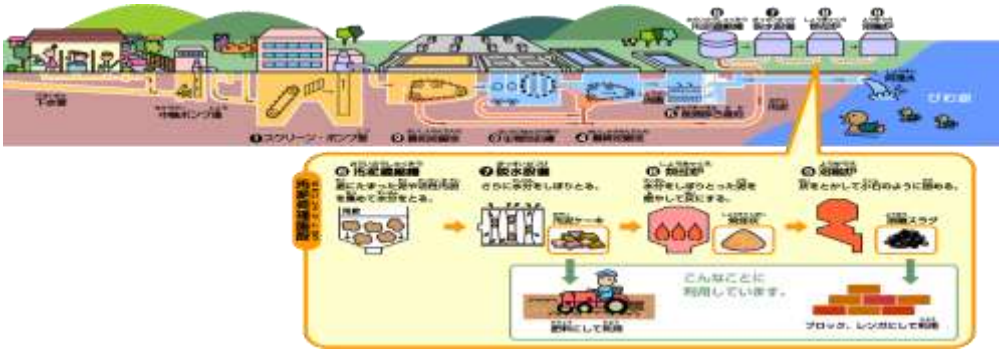

Figure 5.1 Wastewater treatment at the Yasu River basin. 1)screening and pumping; 2)primary settling; 3)recycling in activated sludge champers; 4)final settling; 5)filtration and discharge; 6)dewatering; 7)compacting and reuse in agriculture; 8)further dewatering; 9)casting and block making.(Source: Shiganogesui).

Figure 5.2 shows the degradation of long-chain NPE during wastewater treatment. It was found that 45% of the NPE are still found in the secondary effluents and digested sewage. This percentage is then transformed to one of the possible transformation directions as shown in Figure 5.2.

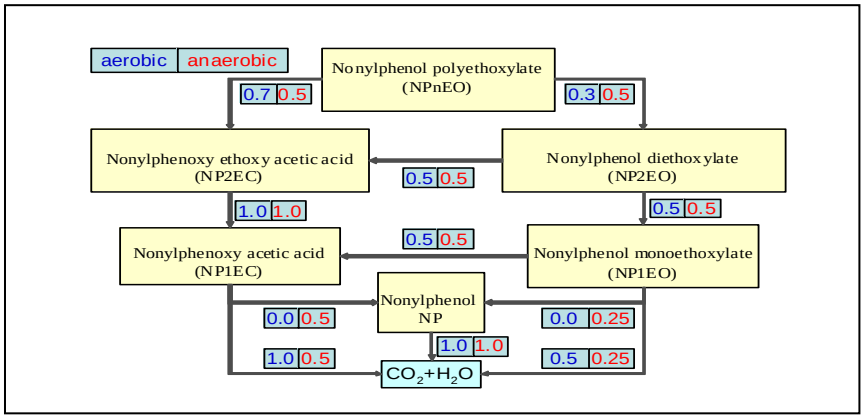

Figure 5.2 Simplified transformation schemes of NPnEO in wastewater treatment plants and in natural environments.

The half-lives data of NPnEO and its transformation products are listed in Table 5.1. They are persistence, toxic to aquatic organisms, and a potential endocrine disruptor.

Table 5-1 Half-lives of NPnEO and its transformation products.

Constant	NPnEO (A)	NP2EC (B)	NPIEC (C)	NP2EO (D)	NPIEO (E)	NP (F)
Half-life in soil (d)	51.6	22.8	22.8	10.0	10.0	32.9
Half-life in water (d)	35.6	27.8	22.8	16.0	12.3	50.3
Half-life in atmosphere (d)	0.08	0.29	0.38	0.26	0.33	0.79
Half-life in sediment (d)	21900	21900	21900	510	392	340

The concentration of NP form the wastewater treatment plant in the atmosphere is simulated using the Gaussian plume method and the generated wind filed in HydroBEAM. The spatial and temporal NP emissions rate is calculated based on the following assumptions:

- Emissions from the wastewater treatment plant into river are estimated by considering the number of sewers connections (population).
- Emissions from the wastewater treatment in the atmosphere are mixed completely with precipitation.
- The accumulated concentration of NP at each mesh is washed by runoff and a certain amount infiltrates into the unsaturated zone according to the distributed soil and land uses, and then ends in groundwater aquifer.
- Separated sewer system (SSS) is assumed.
- The depth of sediment layer in river channel and paddy fields is assumed to be constant.

NP has been detected in atmospheric samples by many researchers, the air concentration of NP ranging from 2.2 to 70 ng/m^3. The two studies suggest that volatilization should also be considered as a degradation mechanism when dealing with the environmental fate of NP, because of its moderate volatility (Henry's law constant ranges from 1.55x10^{-5} to 4x10^{-5} atm-m^3/mole) it enters the atmosphere from the aqueous phase. Gaussian plume model is used for calculating the spatial and temporal concentration of NP at the Yasu River basin. The main assumption is that dispersion in the horizontal and vertical direction take the form of a normal Gaussian curve, and is given by

$$C(x,y,z,t) = \frac{Q_{NP}(x,y,t)}{2\pi V \sigma_y \sigma_z} \exp\left(\frac{-y^2}{2\sigma_y^2}\right) \times \left[\exp\left(\frac{-(z-H)^2}{2\sigma_z^2}\right) + \exp\left(\frac{-(z+H_e)^2}{2\sigma_z^2}\right)\right] \tag{5.3}$$

where, C is the spatial and temporal concentration of NP, QNP is the rate of NP emission, V is the wind speed, σ_y is the standard deviation in the y-direction, σ_z is the standard deviation in the z-direction, y is the distance along a horizontal axis perpendicular to the wind, z is the distance along the vertical axis, and H_e is the effective height of emission. The concentration along the ground, centerline, and with no plume rise is calculated by setting y, z and H_e to be 0.0. Distributed concentrations of NP in atmosphere are shown in A.6, Appendix A. The calculation procedure of H_e, σ_y and σ_z is shown in Table C3, Appendix C.

6 APPLICATIONS OF HYDROBEAM

6.1 Simulation results of water quantity

HydroBEAM is simulating the spatial and temporal water quantity and quality interactions in the atmosphere and in the ground as illustrated by Figure 6.1.

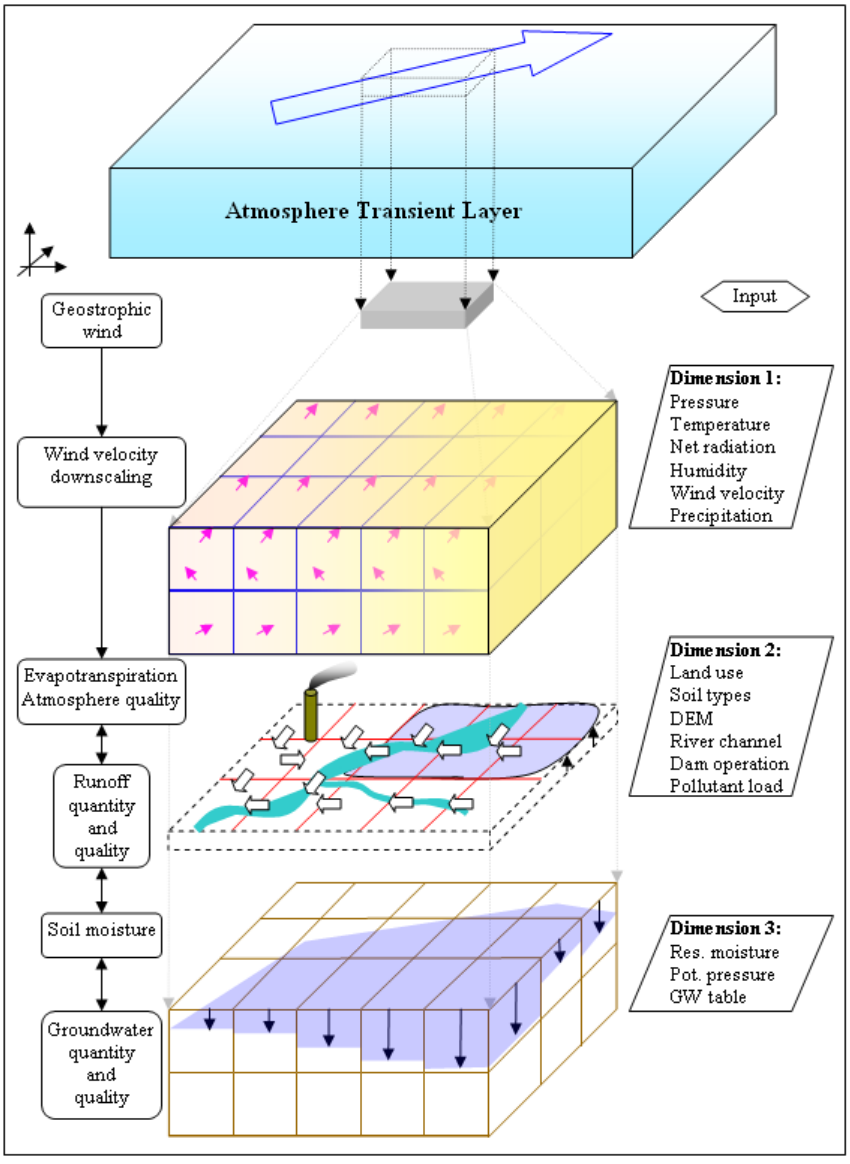

Figure 6.1 Three dimensional river basin simulation with distributed runoff model for water quantity and quality.

HydroBEAM is applied to hourly and daily data from the upper and lower catchments of the Yasu River. Initial saturated depth profiles were evaluated according to the distributed groundwater levels. The undefined parameters were adjusted by trial and error in order to minimize the residual errors between the calculated and the observed data. The simulated and observed snow depths are shown in Figure 6.2 and Figure 6.3 shows the distribution of snow depths at the Yasu River basin.

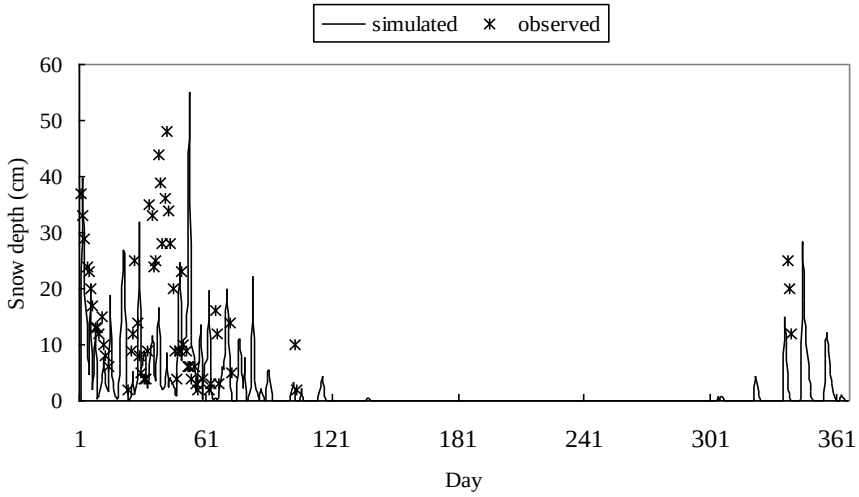

Figure 6.2 Time series of the simulated and observed snow depths at the Yasu Dam. (1997/02/01, time: 00).

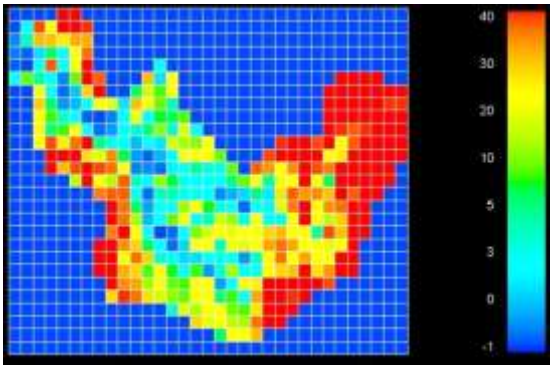

Figure 6.3 The distributions of the simulated snow depths (cm) at the Yasu River basin. (1997/02/01/, time: 00).

Runoff is simulated and averaged every one hour as shown in Figure 6.4. There are three discharge observation stations at the Yasu River basin. The correlation values between observed and calculated values vary within the basin. The fluctuations are caused by the calibration of the model. Since the hydrological parameters of the distributed land uses and soils are varying for each grid, the calibration of the discharge at one station will not necessarily lead to good agreements between the observed and simulated values at other observation stations. The river discharge measurements at the Yasu River are performed daily. The daily measurements do not show the propagation of the kinematic wave from the upper catchments due to averaging of hourly readings. The simulated and observed daily discharges at Minakuchi station are shown in Figure 6.5.

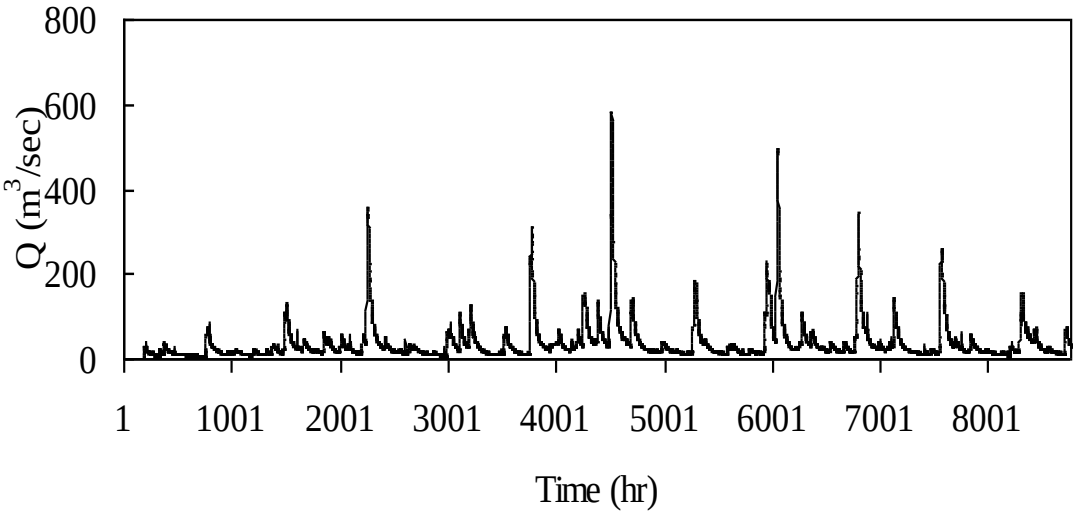

Figure 6.4 Simulated hourly river discharge in lower Yasu River basin (1996).

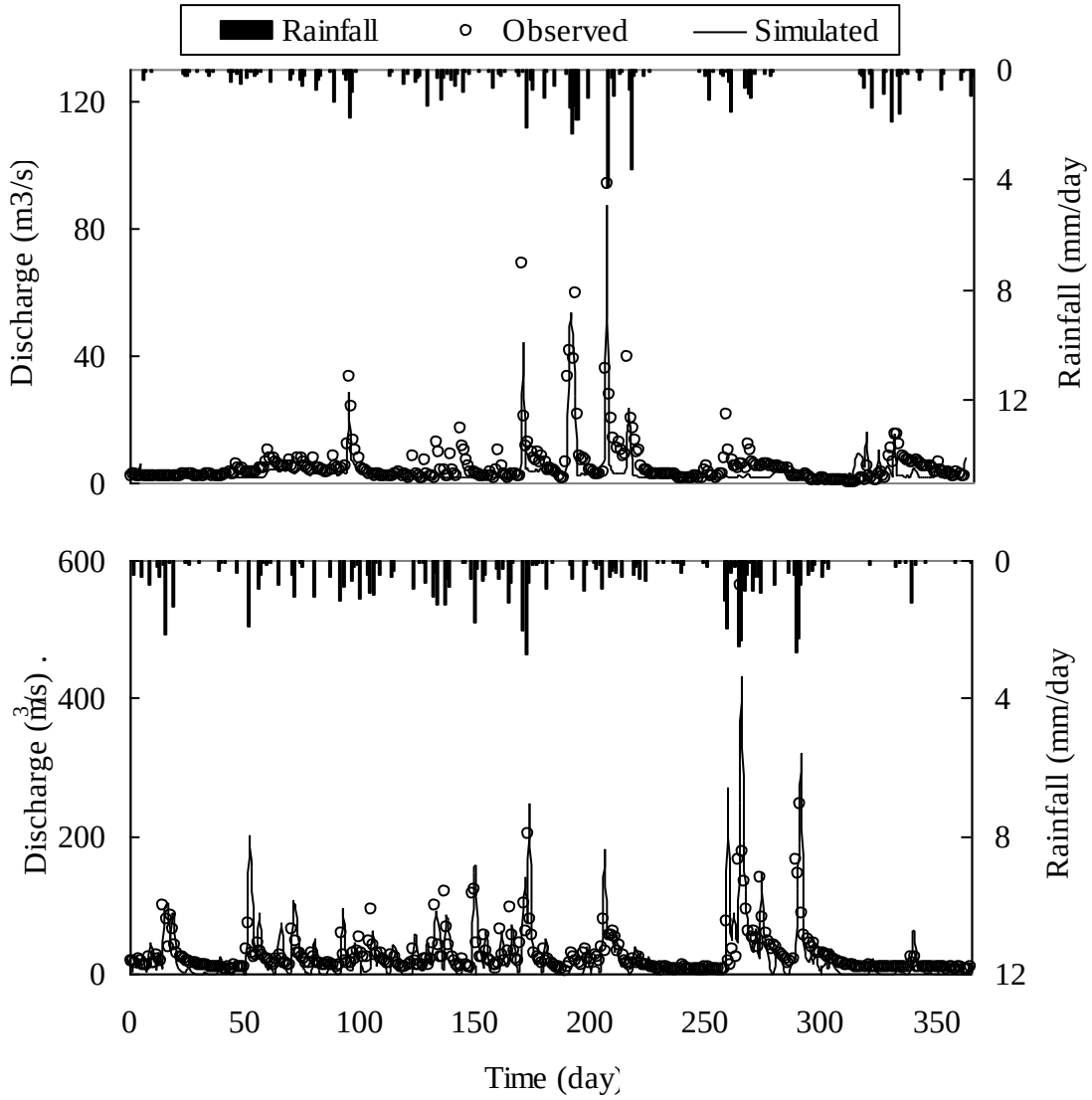

Figure 6.5 Simulated and observed river discharges in lower Yasu River basin; upper chart: (1997), lower chart: (1998).

The response of the river hydrograph due to upstream flow is not the same for upper and lower catchments, the runoff related wave transfers faster in lower catchments. Figure 6.6 and Figure 6.7 show the plots of the flow hydrographs at various points along the river channel in the upper and lower catchments, respectively. It can be seen that the peak discharge is transferred as the runoff wave in the upper streams (1 km,

29 km). In these Figures, the spatial and temporal distribution of the flow hydrograph can be seen for many points along the river channel. This change is caused by the difference in flow accumulation networks and the hydrological characteristics of the catchments. These characteristics include rainfall, parameters for infiltration and roughness coefficients that are highly affected by both land uses and soil distribution.

The model is highly affected by the distribution of both land use and soil type in each grid. Many scenarios have been simulated for identifying the hydrological impacts of urbanization. Figure 6.8 shows the impact of changing (30%) of the agricultural areas into residential areas, and the related change in the river hydrographs in the upper Yasu River basin. In this figure, LU1f and LU2f represent the future shapes of the hydrographs LU1a, and LU2a, respectively. Large points compose the forecasted hydrographs.

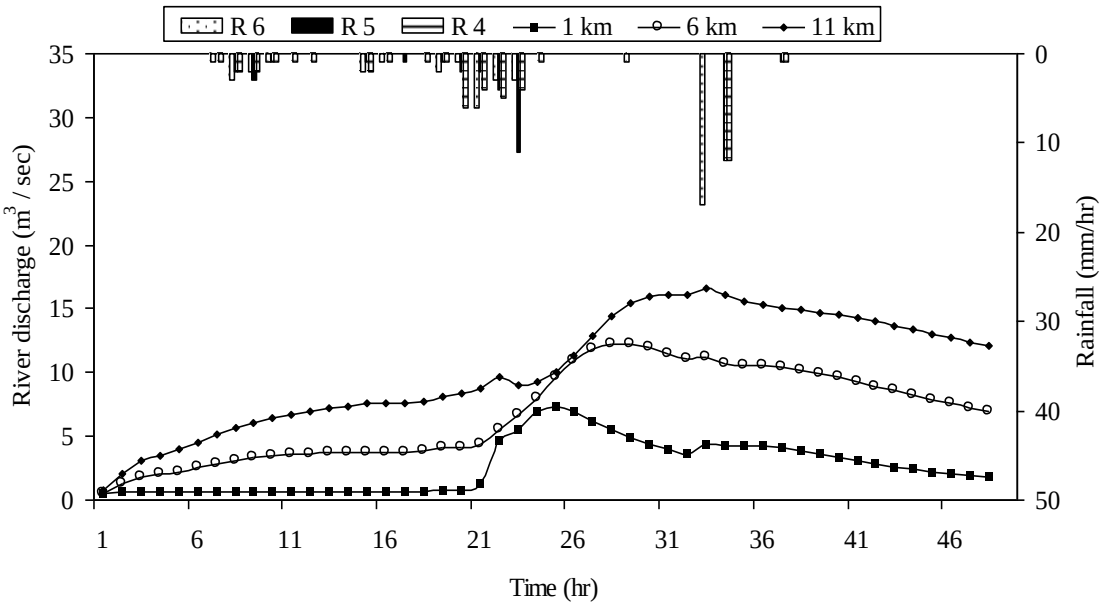

Figure 6.6 Hourly river discharge sequences in upper catchments.

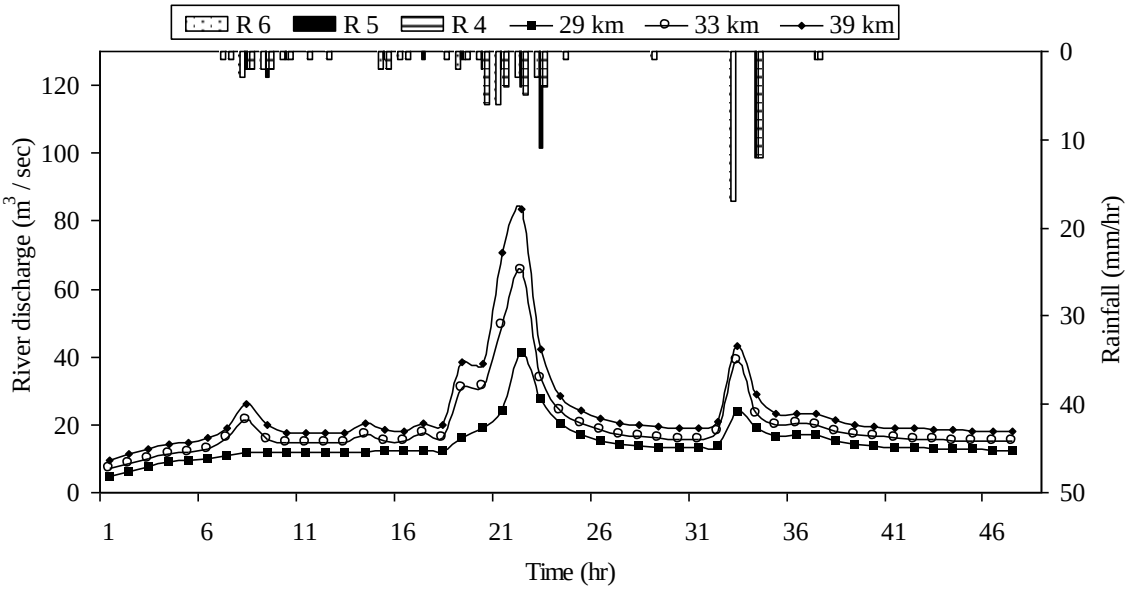

Figure 6.7 Hourly river discharge sequences in lower catchments.

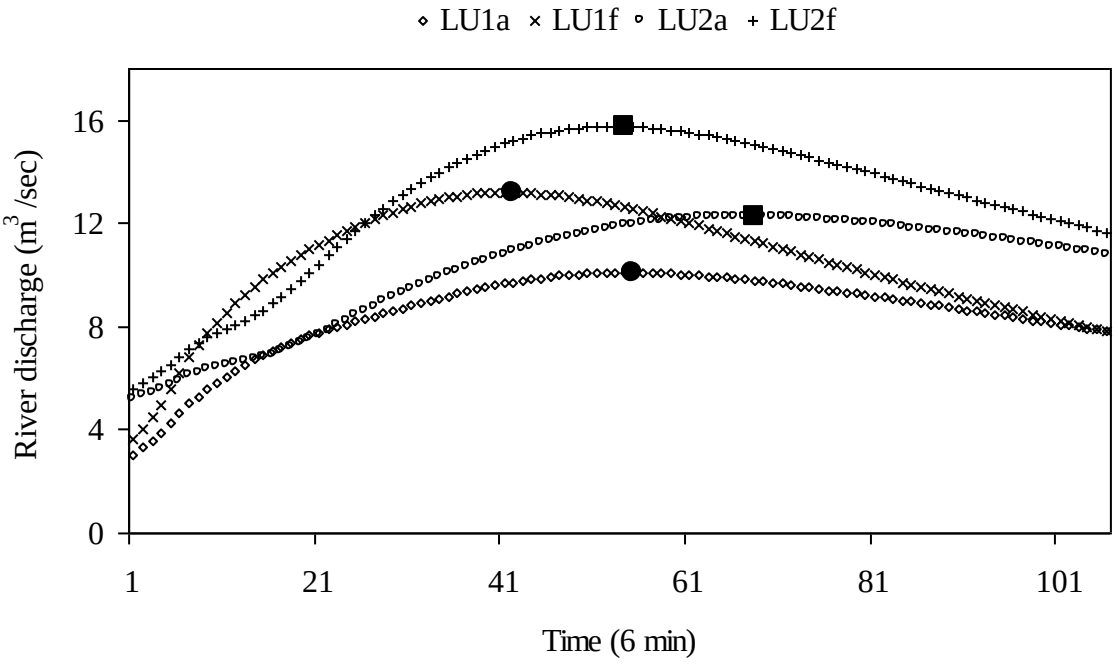

Figure 6.8 River discharge sequences for land use change scenarios. Similar dark points illustrate the changes in magnitude and time of the peak flows at mesh 1a and 2a respectively. LU1a is the existing hydrograph and LU1f.

The distributed soil moisture is highly affected by the existing sources and sinks within the unsaturated subsurface layer. By considering the spatial and temporal parameterization, which is caused by the land use dynamics the soil moisture profile for each cell is simulated. At the start of the rain seasons the soil is assumed to be dry, and according to the soil types and depths of groundwater the potential head at the boundary of the unsaturated layer is evaluated.

At the Yasu River basin the groundwater potential head value ranges from -40 to -100 m, the soil layer is divided into (100) divisions between the surface and the groundwater level. Then the soil moisture and the distribution of the potential head is simulated at every 10 sec, during this small time step the groundwater level is assumed to be steady and doesn't affected by the soil moisture.

At every large time step the groundwater level is updated in order to set the lower boundaries for the unsaturated flow model. Since the initial potential head for dry conditions is smaller than any of the distributed hydraulic conductivities, it is assumed that the soil will absorb a certain amount of the applied sources.

This amount is highly affected by the existing utilization of land and seasonality. Then the calculated soil moistures will be accumulated for every large time step and used for estimating the distributed recharge to groundwater model. Also the model simulates the distributed discharges from groundwater storage, because the accumulated soil moisture can be negative in the case of dry weather conditions, and extensive water uptake from the subsurface layers.

A demonstration for simulating the temporal soil moisture conditions is shown in Figure 6.9.

The groundwater level for each grid is simulated by the dynamic linking between the surface water models and groundwater model in HydroBEAM. The distributed groundwater levels for upper and lower catchments are shown in Figure 6.10. Spatial distributions of river discharges and groundwater levels at Yasu River basin are shown respectively in Figure 6.11 and Figure 6.12.

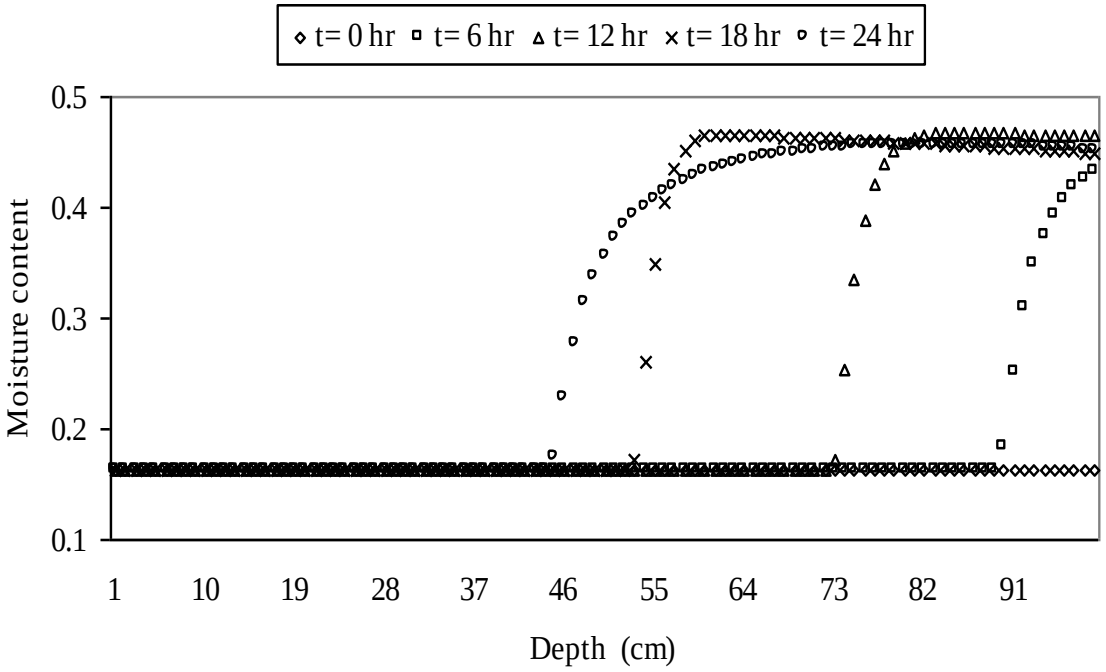

Figure 6.9 Simulated spatial and temporal soil moisture contents in lower Yasu River basin.

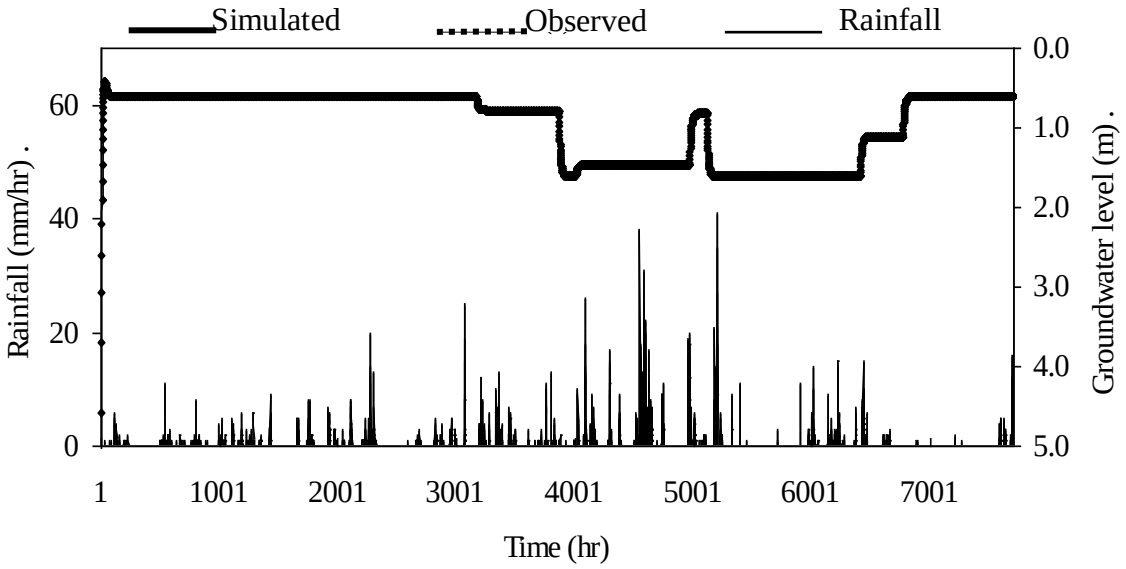

a) Simulated groundwater level in the upper Yasu River basin.

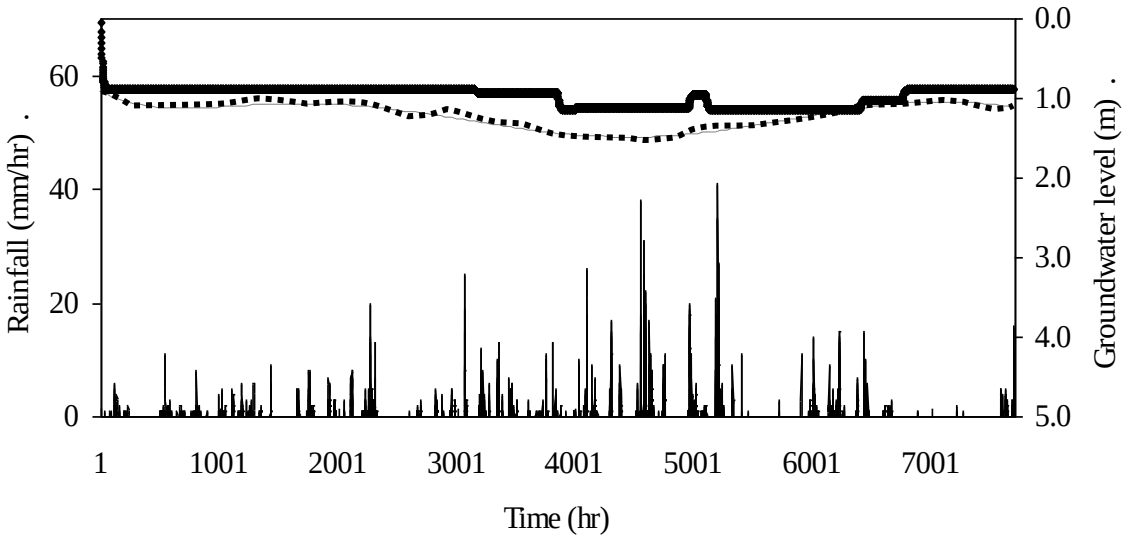

b) Simulated and observed groundwater level in the lower Yasu basin.

Figure 6.10 Simulated groundwater level in the Yasu River basin.

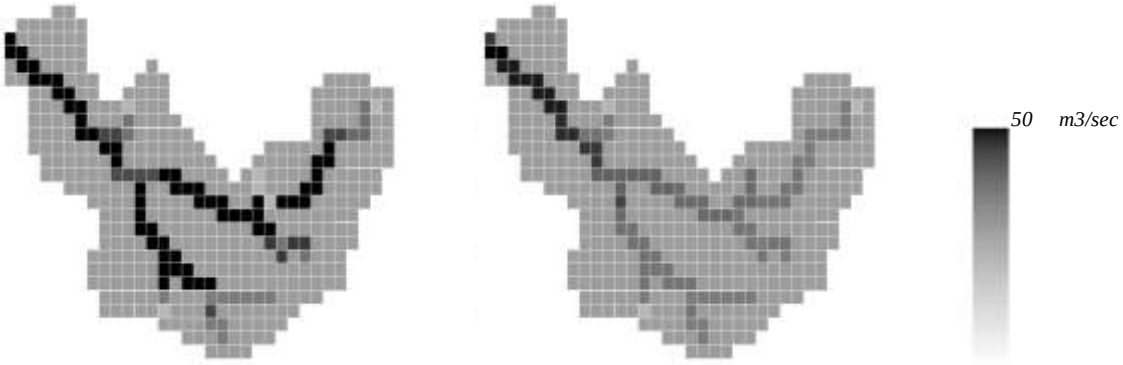

(a) Calculated results at 8:00 AM (b) Calculated results at 11:00 AM

Figure 6.11 Spatial distribution of river discharge at Yasu River. (1997/11/1).

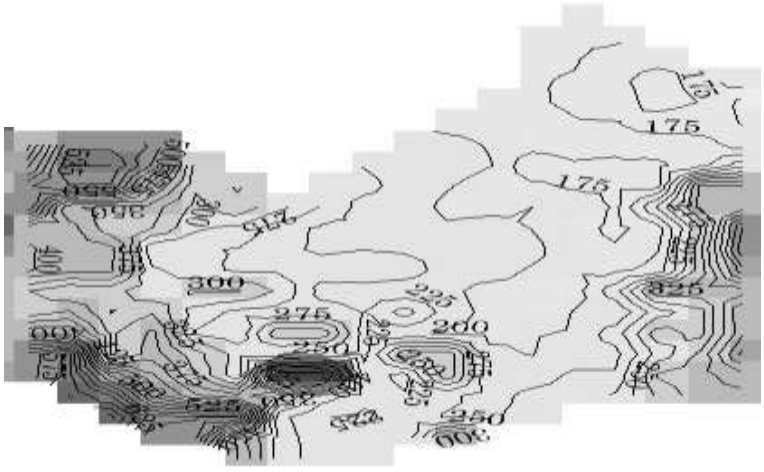

Figure 6.12 Spatial distribution of groundwater level at Yasu River basin. (1997/11/1, 11:00 AM).

The operation of Yasu dam and Ozuchi dam is formulated according to the explained methodology in the previous section. The monthly formulated operation is

applied to Yasu dam, and then the calculated release is added to the simulated runoff in order to estimate the inflow at Ozuchi dam. The operation at Ozuchi dam is evaluated according to the river discharge at Yasu River station, which is located 15 km far away. Figure 6.13 shows the actual release at Ozuchi dam and the periods where the operation of Ozuchi dam has failed to satisfy the monitoring value (1.68 m^3/sec). Therefore HydroBEAM is used to identify these faults in dam operation and optimizes the release by using the iterative operation method. The storage volume at the Ozuchi Dam, and the water intake at the Yasu River basin are shown in Appendix A.

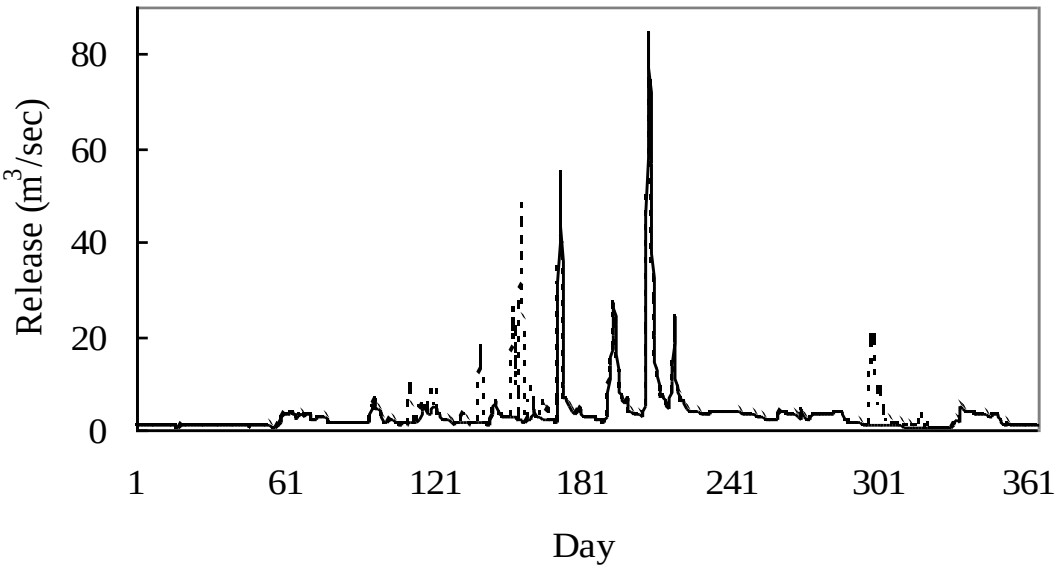

Figure 6.13 Modified dam release at Ozuchi Dam (*dashed line*), 1997.

6.2 Simulation results of Atmosphere quality

The generated wind in HydroBEAM is used with Gaussian plume model to calculate the distribution of NP that when emitted form a single point source located at Minaguchi. Since emission data was not it is approximated based in daily generation of wastewater. Figure 6.14 shows the spatial distribution of NP.

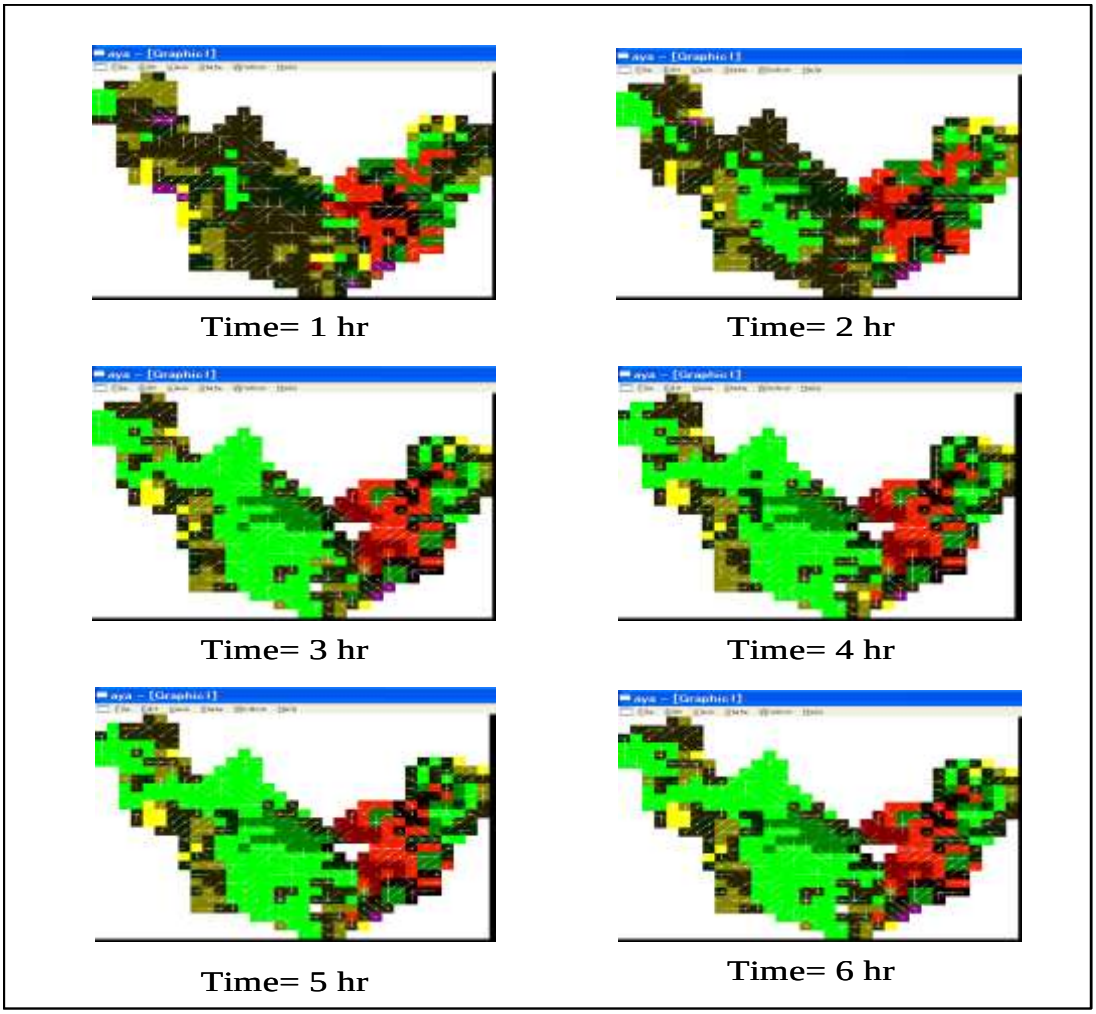

Figure 6.14 Spatial and temporal distribution of NP, in green, and its concentrations that ranges form 90 ng/m^3 near the emission source and 2.2 ng/m^3 15 km far away.

7 UNGAUGED WATERSHEDS

7.1 Introduction

In chapter 3 and 4 the explained methodology for hydrological characterization of the watershed requires both high quantity and quality of spatial and temporal hydrological data. Ungauged watershed is the watershed that has no hydrological data or has no representative hydrological data. Observed data is needed to analyze the characteristics of watershed statistically (inference or predictive), and for the initiation, calibration and validation of hydrological models, the missing data can be obtained using physical or statistical downscaling form global circulation models or design of a hypothetical storm events. The proposed approach in this chapter is to validate the daily simulations of distributed runoff model using the analytical solution of the main governing equations. This chapter shows the way that HydroBEAM can be reformulated in order to form the basis for hydrological modeling for ungauged river basins. It is proposed that a more realistic estimate of watershed characteristics can be obtained when global and observed dataset are used as an input in HydroBEAM.

7.2 Derivation of hydroclimatic data from GCM

Global circulation models calculate the velocity, temperature and water-vapor content in the troposphere and lower stratosphere. In these models the globe is divided to square grids. The surface temperature and water-vapor are located in the center of each grid, and the horizontal velocity components are located at the corners of the grid. The topography of the model is that obtained by area-averaging the 1^o x 1^o, the surface temperature is extrapolated from the temperature at the lowest level (about 80 meter elevation) with the dry-adiabatic lapse rate (9.8 ^{0}C/km), the ground temperature is calculated from the prognostic heat budget, the soil wetness is calculated from the

prognostic water budget that includes precipitation, snowmelt and evaporation. Precipitation falls as snow if the temperature of the lowest level is less than $0\ ^0$C.

7.2.1 Delineation of distributed hydroclimatic processes

The watershed is girded into identical grids. Accurate initialization of grid hydroclimatic processes is critical for distributed hydrological and meteorological models because of their spatial and temporal regulation of runoff, and energy fluxes between the ground and the atmosphere.

The approach in this section is to use the bilinear interpolation method, which is illustrated by Figure 7.1, to incorporate topography and GCM daily records of temperature and precipitation data at few locations, in order to delineate the hourly records of distributed temperature, precipitation, snowfall, and snowmelt. The data at meteorological stations is used to derive the physical parameters that describe spatial and temporal variability of hydroclimatic processes such as lapse rate and threshold temperature for snowfall occurrence.

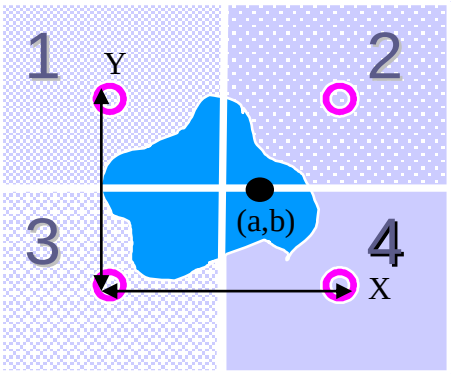

$$T(a,0,t) = ((X-a)\times T(0,0,t) + a\times T(X,0,t))/X$$
$$T(a,y,j) = ((Y-a)\times T(0,Y,j) + a\times T(X,Y,j))/Y$$
$$T(a,b,j) = ((Y-b)*F(a,0,j) + b\times T(a,Y,j))/Y$$
$$T^{*}(a,b,j) = T(a,b,j) - (Ele(a,b) - 130)\times\alpha$$

Figure 7.1 Delineation of the spatial and temporal temperatures methodology. *Ele* is the elevation of a grid located at point (*a*,*b*), *t* is daily time step, *X*,*Y*=280 km, and 130 is the assumed ground elevation.

The delineation of the spatial and temporal precipitation data is achieved by assuming that the distribution of precipitation is calculated by using an empirical interpolation method,

$$Rain(a,b,t) = \frac{\sum_{k=1}^{4} Rain(X_k, Y_k, t)/r_k}{\sum_{k=1}^{4} 1/r_k} \tag{7.1}$$

The occurrence of snowfall is determined by using the following empirical formula that is derived form historical data and given by,

$T(a,b,t) < 4.0°C$. and. $Rain(a,b,t) > 0.0 \Rightarrow$ Snowfall

7.3 Initialization and calibration of ungauged watershed

It is difficult for a GCM model to quantitatively predict the regional rainfall or other meteorological data at high resolutions. The approach in this section is to make a knowledge based assumption of spatial and temporal rainfall events, then to calculate the analytical solution of the main governing equations. The analytical solution is not achievable unless a simple boundary and initial conditions are identified, the simplifications are achieved by ignoring the spatial and temporal effective rainfall term in Eq. (2.32), and then modifying the left terms, or

$$\begin{aligned} &\frac{\partial A}{\partial t}+\frac{\partial Q_g}{\partial x}=0, \\ &Q_g=\sum Q+Qstr \end{aligned} \tag{7.2}$$

where Q_g is the flow rate including the spatial and temporal effective rainfall Q_{str}. The analytical solution of Eq. (7.2) is calculated and given by,

$$T_t(g,t)=\frac{3}{5}\left[n(g,t)B(g)^{\frac{2}{3}}\sqrt{S_0(g)}\right]^{\frac{3}{5}}Q(g,t)^{\frac{-2}{5}}L \tag{7.3}$$

where g is the grid number, B is a hypothetical channel width in each grid, L is the length of this channel and S_0 is the average slope. Figure 7.2 shows the shape of the output hydrographs using Eq. (7.3) and using the detailed formulation of Eq. (2.32).

a) High flows in gauged basin

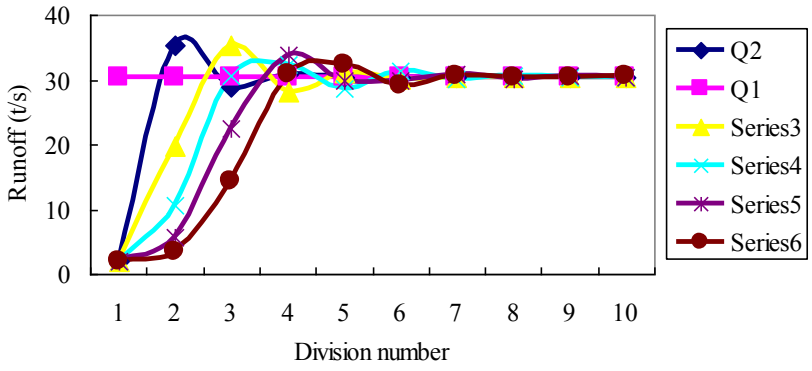

b) Low flows in gauged basin

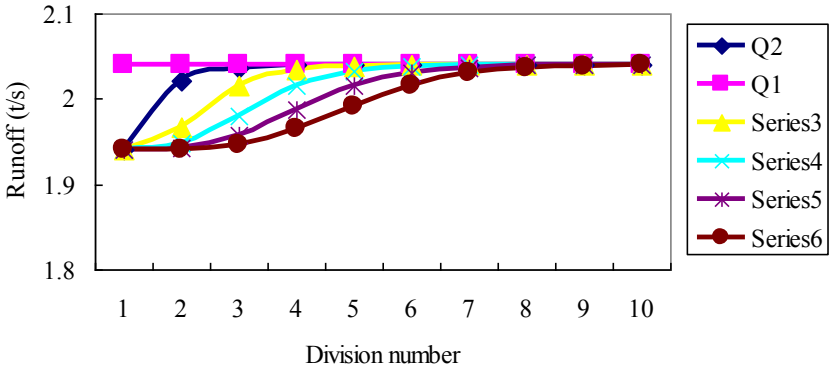

c) Ungauged basin

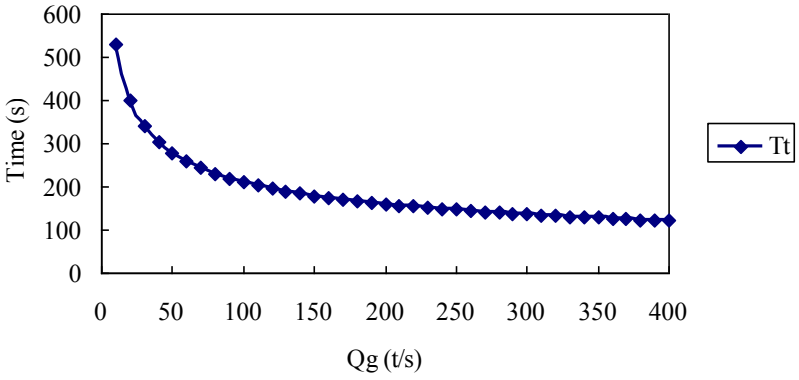

Figure 7.2 Relationship between the kinematic wave travel time and the flow rate.

7.3.1 Evaporation

The distributed temperatures are downscaled from DCM model using the nonlinear interpolation method, and modified according to change in topography. Distributed air pressure is calculated by using the ideal gas equation. Vapor pressure e_a, can be obtained by assuming that dew point temperature is near the daily minimum temperature (T_{min}), or $e_a = 0.611\exp\left(\frac{17.27T_{\min}}{T_{\min}+273.3}\right)$ (7.4)

The average wind speed estimates may be selected from information available for the regional climate, but should take seasonal changes into account. General values are suggested as follows :mean monthly wind speed at 2 m, light wind:1.0 m/s, light to moderate wind: 1 - 3 m/s, moderate to strong wind: 3 - 5 m/s, strong wind: 5.0 m/s

Where no wind data are available within the region, a value of 2 m/s can be used as a temporary estimate. This value is the average over 2000 weather stations around the globe (FAO). An alternative equation for calculating the potential evaporation E_0, when meteorological data is missing, by using the Hargreaves equation,

$$E_o = 0.0023(T+17.8)\sqrt{\delta_t}R_a \quad (7.5)$$

where δ_t is the difference between the maximum and minimum temperature for a given month, averaged over several years, and R_a is the extra terrestrial radiation in (mm/day).

7.3.2 Groundwater flow

In the case of ungauged watershed the groundwater flow in a pours medium resting on a slopping impermeable bed, with direction parallel to this bed. Since neither monitoring wells nor soil profile are available, groundwater flow modeling using classical models is unrealistic and based on many assumptions that harden the verification or validation of these models.

The approach in this dissertation is to make similarity between the simplified kinematic wave model and the groundwater flow model. Thus, the assumption is that, Eq. (7.3) can be used to describe the spatial and temporal groundwater flow, the only difference is the definition of *n*, which will be defined as a coefficient of groundwater flow, and this coefficient is derived from historical data using methods for hydrograph analysis and separation.

7.4 The case of the Seyhan River basin

For the Seyhan River basin, HydroBEAM is provided by DEM data from global topographical data, which has a resolution of one kilometer by one kilometer square grids. Because the boundaries of the basin are not available, HydroBEAM delineates the boundaries by using the eight-directions based routing and approximate initial boundaries, which have been estimated form previous studies and several filed studies. Figure 7.3 illustrates the delineation of the Seyhan river basin.

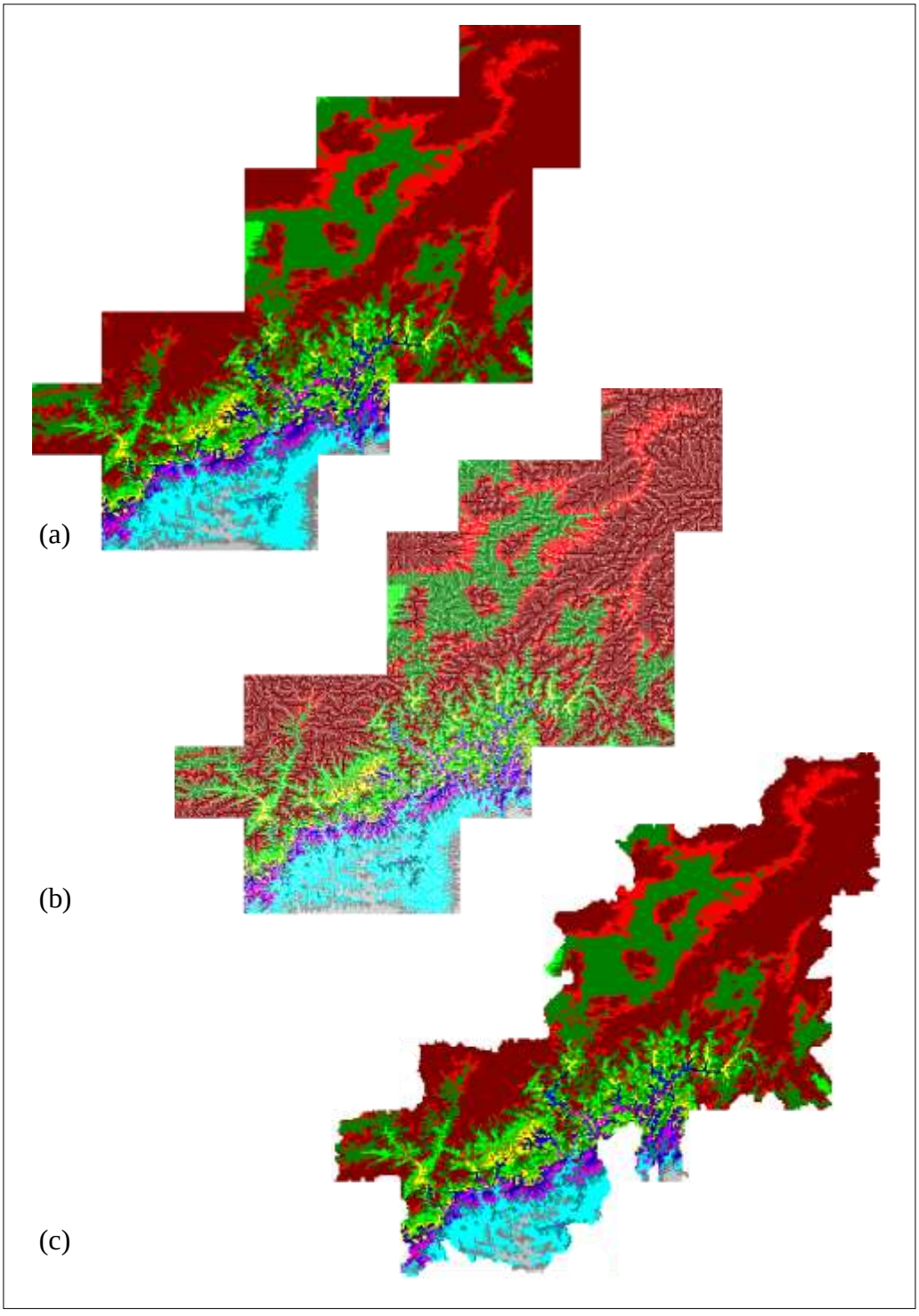

Figure 7.3 Delineation of the Seyhan River basin boundaries. a) DEM for initial boundaries (*Source: GOTOPO30*), b) Grid-to-grid drainage network, c) Approximated river basin boundaries.

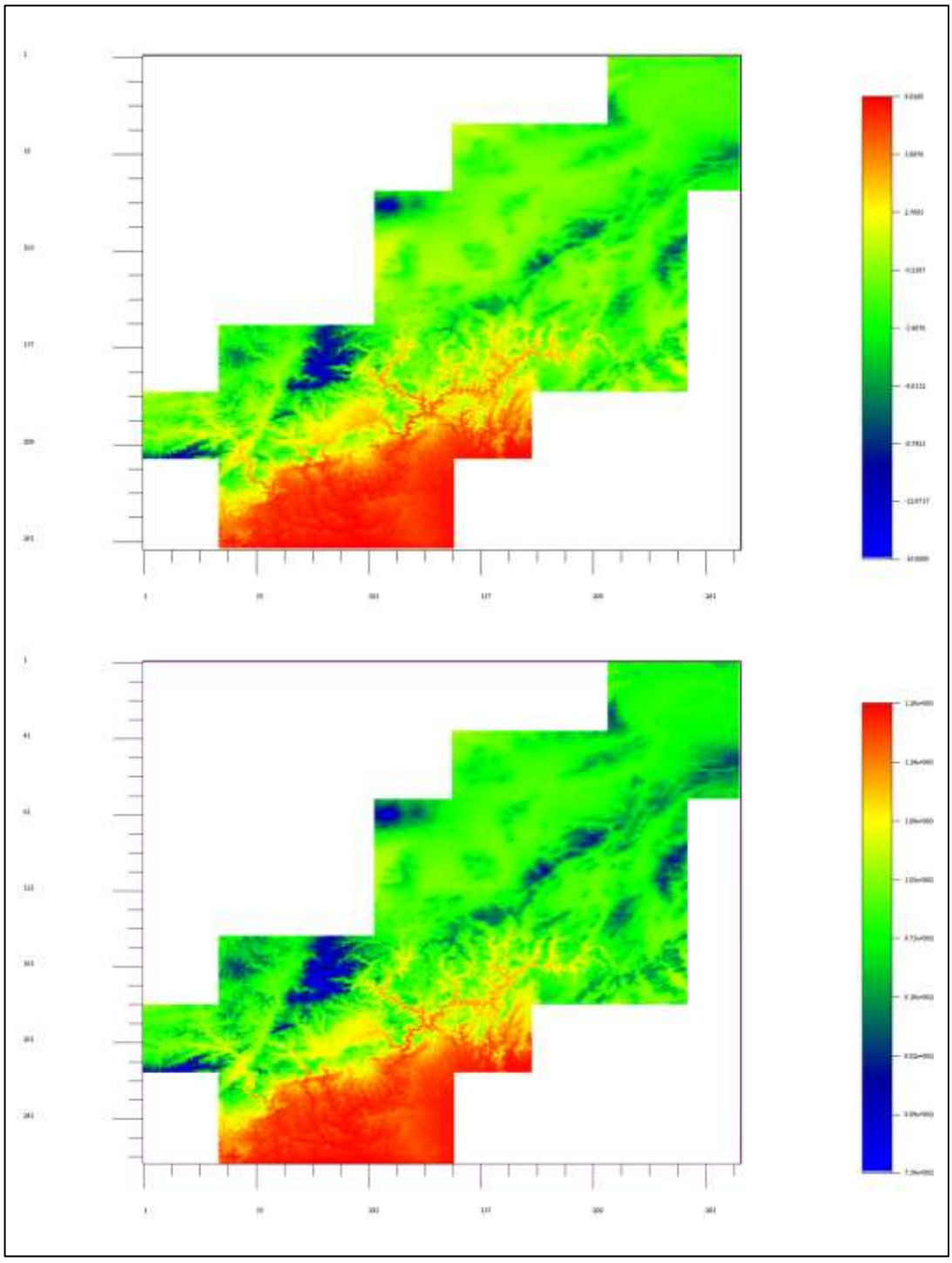

Figure 7.4 Distribution of the daily ambient temperature and air pressure at the Seyhan River basin. (2000/01/01).

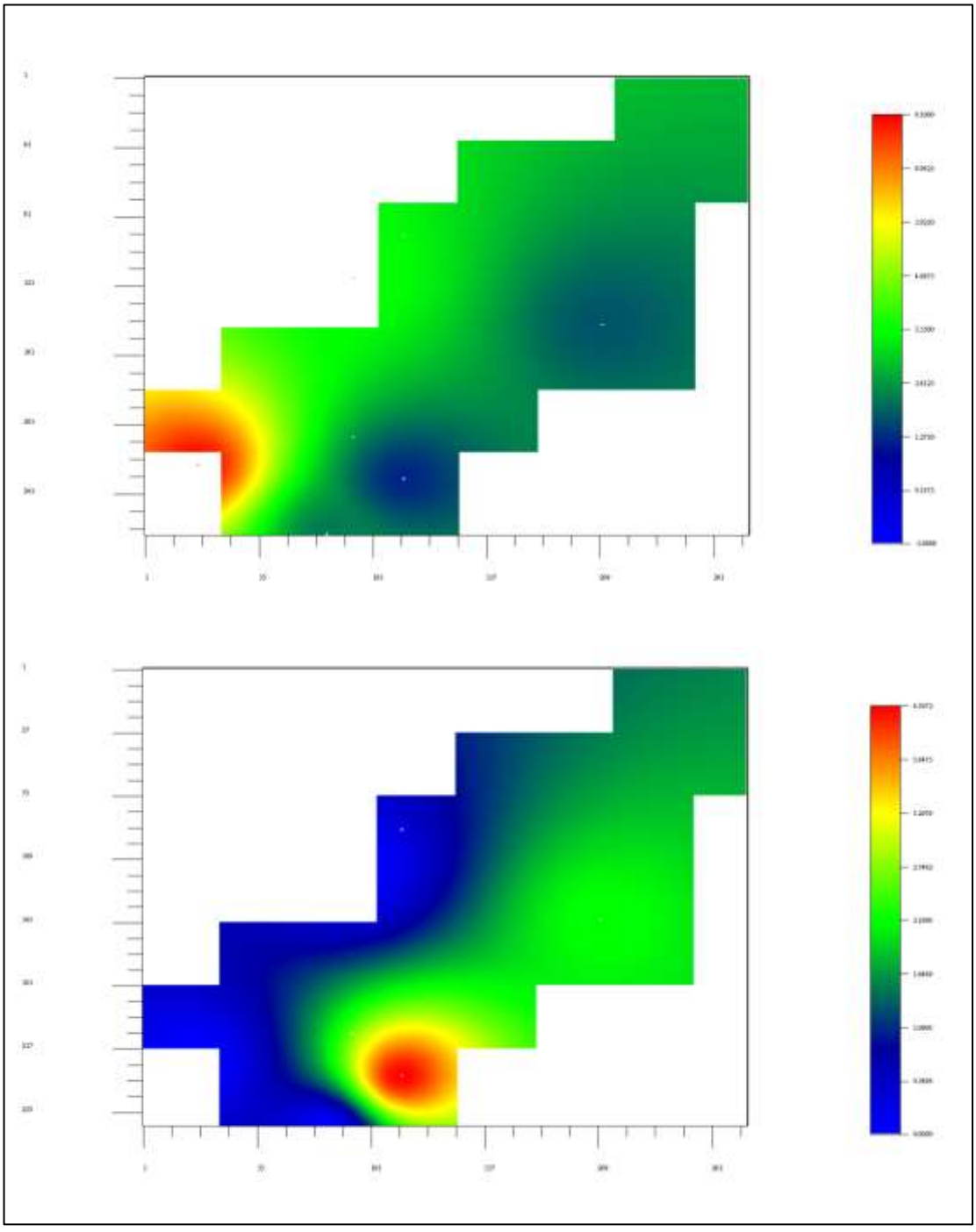

Figure 7.5 Distribution of wind field and rainfall based on empirical method at the Seyhan River basin. (2000/01/01).

In the Seyhan river basin, snowmelt is one of the main important events of the water year. The snowmelt runoff supplies Goksu and Zamanti rivers, Catalan and Seyhan dams, and groundwater recharge. Snowmelt usually starts in spring, some of the greatest floods resulted form snowmelt. According to many hydrological studies in and around the Seyhan River basin the snowmelt starting elevation is 1250 meter above the sea level, the highest elevation of melting zone at which freezing temperature is 0 ^{0}C, which is calculated by using the method of meteorological characterizing in HydroBEAM.

The snowmelt runoff can be calculated in centimeters per degree-day above 0^{0}C, which is varies between 0.15 and 0.38 (JICA, 1990). Also it can be calculated using the energy balance method, which is accomplished by dividing the watershed into grid squares by using the method of watershed meteorological characterizing in HydroBEAM. Figure 7.6 shows the relationship between ambient temperature and snow depth in different weather stations (see Appendix B). Figure 7.7 shows the distributions of potential evaporation and Figure 7.8 shows the snow cover during February and March respectively. Figure 7.9 shows the daily rainfall data and the corresponding simulated river discharges in Catalan Dam.

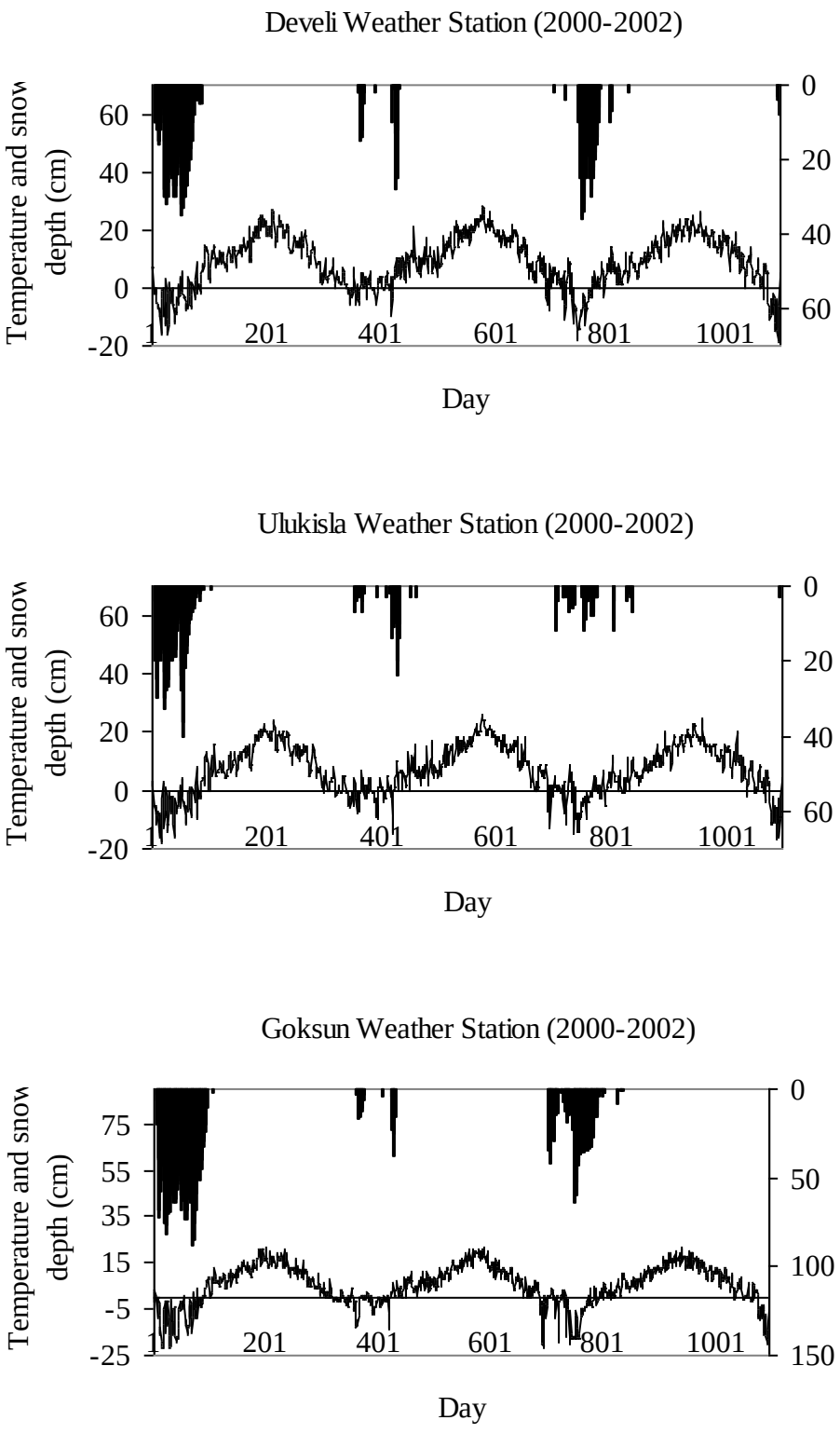

Figure 7.6 Relationship between snow depth and ambient temperature.

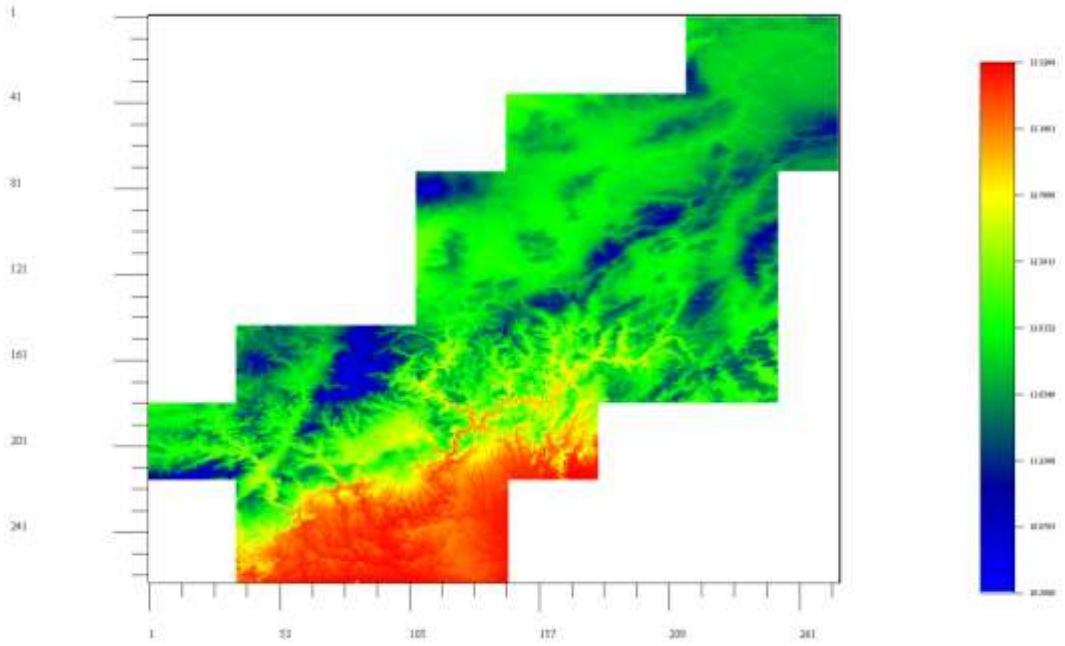

Figure 7.7 Simulated potential evapotranspiration (mm/day) in the Seyhan River basin. (2000/05/01).

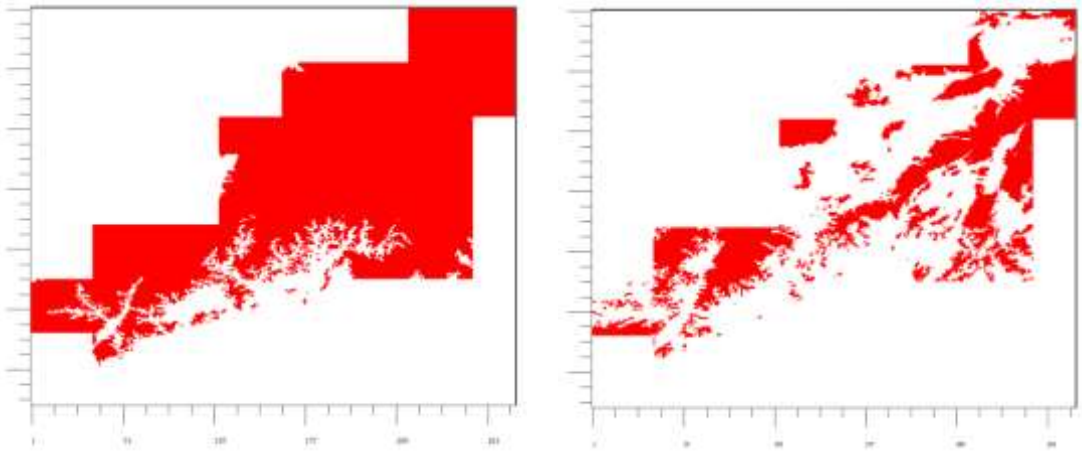

Figure 7.8 Simulated snow cover in the Seyhan River basin. Right: (2000/02/01), left: (2000/03/01).

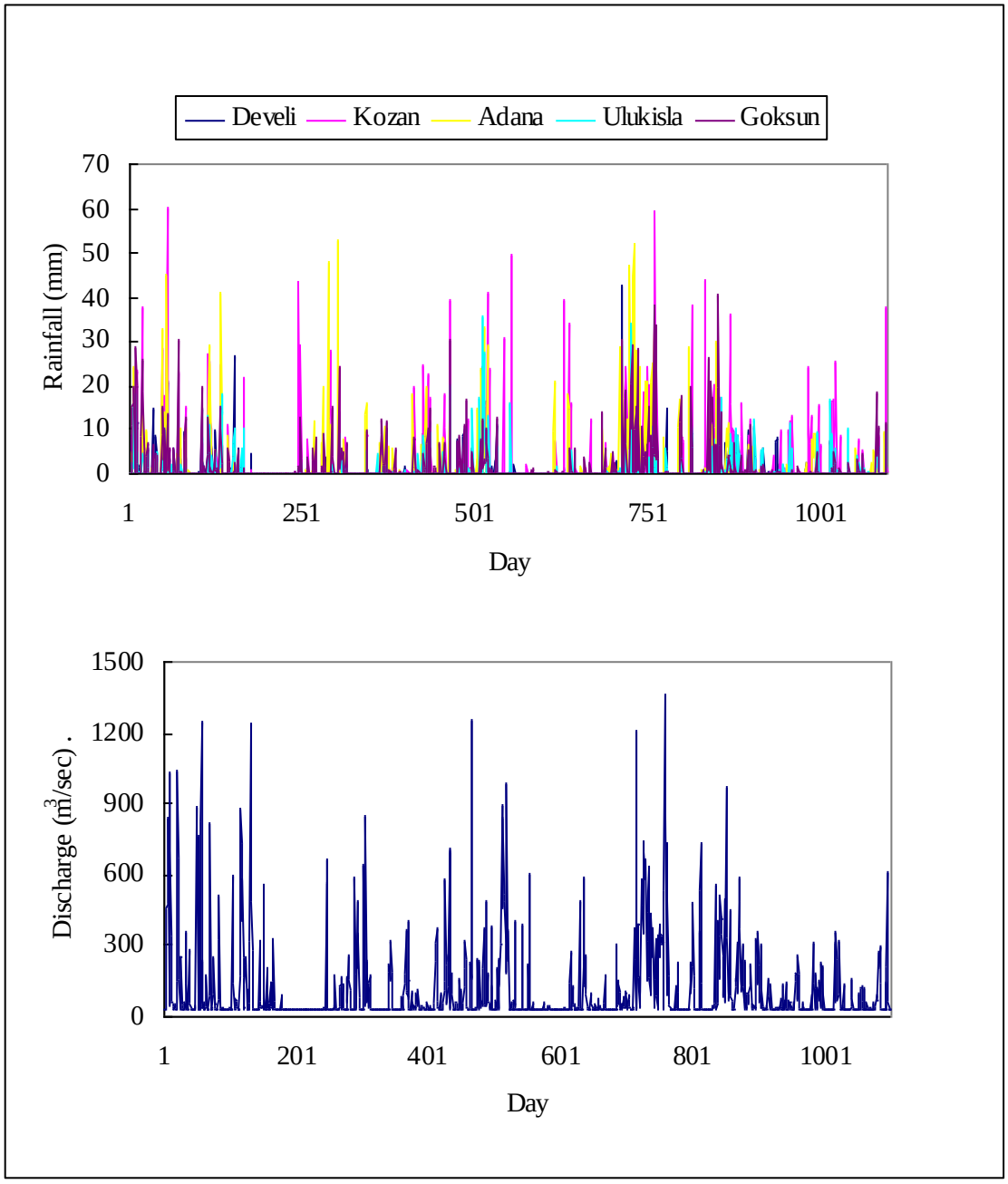

Figure 7.9 Daily rainfall data, and simulated river discharges in Catalan Dam, Seyhan River basin. (2000-2002).

7 CONCLUSIONS

8.1 Synopsis of the methodology

The main objective of this dissertation was to establish dynamically linked and physically based mathematical relationships with numerical approaches between distributed runoff models, groundwater and atmosphere models in order to simulate the hydrological interactions in the three zones. A general framework for the three dimensional hydrological modeling has been presented. The framework includes three main linked models; distributed rainfall-runoff model, groundwater flow model, and simplified atmosphere model. The importance of linking the three models for water quantity and quality has been illustrated and emphasized.

The mathematical formulations of the interactions in three zones using the dynamic linking have been achieved by using of the watershed characterization methodology. In HydroBEAM the characterization subroutines are dynamically linked with the main workspace, this allows for including the dynamic behavior of a watershed and its hydrological systems. The hourly records at few locations can be used to estimate the spatial and temporal ambient temperature, atmosphere pressure, and wind velocity in each grid. And then water quantity is simulated, and water quality can be simulated using the compartmental ("well-mixed" media) model. The present methodologies requires many hydroclimatic data, which is not available for many watersheds, therefore downscaling of hydroclimatic data from GCM data was introduced, and proposed simplifications for the main governing equations were illustrated.

8.2 Comprehensive remarks

In Chapter 2, the HydroBEAMs'mathematical formulations and their numerical solving approaches were introduced. This means the governing main equations were derived by considering the (x,y,z,t) dimensions.

In Chapter 3, the watershed characterization methodology was developed. It has been implemented mathematically and physically at a very high resolution (1 km) land data, involving several categories such as: land uses, soil types, topography, and geology. It includes reservoir routing, and an integrated hydrological parameterization in each grid. Since the characterization subroutines are dynamically linked with the main workspace, this allows for including the dynamic behavior of a watershed and its hydrological systems.

In chapter 4, accurate evaluation of grid hydroclimatic parameters is described for distributed hydrological and meteorological models because of their spatial and temporal regulation of runoff, and energy fluxes between the ground and atmosphere. The spatial and temporal ambient temperature, atmosphere pressure, and wind velocity in each grid were calculated using physically based analytical approaches, such as the idealized Ekman boundary layer with an empirical data-driven formulation in order to downscale the characteristic of upper atmosphere and then distribute it for each grid within the river basin.

In Chapter 5, A compartmental ("well-mixed" media) model of environmental fate and transport, which describes the entry, movement, and spatial and temporal

concentration of Nonylphyenol Ethoxylate in the ground and in the atmosphere, was introduced making use of the diffusion transport mechanism and Gaussian plume rise model.

In Chapter 6, the developed HydroBEAM was applied for the case of the Yasu River basin. The spatial and temporal water quantity was presented and the simulations were compared with the observed data. Manual calibration has been conducted for the case study of the Yasu River basin. The simulated groundwater levels and the river discharges showed good agreements with the corresponding observed values.

In Chapter 7, HydroBEAM was modified in order to be applied to ungauged river basin, daily temperature and precipitation are extracted from GCM model and downscaled to finer resolutions. Temperature is downscaled using the nonlinear interpolation method, and then it is modified with respect to topography. Precipitation is downscaled using an empirical interpolation method, and then snowfall and snowmelt are evaluated empirically. The kinematic model was simplified in order to get an analytical solution that can simulate the travel time for surface runoff and groundwater flow. The developed HydroBEAM was applied for the case of the Seyhan River basin.

In this dissertation deterministic, physical, empirical, and numerical mathematics are employed. Only relatively simple numerical formulation is used for the atmosphere. The added value lies in the dynamic linking between different hydroclimatic processes, which have different spatial and temporal domains. This

resulted in a new integrated hydrological model for numerical watershed management with relatively small spatial and temporal time steps.

There is a considerable amount of further work that requires investigation. For example, Formulations of physically based distribution of rainfall data that requires a more robust and accurate approximation of the hydrological interactions between the surface and the atmosphere. This can be considerably difficult to obtain, especially if a simplified approximation of the atmosphere hydroclimatic processes are conducted and all the formulations and numerical schemes introduced in one and two dimensions. Numerical schemes that can use small spatial and temporal dimensions, such as combined implicit-explicit schemes need to be examined with the unsteady formulations. Also for the kinematic wave model, instead of simplified conservation of momentum equation and flow routing in flat catchments, an approximation of these two simplified parts can be obtained instead by using less conservative solution of the St. Venant equations. This enables a more accurate numerical approximation to be obtained.

REFERENCES

[1] Amorocho, J., and B. Espildora, "Mathematical simulation of snow melting process", *Water Science and Engineering*. Paper No 3001, University of California, (1968).

[2] Anderson, E.A., and Crawford N.H., "The synthesis of continuous snowmelt runoff hydrographs on a digital computer", Department of Civil Engineering, Stanford University, Stanford, California, Technical Report No 36, (1964), pp. 103.

[3] Baker D.L., "Darcian weighted inter- block conductivity means for vertical unsaturated flow", *Groundwater*, Vol. 33, No. 3, (1995b), pp. 385-390.

[4] Beldring S., "Kinematic wave approximations to hillslope hydrological processes in tills", *Hydrological Process*, Vol. 14, No. 1, (2000), pp. 727-745.

[5] Beven K., "On subsurface storm flow: an analysis or response times", *Hydrological Science Journal*, Vol. 4, No. 1, (1982), pp. 505-521.

[6] Beven K.J., R. Lamb, P. Quinn, R. Romanowicz and J. Freer," TOPMODEL. In V.P. Singh (Ed.), Computer Models of Watershed Hydrology", *Water Resources Publications*, (1995), pp. 627-668.

[7] Bouwer H., *"Water resources and environmental engineering"*, 1st edition, MGraw- Hill, (1978).

[8] Bras R., *"Hydrology: an introduction to hydrologic science"*, 1st edition, Addison-Wesley Publishing Company, Inc, (1990).

[9] Chow V., *"Applied hydrology"*, 1st edition, McGraw-Hill, (1988).

[10] Curtis D.C., and Eagleson P.S., "Constrained stochastic climate simulation", MIT Department of Civil Engineering, Technical Report No 274, (1982).

[11] Crawford C.B., and Legget R.F., "Ground temperature investigations in Canada", *Engineering Journal*, Vol. 40, No. 3, (1957), pp. 263-269.

[12] Eagleson P.S., *"Dynamic Hydrology"*, 1st edition , McGraw-Hill, (1970).

[13] FAO,"Crop evapotranspiration guidelines for computing crop water requirements", Irrigation and drainage paper No 56, (1998).

[14] Feldman, A.D., "HEC-1 Flood Hydrograph Package. In V.P. Singh (Ed.)", *Computer Models of Watershed Hydrology*, Water Resources Publications, (1995), pp. 119-150.

[15] Fenner K., Kooijman C., Scheringer M., and Hungerbuhler K., "Including transformation products into risk assessment for chemicals: The case of Nonylphyenol Ethoxylate usage in Switzerland", *Environ.Sci.Technol.*, Vol. 36 , (2002), pp. 1147-1154.

[16] Hiroh A., Shioshige K., and Ootaki A., "Simulation of the plume model with the curved trajectory on the data of a diffusion experiment", School of Science and Engineering, Waseda University, (1992).

[17] Huber W.C., "EPA Storm Water Management Model - SWMM. In V.P. Singh (Ed.), *Computer Models of Watershed Hydrology*", Water Resources Publications, (1995), pp. 783-808.

[18] Impact of Climate Changes on Agricultural Production System in Arid Areas, Interim Report of ICCAP, (2004).

[19] Idso, S.B.," A set of equations for full spectrum and 8- to 14 m and 10.5-um, Thermal radiation from cloudless skies", *Water Resources Res.*, Vol. 17 (2), (1981), pp. 295-304.

[20] Ishihara T. and Takasao T. , "Fundamental researches on the unit hydrograph method and its application", *Japan Society of Civil Engineers*, Vol. 60, No. 3-3, (1959), pp. 19.

[21] Horton R. E., "Rainfall Interception", *Monthly Weather Review*, Vol. 47, No. 1, (1919), pp. 603-623.

[22] Jansson P.E.,"SOIL: simulation model for soil water movement and heat conditions", Technical Report No 165, Swedish University of Agricultural Science, Department of Soil Science, (1991), pp. 73.

[23] Jennifer P., Mark P., William j., Gutowski, Thomas C., "Putting aquifers into atmospheric simulation models: an example from the Mill Creek Watershed, northeastern Kansas", *Advances in Water Resources*, Vol. 25, No. 1, (2002), pp. 221-238.

[24] Johansson P., "Diurnal groundwater level fluctuations in sandy till-a model analysis", *Journal of Hydrology*, Vol. 87, No. 1, (1986), pp. 125-134.

[25] Kato T., *"Research on the water cycle for the upper basin of the Yasu River"*, 1st edition, Kyoto University, (2002).

[26] Kite, G.W., 1995. The SLURP Model. In V.P. Singh (Ed.), *Computer Models of Watershed Hydrology*: 521-562, Water Resources Publications, Highlands Ranch, CO.

[27] Kimaro T., "Groundwater modeling coupled with SVAT model and its application to the Yasu River basin", *Annual DPRI, Kyoto University*, Vol. 45, No. 1, (2002), pp. 163-170.

[28] Kojiri T., "GIS-based environment model for water quantity and quality with river basin simulation", *Annual DPRI, Kyoto University*, Vol. 44, No. 1,(2000), pp. 150-160.

[29] Kuch H., and Ballschmiter K., "Determination of endocrine-disrupting phenolic compounds and estrogens in surface and drinking water by HRGC-(NCI)-MS in the picogram per liter range", *Environ. Sci. Technol.*, Vol. 35, (2001), pp. 3201-3206.

[30] Mark, D.M., "Automatic detection of drainage networks from digital elevation models". *Cartographica*, Vol. 21, no. 2/3, (1984). pp. 168-178

[31] Meyer W.S., "Standard reference evaporation calculation for inland, south eastern Australia", CSIRO Land & Water, Technical Report No 98, (1998).

[32] Park j., Kojiri T., Tomosugi K., "Development of GIS based distributed runoff model for environmental assessment", *Japan Soc. Hydrol. & Water Resources*, Vol. 16, No. 1, (2003), pp. 541-555.

[33] Pielke R. A., "Mesoscale Meteorological modeling", (1984), Academic Press, Orland.

[34] Potter T.L., Simmons K., Wu, J., Sanchez-Olvera M., Kostecki P., and Calabrese E.," Static die-away of a Nonylphenol Ethoxylate surfactant in estuarine water samples", *Environ. Sci. Technol.*, Vol. 33, (1999), pp. 113-118.

[35] Refsgaard, J.C. and B. Storm, "MIKE SHE. In V.P. Singh (Ed.)", *Computer Models of Watershed Hydrology*: 809-846, Water Resources Publications, Highlands Ranch, CO, (1995).

[36] Richards L. A., "Capillary conduction of liquids through porous media". *Physics 1*, (1931), pp. 318-333.

[37] Singh V.P., "Computer Models of Watershed Hydrolog", *Water Resources Publications*, (1995).

[38] Shen H., *"Modeling of rivers"*. 1st edition, Wiley, (1979).

[39] Snyder S., Keith T., Verbrugge D., Snyder E., Gross T., Kannan K., and Giesy J., "Analytical methods for detection of selected estrogenic compounds in aqueous mixtures", *Environ. Sci. Technol.*, Vol. 33, (1999), pp. 2814-2820.

[40] Tennessee Valley Authority, "Heat and mass transfer between water surface and the atmosphere", Technical Report No 14, Water Resources Research Report No 0-6803, (1972).

[41] Wang H., Anderson M., *"Introduction to groundwater modeling"*, Academic Press, (1982).

APPENDIX A

The Yasu River Basin, Japan

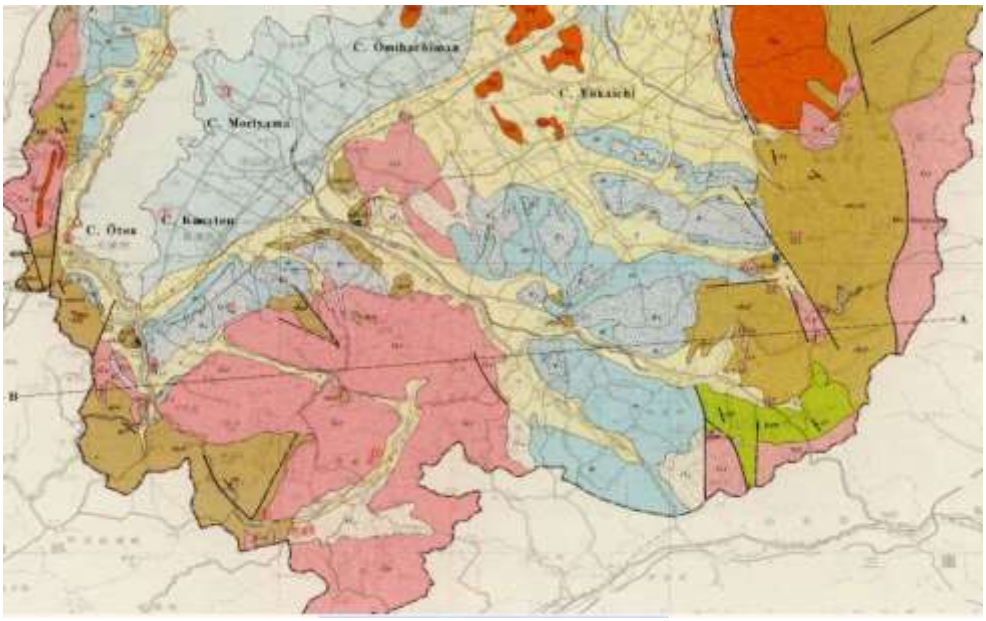

(a)

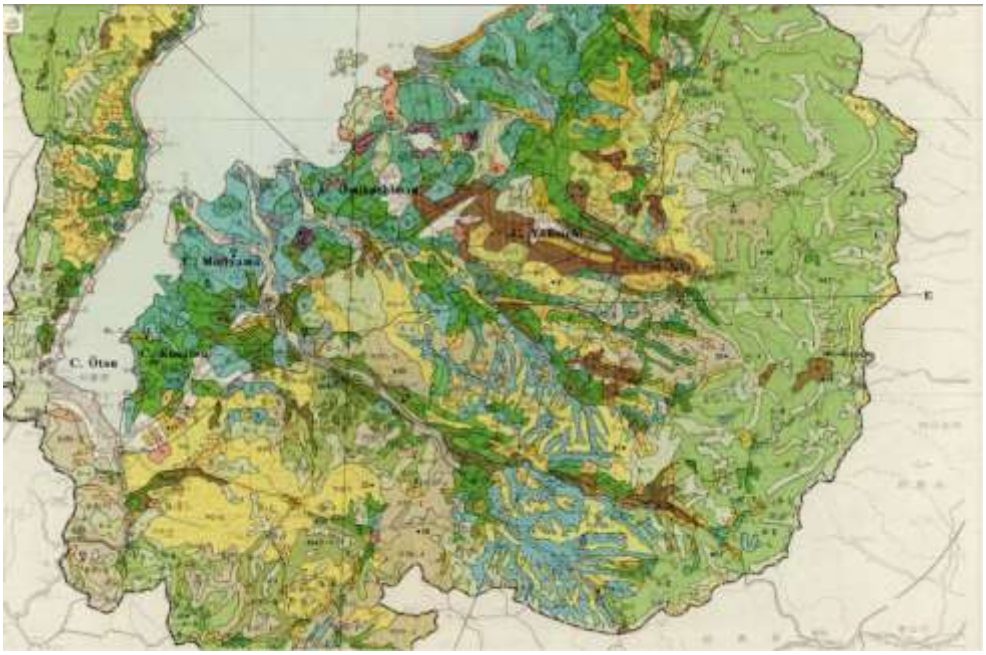

(b)

Figure A.1 Hard copy maps, (a) geological map; (b) Soil map the, Yasu River basin.

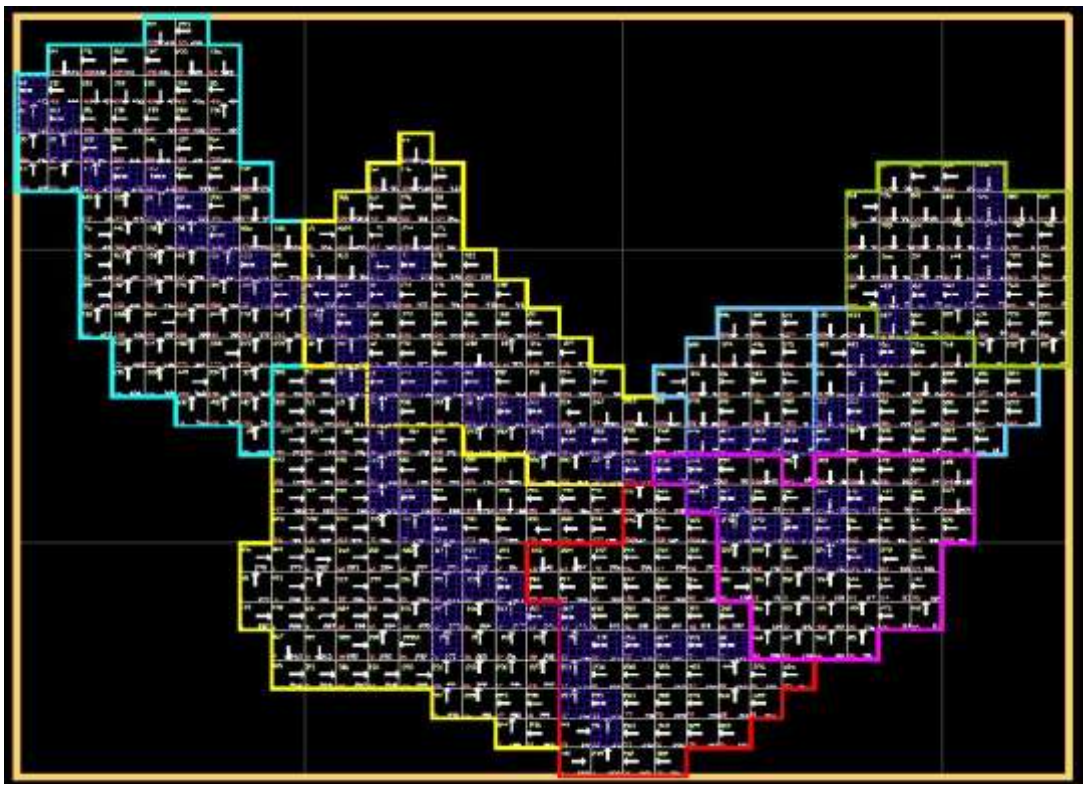

Figure A.2 Flow routing map with four directions on surface runoff.

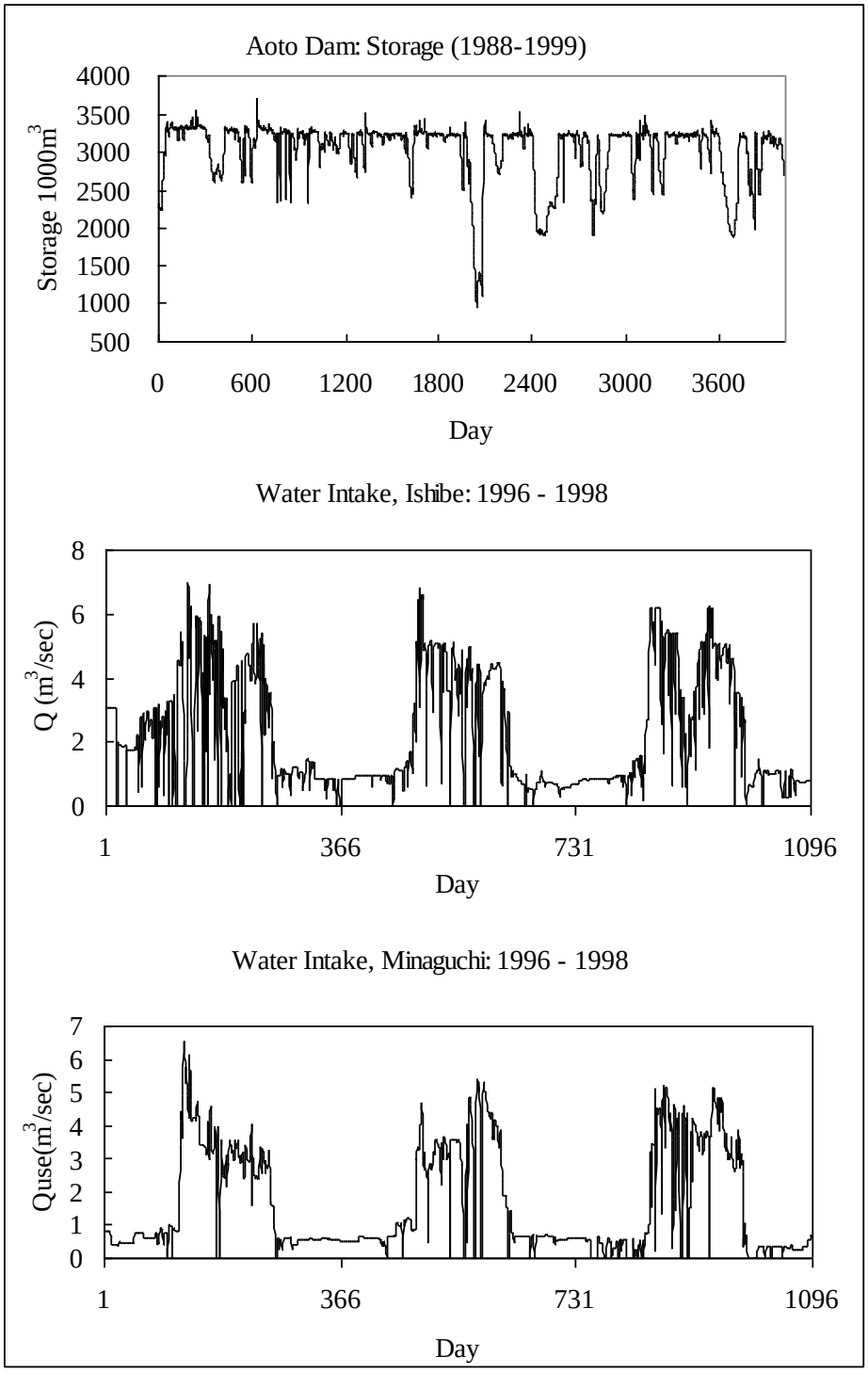

Figure A.3 Water Intake in the Yasu River basin.

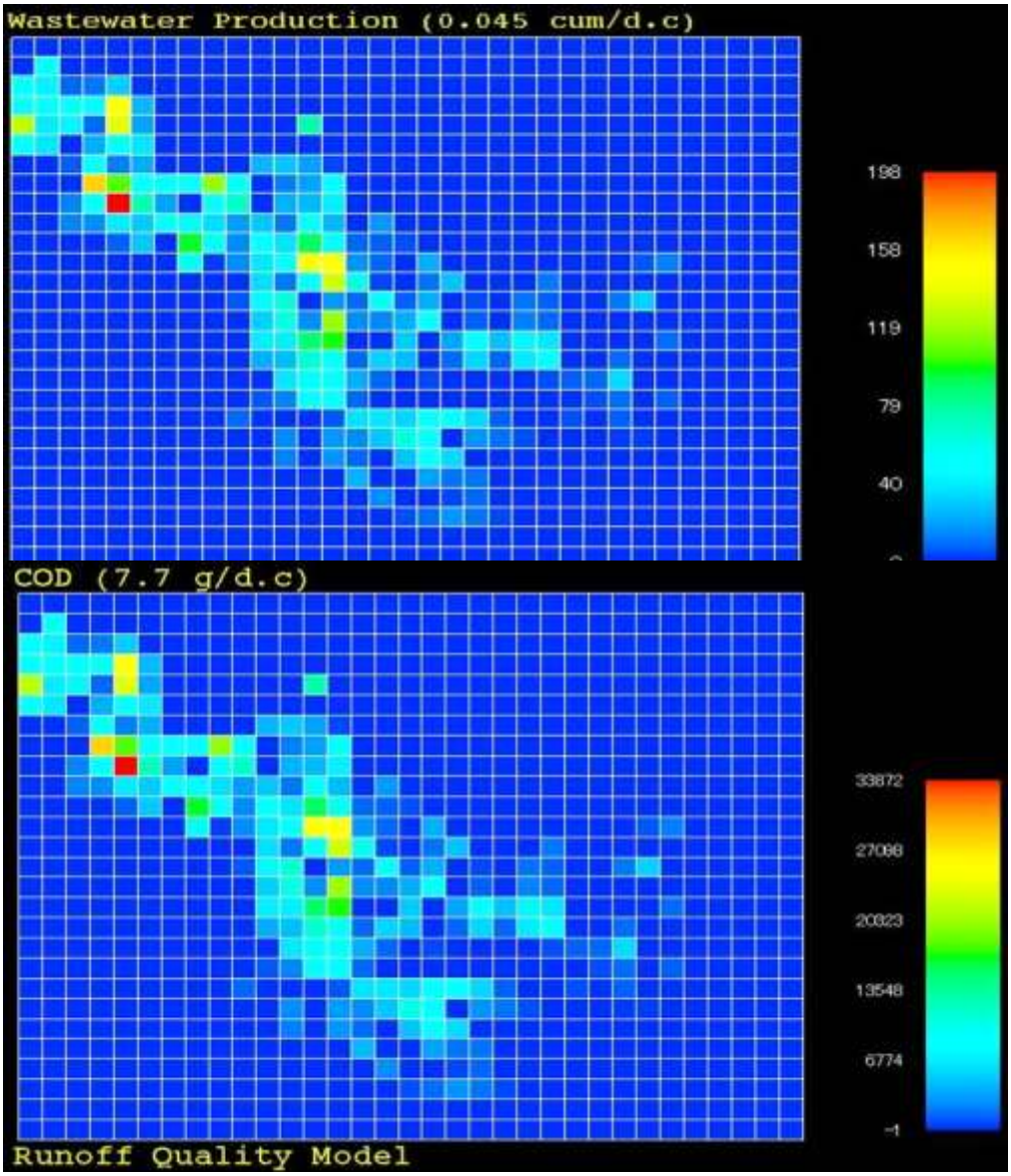

Figure A.4 Distribution of wastewater effluents and the corresponding concentration of COD in the Yasu River basin.

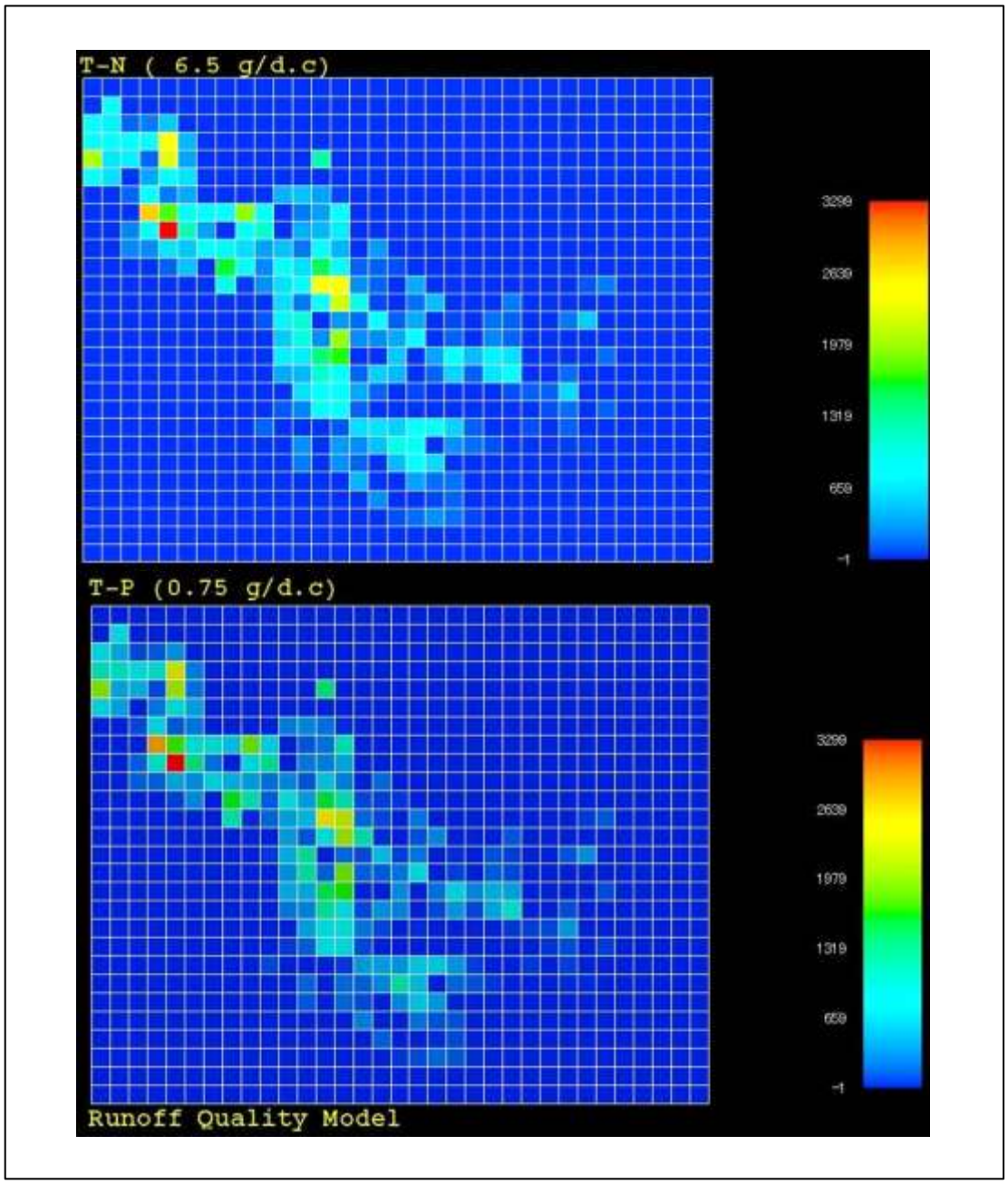

Figure A.5 Distribution of total- N and total-P in the Yasu River basin.

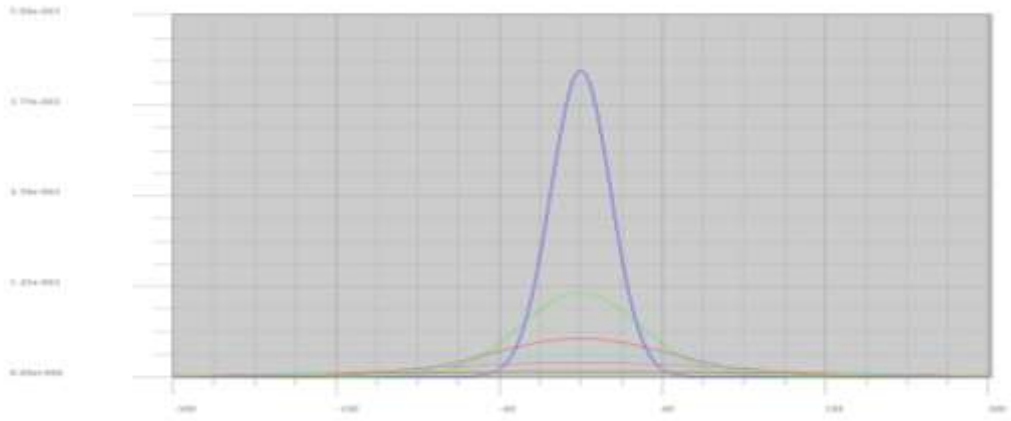

(a)

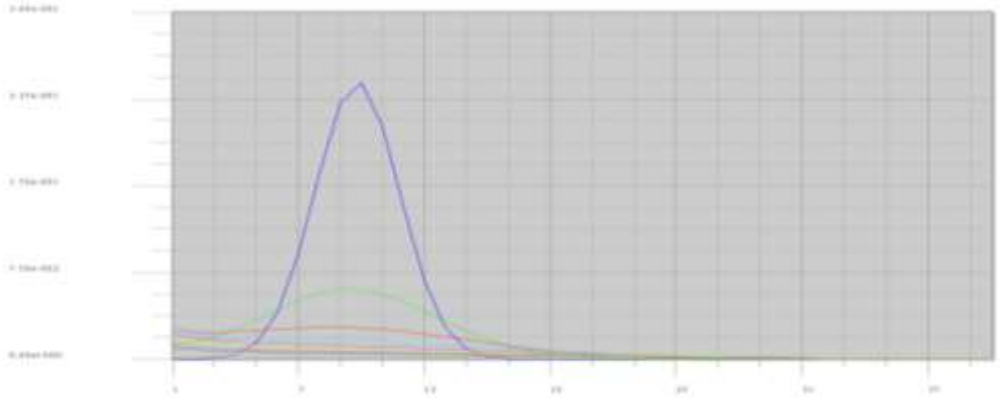

(b)

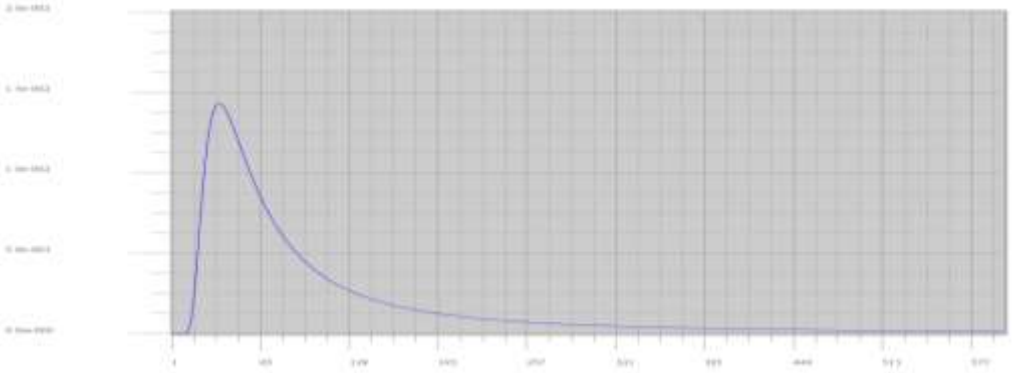

(c)

Figure A.6 NP concentration, a) along the ground, z=0, b) along the centerline, y=0, c) along the ground on the centerline, y=0, z=0.

APPENDIX B

The Seyhan River Basin, Turkey

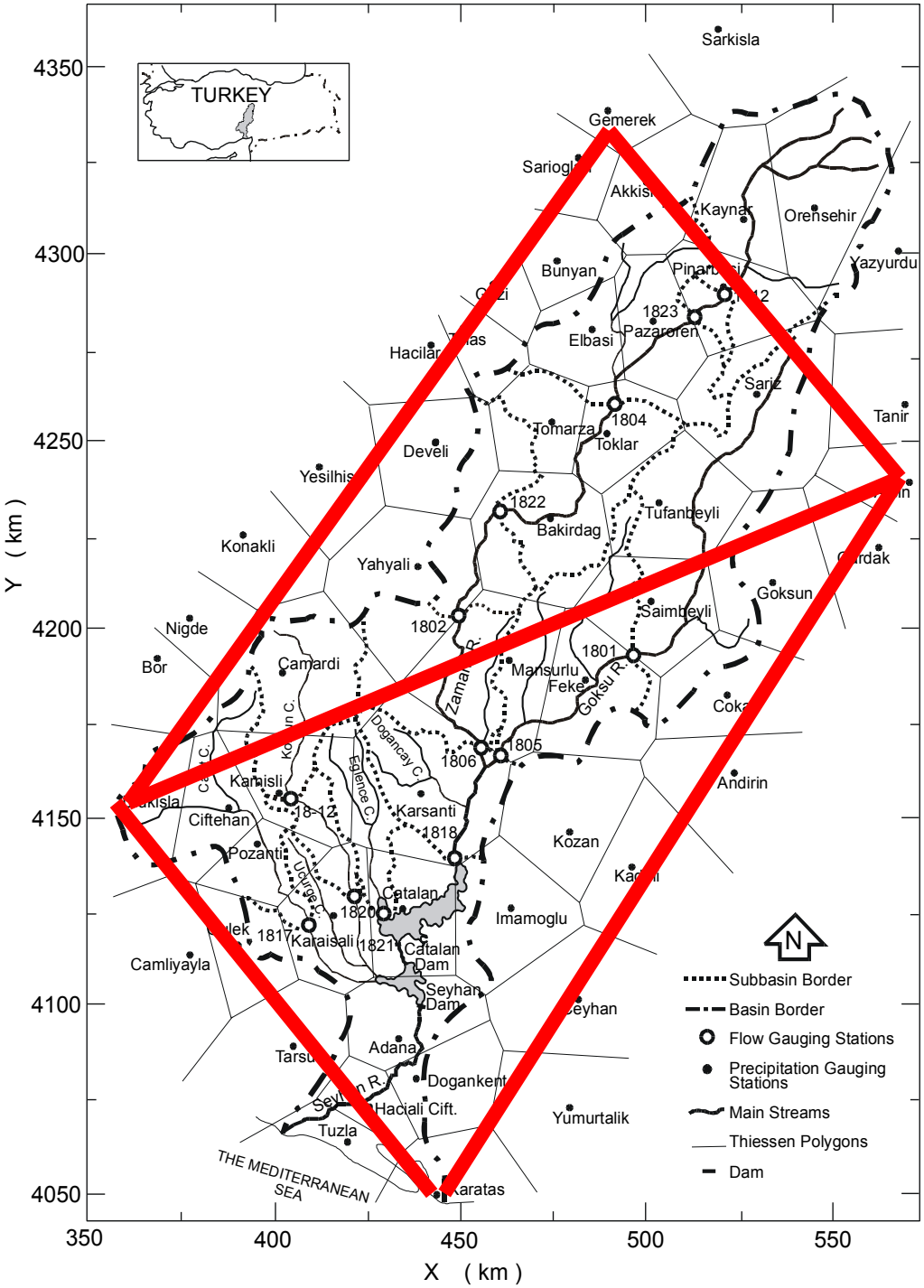

Figure B.1 The Seyhan River basin and Thiessen polygons of the main weather stations, (*Source: ICCAP*).

APPENDIX C

Plume Rise

Table C-1 Stability classes.

Surface Wind Speed at 10 m (m/s)	Day			Night	
	Incoming Solar Radiation			Cloud Cover	
	Strong	Moderate	Slight	Thinly Overcast or ≥50% Clouds	Mostly Clear or $\leq\frac{3}{8}$ Clouds
<2	A	A–B	B	—	—
2–3	A–B	B	C	E	F
3–5	B	B–C	C	D	E
5–6	C	C–D	D	D	D
>6	C	D	D	D	D

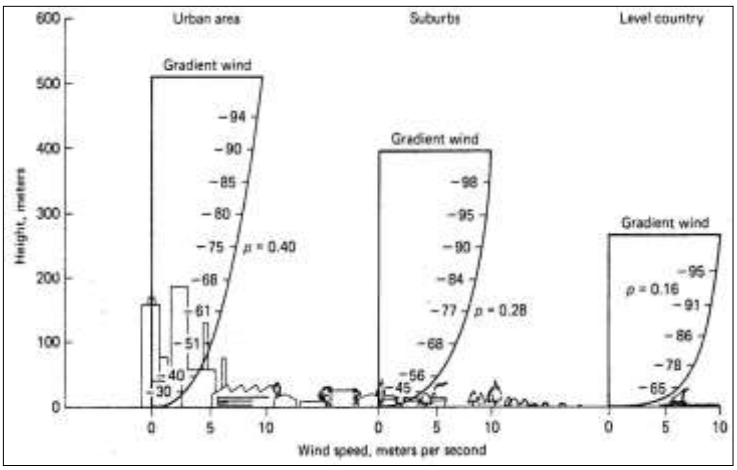

Figure C.1 Wind speed with height.

Table C-2 Briggs plume rise.

Unstable or Neutral Atmospheric Conditions				Stable Atmospheric Conditions	
for $F_b < 55\frac{m^4}{s^3}$, $(\Delta T)_c = 0.0297 T_s \frac{v_s^{1/3}}{d_s^{2/3}}$		for $F_b \geq 55\frac{m^4}{s^3}$, $(\Delta T)_c = 0.00575 T_s \frac{v_s^{2/3}}{d_s^{1/3}}$		$(\Delta T)_c = 0.019582 T_s v_s \sqrt{s}$	
if $\Delta T < (\Delta T)_c$, momentum dominated	if $\Delta T \geq (\Delta T)_c$, buoyancy dominated	if $\Delta T < (\Delta T)_c$, momentum dominated	if $\Delta T \geq (\Delta T)_c$, buoyancy dominated	if $\Delta T < (\Delta T)_c$, momentum dominated	if $\Delta T \geq (\Delta T)_c$, buoyancy dominated
$\Delta h = 3 d_s \frac{v_s}{u}$	$\Delta h = 21.425 \frac{F_b^{3/4}}{u}$	$\Delta h = 3 d_s \frac{v_s}{u}$	$\Delta h = 38.71 \frac{F_b^{3/5}}{u}$	$\Delta h = 1.5 \left(\frac{F_m}{u\sqrt{s}}\right)^{1/3}$ or $\Delta h = 3 d_s \frac{v_s}{u}$ whichever is lower	$\Delta h = 2.6 \left(\frac{F_b}{u\, s}\right)^{1/3}$

Table C-3 Briggs formulas.

Pasquill Stability Category	σ_y (meters)*
A	$0.32\,x\,(1.0 + 0.0004\,x)^{-1/2}$
B	$0.32\,x\,(1.0 + 0.0004\,x)^{-1/2}$
C	$0.22\,x\,(1.0 + 0.0004\,x)^{-1/2}$
D	$0.16\,x\,(1.0 + 0.0004\,x)^{-1/2}$
E	$0.11\,x\,(1.0 + 0.0004\,x)^{-1/2}$
F	$0.11\,x\,(1.0 + 0.0004\,x)^{-1/2}$
Pasquill Stability Category	**σ_z (meters)***
A	$0.24\,x\,(1.0 + 0.001\,x)^{1/2}$
B	$0.24\,x\,(1.0 + 0.001\,x)^{1/2}$
C	$0.20\,x$
D	$0.14\,x\,(1.0 + 0.003\,x)^{-1/2}$
E	$0.08\,x\,(1.0 + 0.015\,x)^{-1/2}$
F	$0.08\,x\,(1.0 + 0.015\,x)^{-1/2}$

* Where x is in meters